Department of Precision and Microsystems Engineering

# Relax To Stress

M. Blaakman

Report no : 2024.089
Coach : dr. ir. G. Radaelli
Professor : dr. ir. G. Radaelli
Specialisation : MSD
Type of report : Master Thesis
Date : 25 October 2024

# From zero-stiffness to neutral stability

## The use of stress relaxation to make an initially zero-stiffness mechanisms neutrally stable

Master of Science Thesis

For the degree of Master of Science in Mechanical Engineering - High Tech Engineering at Delft University of Technology

M. Blaakman

October 14, 2024

Faculty of Mechanical, Maritime and Materials Engineering (3mE) · Delft University of Technology

Delft University of Technology
Department of
Precision and Microsystems Engineering (pme)

The undersigned hereby certify that they have read and recommend to the Faculty of Mechanical, Maritime and Materials Engineering (3mE) for acceptance a thesis entitled

From zero-stiffness to neutral stability

by

M. Blaakman

in partial fulfillment of the requirements for the degree of

Master of Science Mechanical Engineering - High Tech Engineering

Dated: October 14, 2024

Supervisor(s):

dr. ir. G. Radaelli

Reader(s):

dr. ir. G. Radaelli

prof. dr. ir. J.L. Herder

prof. dr. ir. K.M.B. Jansen

# Preface

After years of hard work and many coffee breaks, I am proud to be finalizing my studies at the Technische Universiteit Delft with this Master Thesis. My interests in the field of compliant mechanisms have far surpassed my expectations. I started this project with so many questions, and after gaining some valuable insights I ended up with many more.

Completing this final project was however not a solo effort. First of all, I would like to thank my supervisor Giuseppe Radaelli for his continuous support, insight and guidance. The conversations in our fortnightly meetings kept me sharp, and the appreciation for my work made me tone down on my sometimes overly critical attitude. All in all, I learned a great deal and I attribute a big portion of that progress to my supervisor.

My gratitude also goes towards PME's lab support, who have always been there to help me tackle practical issues, especially in the experimental phase of this research.

I would finally like to thank my friends, family and girlfriend for taking my mind off of studying and enabling me to vent about my struggles. Having them beside me made the whole process of doing this research a number of magnitudes more enjoyable.

To give credit where credit is due, D. Farhadi Machekposhti supplied a basic template for all simulations done using Ansys parametric design language. Also, this master thesis is written in the template of Delft Center for Systems and Control.

*Thies Blaakman*

*Delft, October 2024*

# Table of Contents

# Glossary

List of Acronyms

| | |
|---|---|
| **NS** | neutrally stable |
| **ZS** | zero-stiffness |
| **WLF** | William-Landel-Ferry shift function |
| **UV** | ultraviolet |
| **TTS** | time-temperature-superposition principle |
| **DoF** | degrees of freedom |
| **PI** | Physik Instrumente |
| **FDM** | fused deposition modelling |
| **ID** | initial deformation |
| **RD** | returning deformation |
| **SRPS** | stress relaxation prestressing |
| **PLA** | polylactic acid |
| **MJF** | multi jet fusion |
| **BSP** | Boltzmann superposition principe |
| **PA12** | Nylon |

# Chapter 1

# Introduction

In the field of compliant mechanisms, an overarching goal has always been to create compliant alternatives that would be able to replace traditional rigid body mechanisms. One of the single most difficult tasks in this regard is, due to the inherent stiffness of materials, the creation of hinges and joints which do not require the application of an actuation force in order for them to move along their desired degree of freedom.

The class of compliant mechanisms which do possess the aforementioned desired ability without the need of a force keeping them in a specific configuration, are called neutrally stable compliant mechanisms. These type of mechanisms do not have a preferred configuration. Take for example the Anglepoise lamp from Schenk and Guest [1], which uses springs to balance the weight of its links. Where this example consists of an assembly of rigid parts and compliant parts, the neutrally stable tape spring from Murphey and Pellegrino [2], is a monolithic example. In both cases, a type of prestress is added to the mechanism in order for it to become neutrally stable. The lamp would collapse without its springs, and the tape spring would be monostable in case of force misalignment.

In reality, no compliant mechanism is purely neutrally stable. This issue stems from achievability of manufacturing tolerances, especially in 3D printed materials, and the difficulty of matching the applied prestress with the original stiffness in order to counter it. Especially in monolithic structures. As a result, there are very few examples of monolithic neutrally stable structures. And even fewer of complex examples.

In this research, a method is proposed for applying prestress in a predictable manner in order to consistently create neutrally stable mechanisms, from a variety of monolithic zero-stiffness mechanisms, both simple and complex. The prestressing method relies on the requirement of zero-stiffness in combination with the requirement of the existence of a near mirror image of the deformed mechanism, after deformation.

After this first introductory section, a paper can be found in which, after a short introduction, a section is dedicated to the explanation of the viscoelastic effects, creep and stress relaxation. In this section the idea behind the working principle of the prestressing method is also demonstrated. Then, two different mechanisms are proposed to demonstrate the prestressing method on. Next up is the method section in which simulations and experiments, for both mechanisms respectively, are discussed. Afterwards a section is dedicated to visualising the findings from the simulations and experiments. The presentation of these results is then followed by a discussion in which they are are interpreted. The final section reflects back on the whole paper. For an in depth review on viscoelastic effects in different materials and suitable models, and a categorisation on prestressing techniques, see Appendix A.

# Chapter 2

# From zero-stiffness to neutral stability using stress relaxation

***Abstract*** **- The creation of neutrally stable compliant mechanisms is a balancing act between knowledge on the system and the application of a stiffness countering prestress.**

**This paper presents a novel prestressing method for polymeric compliant zero-stiffness mechanisms, utilizing stress relaxation as an actor for imprinting a permanent elevated internal stress state. The method in question does not require a complex mechanical setup for application of the prestress. A sensitivity analysis is performed for the variables of relaxation time and imposed deformation.**

**Two mechanisms with different origins for zero-stiffness behaviour are presented, and made neutrally stable. The simulations for one of the two examples, after correcting for a stretch in the force-displacement relationship, match with the experimental results for both the variation in relaxation time and imposed deformation. For the second mechanism, the simulation for relaxation time matches that of the experiment, but for the imposed displacement this does not seem to be the case.**

***Index terms*** **- Neutral stability, Zero-stiffness, Snap-through buckling, Prestress, Viscoelasticity, Stress relaxation, Creep, Compliant mechanisms**

## I Introduction

In the field of compliant mechanisms, the most often used materials are polymers due to their high yield strength to Young's modulus ratio [3]. One of the biggest obstacles in working with polymers is their inherent viscoelastic behaviour. Viscoelastic effects such as creep and stress relaxation occur at almost any level of deformation induced stress, and can therefore impact the predictability of polymeric mechanisms' behaviour. More on creep and stress relaxation can be found in section II.

One of the main objectives of compliant mechanisms is mimicking the functionality of regular joints. Where typical joints have no preferred configuration as long as their internal friction is overcome, compliant mechanisms struggle on this front. The obvious reason for this is that the bending and twisting of material results in a reaction force attempting to undo the deformation. Combatting this tendency to deform back is normally done either by the addition of elements of different, sometimes negative, stiffness to mechanisms, or plastically deforming them. This is what is referred to as prestressing the mechanism. The process of prestressing is often a difficult balancing act. Especially monolithic structures are difficult to enable to behave neutrally stable (NS). Where creating NS monolithic structures is usually limited to very simply shaped mechanisms, take the tape spring from Murphey and Pellegrino [2] or the coiled strip from Seffen and Guest [4], the prestressing method presented in the next section is not.

This paper shows how, based on two criteria, a zero-stiffness (ZS) mechanism can be transformed into a NS mechanism utilizing the viscoelastic phenomenon stress relaxation. The method described in this paper enables for a transformation of monolithic zero-stiffness mechanisms with complex geometry into neutrally stable mechanisms, using a novel prestressing method. The prestressing method is reffered to as the stress relaxation prestressing (SRPS) method.

After this introduction, the paper continues with the working principle section, in which important definitions and concepts are explained. In this section, the method of applying a prestress using stress

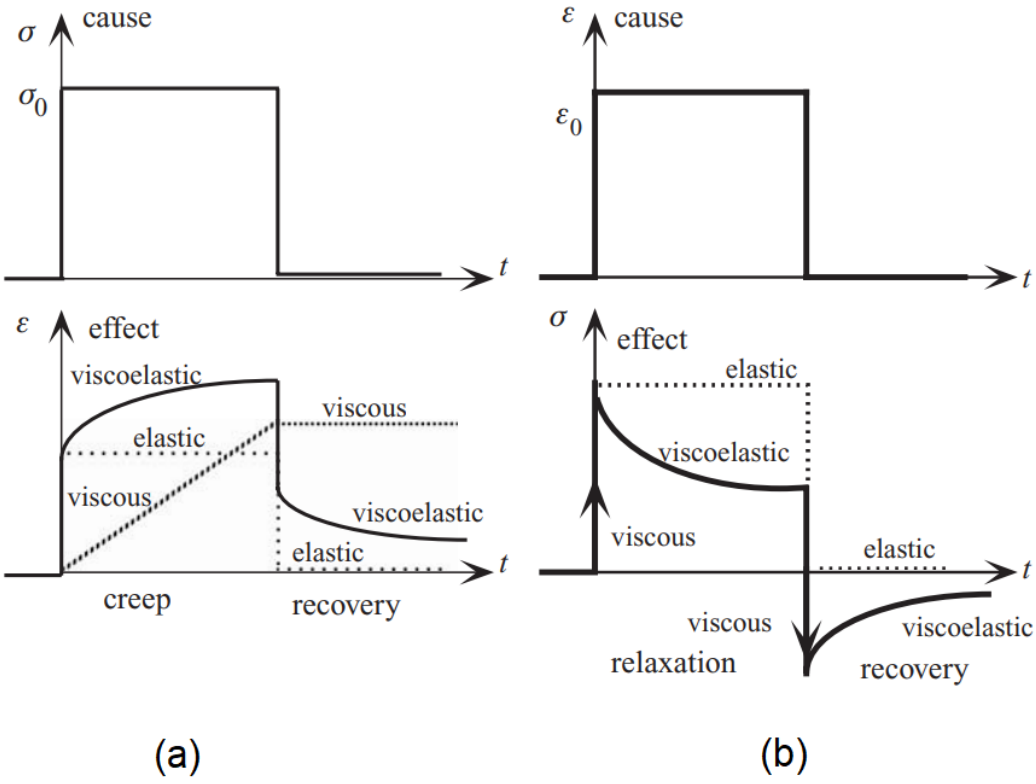


**Figure 2-1:** Generic stress-time and strain-time diagrams for creep (a) and stress relaxation (b) [5].

relaxation will be explained in combination with two different examples: a linear guide and a helicoidal shell mechanism. A clear distinction will be given on the reasons for the ZS behaviour of the two mechanisms. The method section follows, discussing the numerical model used to predict the behaviour for a given deformation and relaxation, and explaining the experimental setup to validate the model in question. The results section will follow, showing the neutral stability of both mechanisms through the SRPS method as mentioned in the working principle section. The discussion section, will reflect on the obtained results, along with an attempt to explain discrepancies between the numerical model and the experimental results. Some recommendations for future research will also be given here. This paper ends with the subsequent conclusions that can be drawn from the results and the discussion section.

## II Working principle

Before diving into prestress method, a few concepts are explained to give a better understanding as to what is happening during the prestress process.
Firstly, we address creep and stress relaxation. Then, we explain the idea of using stress relaxation as a means of applying prestress. Here two requirements for mechanisms for which this method is suitable are proposed. Finally, two different mechanism are given, explaining how they adhere to the proposed requirements.

### *A. Viscoelasticity*

Viscoelastic behaviour has many facets, but the most important phenomena of concern in this work are called creep and stress relaxation. The concept of creep is defined as an increasing strain over time for a constant force level, see figure 2-1(a). This can be visualised with a real world example of an elastic band that is being held in the air at one point and on the other end has a mass attached, see figure 2-2. Over time, even though the mass, and thus force, doesn't change, the length of the band will increase. The origin of this behaviour in polymers lies in the rearrangement of polymeric bands on a micro scale in the material itself through straightening or unwrinkling, in addition to sliding relatively to each other in response to sustained loads [6].

Stress relaxation on the other hand is defined as a reduction of stress over time for a constant value of imposed strain, see figure 2-1(b). For a physical example, take a look at figure 2-3. In the figure, an elastic band is first held at an undeformed length of L. Then the elastic band is stretched by an amount dL, and held deformed for some time. During this time, the internal polymeric chain structure rearranges. As a result, now moving the hands

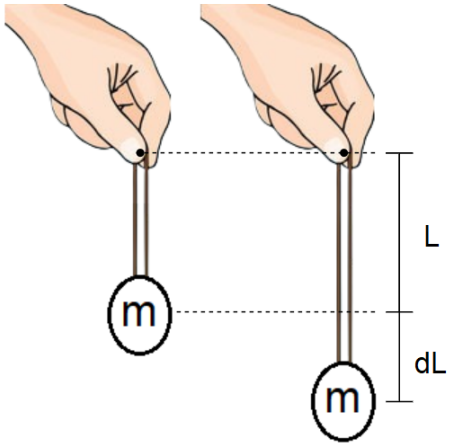


**Figure 2-2:** Physical example of creep: an elongation of an elastic band after some time with a constant load.

closer together again so that the distance between the attachment points is L again, it can be seen that the band is hanging slack. Ergo, the internal stresses that caused the tensile force in the elastic band have partially dissipated. The terms creep and stress relaxation might seem very similar, and rightfully so. While the definitions from the point of view of mechanics might be different, the underlying phenomenon is the same [7]. The terms are even sometimes used interchangeably [8].

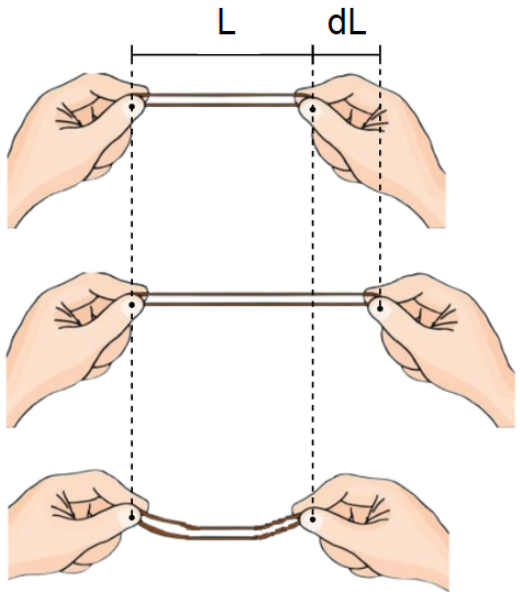


**Figure 2-3:** Physical example of stress relaxation: after extension from its original length for some holding time, and then returning to the original length, the elastic band is now slack.

The degree of relaxation in a mechanism depends on factors such as time, temperature, the level of stress in the material, humidity and the exposure to ultraviolet (UV) radiation, over the whole time span of the existence of the mechanism. For linear viscoelastic materials, this phenomenon is explained with the Boltzmann superposition principe (BSP), which states that the induced stresses from two different deformations are additive and create a proportional strain [6]. The cumulative effect of stresses is highly apparent in polymers [9]. An assumption that is made at the start of this research is that an increase in stress leads to an increase in relaxation, regardless of the type of stress (eg: tension versus compression), due to the increased energy state of the polymer chains in the mechanism [10] .

### *B. From zero-stiffness to neutral stability*

For regular ZS mechanisms, the force-deflection curve looks somewhat similar to the initial deformation (ID) phase of figure 2-4, with a constant force-level of $a$. If the system is deformed from its initial configuration to a deformed configuration, such as at the end of the ID phase, a set amount of work has to be done. If the mechanism in question is held in its deformed position for an extended amount of time, see the relaxation phase of figure 2-4, the internal stresses will dissipate through stress relaxation and therefore the force on the mechanism will drop to zero at some point in time. In the physical world, the mechanism would now not configure back to its initial state. Releasing the mechanism at this point in time, its internal rearrangements will have led to this configuration being the new 'preferred' configuration of the system. If the deformed configuration of the mechanism would be a a near mirror image of the original configuration, it would be expected that the force-deflection curve inverts when the new preferred configuration is assumed. The reason for this is that a mechanism, when fully relaxed after deforming it to its mirror image configuration, would behave as if it was fabricated in this mirrored configuration. As such, the ZS region would have vertically shifted from a force value of $a$ to a value of $b$ as can be seen in the figure in the returning deformation (RD) phase. What this means in practise is that now the system will require a set amount of work to move from the deformed configuration back to the initial configuration, as it no longer 'wants' to move back to its initial state. The question now arises if there is also a point in time where the mechanism ís deformed, but not yet to the point that the ZS region has shifted from $a$ to $b$, but from $a$ to 0, as depicted in the RD phase in figure 2-5, rendering the mechanism neutrally stable.

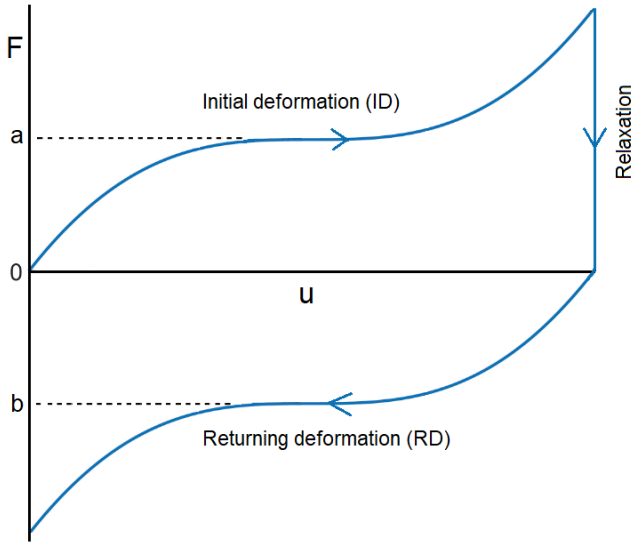


**Figure 2-4:** Force-deflection curve of generic zero-stiffness mechanism with full relaxation in order to invert the force-deflection curve.

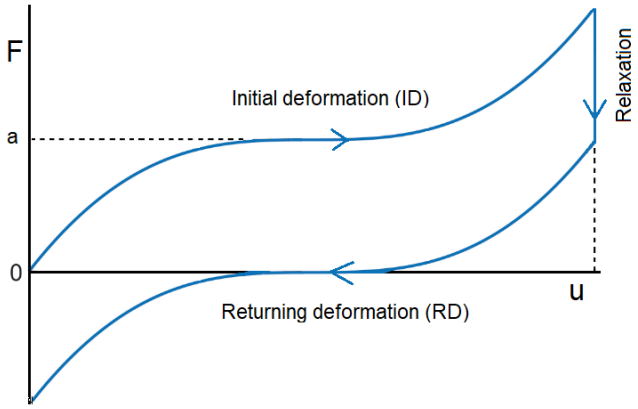


**Figure 2-5:** Force-deflection curve of generic zero-stiffness mechanism with partial relaxation, in order to achieve neutral stability.

The set of compliant mechanisms that has been researched in this paper in order to see if they can be made NS using the SRPS method is limited to mechanisms which adhere to the following two requirements:

I. The mechanism can be deformed in a way that its deformed configuration is a near mirror image of its undeformed configuration.

II. The mechanism has a zero-stiffness region.

The first criterion stems from the fact that a relaxation phase in a non-mirrored configuration might lead to a whole different curve in the RD phase, meaning that the system will no longer be NS if it ever were ZS. This would also imply that mechanisms which are not ZS in the first place might still become NS when using the SRPS method, however the investigation of this thought is left for future research.

The second criterion as mentioned only gives an initial shape to a shifting curve on the force axis of the force-displacement diagram. If this curve can be made to retain its original shape, making the assumption that a mirrored relaxation phase does not alter the mechanism's slope, the system will become neutrally stable after the relaxation phase.

### C. *Linear guide*

The simplest example of a mechanism that shows the working principles of this paper is the linear guide, the most uncomplicated version of which can be seen schematically in figure 2-6. In the figure, a pinned-pinned connection for a snap-through beam is visible. It is obvious that deforming the mechanism beyond its snap-through region leads to a mirror image of the original configuration of the mechanism if the offset $d_o$ of the beam is the same for both configurations.

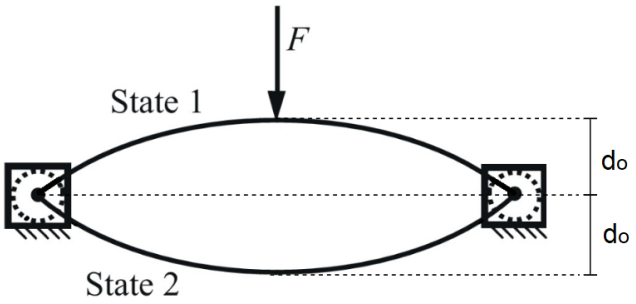


**Figure 2-6:** Simple snapping beam [11] with state 2 being a mirror image of state 1.

Normally, a snapping beam's force-deflection diagram has a curved appearance. The thinner the beam, the more pronounced this undulating shape. The system will behave bistable when the beam is very thin, creating an almost sinusoidal shape. On the other hand, the thicker the beam, the more it behaves like a simple bending beam, losing its bistable behaviour. The resulting shape of the force-deflection curve is an increasingly straighter line. By optimizing for thickness a ZS snapping beam can be generated as a middle ground between an undulating shape and a straight line. In figure 2-7 a generic example of such an optimisation is depicted. It is important to note that increasing the arc of the beam will also lead to an increasingly wave-like shaped force-deflection curve. It should

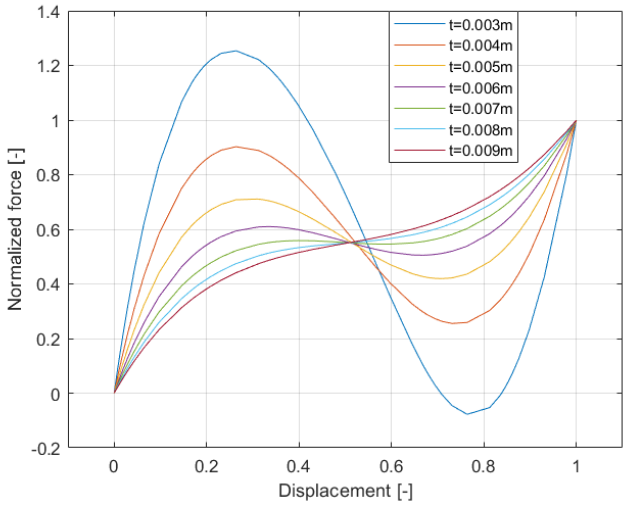


**Figure 2-7:** Force displacement curve of snap-through buckling beam for a variation in beam thickness.

be trivial to state that the linear guide meets the requirement I.

To accurately capture the mechanism's behaviour, two of the snapping beams have been added in parallel in order to create symmetrical snapping behaviour. The final mechanism to be tested can be seen in figure 2-8(a). The geometric parameters for the linear guide are height h = 81mm, offset $d_o$ = 2mm, thickness t = 3mm, width between splines w = 20mm, and in plane depth d = 7.5mm, see figure 2-8(b).

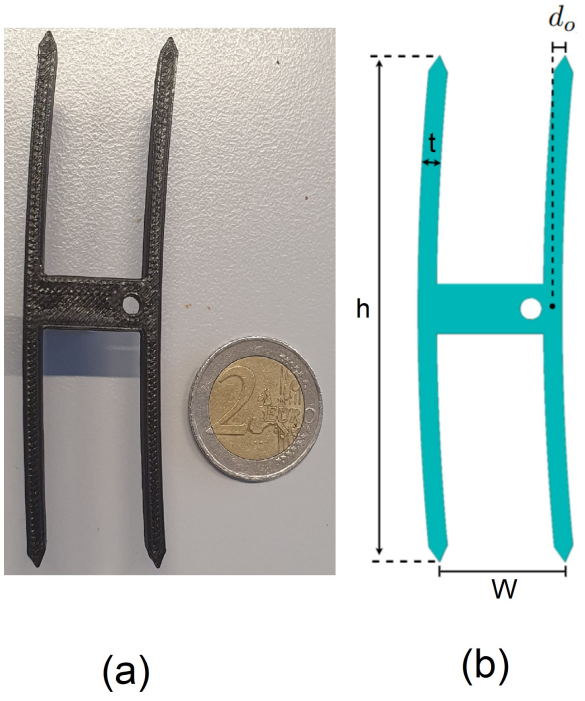


**Figure 2-8:** Physical linear guide (a) and a schematic with reference geometry (b).

### D. Helicoidal shell

In order to show that the proposed idea applies to more complex mechanisms, the ZS helicoidal shell designed by Radaelli [12] has been chosen as a second example to be made neutrally stable. Radaelli displays the synthesis of a helicoidal shell structure consisting out of 6 flanges, attached at a symmetry axis, see figure 2-9(a). The exact geometry has been adopted for this paper with height h = 0.1m, width w = 0.01m, pitch angle $\theta = 180°$, and flange thickness t = 0.4mm (not shown), see figure 2-9.

.

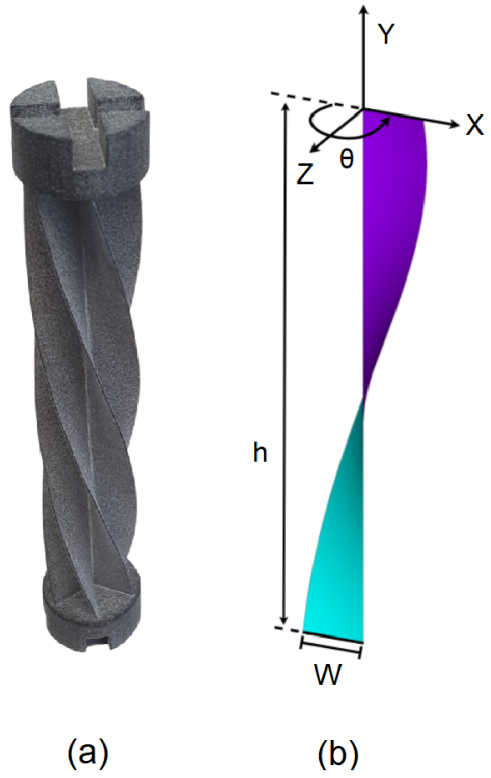


**Figure 2-9:** Physical helicoidal shell [12] (a) and a schematic with reference geometry (b).

When taking a look at the helicoid, it is plain to see how the twisting of the mechanism around its symmetry axis results in a mirrored version of the original, especially if you compare figure 2-10(a) and figure 2-10(d).

The mechanism derives its ZS from the fact that when one end is clamped and the other is rotated around its symmetry axis, after the initial buckling region, the only deformation happening is a propagation of the buckled region along its length. Therefore, a constant amount of work is being done when rotating further. For the full deformation to a mirrored configuration, see figure 2-10(a)-(d).

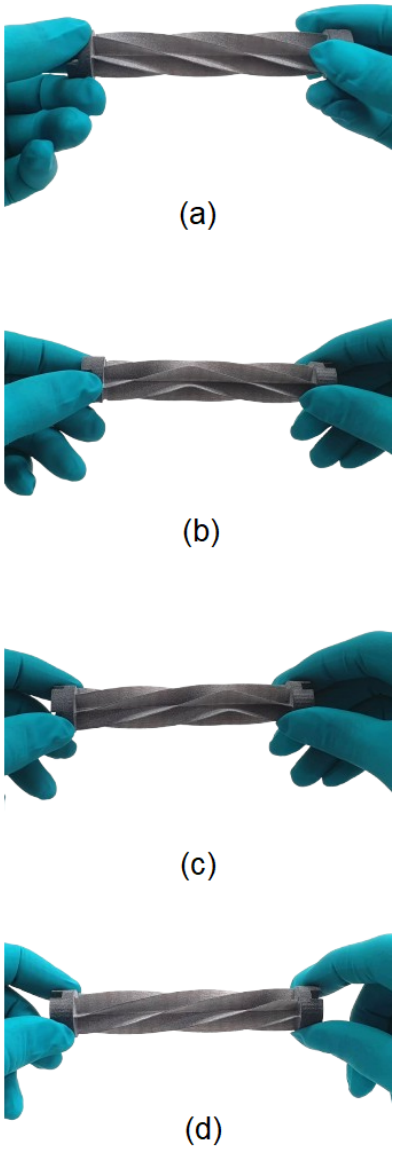


**Figure 2-10:** Helicoidal shell propagation deformation zone. From fully undeformed (a), to partially deformed (b)(c), to fully mirrored (d).

## III Method

In order to asses if the SRPS method achieves NS in the given examples, first numerical models are made for both the linear guide and the helicoid. In an attempt to validate these numerical models, an experiment which replicates the simulated boundary conditions is performed. This section provides the necessary means for reproducing the simulations and experiments. The modelling setup and experimental setup for the linear guide will be explained. In the same fashion, the numerical model and experiment for the helicoid will be elaborated on. A sensitivity analysis will be perfomed in both simulation and experiment in order to see if increasing the parameters of relaxation time and deforming displacement, or twist in case of the helicoid, will result in increased relaxation.

Testing for a varying temperature will not be performed, although temperature dependence is taken into account in the simulation, as controlling the temperature of the mechanisms would require too complex of a setup for the scope of this research. It is however generally accepted that an increase in temperature, along with an increase in stress, accelerates the rate at which a deformed mechanism relaxes, provided there are no phase transitions [13]. This phenomenon is called the time-temperature-superposition principle (TTS) or sometimes the time-temperature-stress superposition principle. Figure 2-11 shows how an increase in temperature vastly reduces the time it takes for the relaxation modulus, which is the time-dependent Young's modulus, to decay when subjected to an imposed strain.

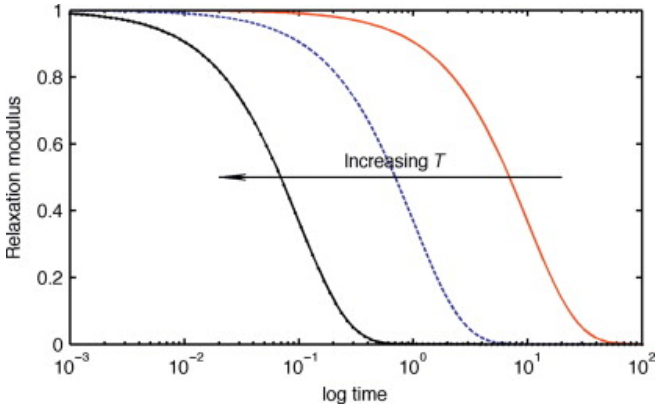


**Figure 2-11:** Time-temperature equivalence diagram showing an increase in relaxation with increased temperature [14].

### *A. Numerical Model Linear Guide*

The linear guide is modelled in using the same geometry as depicted in figure 2-8. The geometry has been created using Solidworks 2023, and imported into Ansys Mechanical APDL 2022 R2 as a parasolid. A static structural analysis was performed using this software. The physical guide has been simplified to a model consisting out of two symmetrical splines, with an offset $d_o$ of 2mm of the midpoint to create the curvature. The model consists out of a SOLID187 element. The material model consists of a combination between a viscoelastic material model, and a linear elastic material model, the material properties which can be found in table 2-1. In linear elastic analyses, the interconnection between nodes is modelled as a simple linear spring. In a viscoelastic model, this spring is put in parallel with one or multiple sets of spring-damper components. In the table the Young's modulus and poisson ratio, E and v, are the linear elastic parameters. The Young's modulus, E, was approximated

numerically and the poisson ratio, v, was found in the literature [15].

The assumption is made that the material in question is nearly incompressible due to the fact that most of the deformation in the material comes from the shearing of the polymeric chains, also referred to as monomers [16]. Making this assumption enables for deriving a direct relationship between the general relaxation modulus, $E(t)$, and the shear relaxation modulus, $G(t)$, the normalized version of which is required in Ansys, given as

$$G_0(t) = \frac{E_0(t)}{2(1+\nu)} = \frac{E_0}{3}. \tag{2-1}$$

To model the decay from experimental data, a 5th order Prony series curve fit has been made. This series is often used to model viscoelastic behaviour. It relies on the solving of an initial value problem for a Generalized Maxwell model of n-th order [17], in our case n = 5. The formula for the Prony series of the generalized shear relaxation modulus is given as

$$G_0(t) = \alpha_0 + \Sigma_{i=1}^{N} \alpha_i \cdot e^{-\frac{t}{\tau_i}}. \tag{2-2}$$

The Prony constants are derived from a linear stress relaxation test using a tensile test bench extending a dog bone-like structure, see figure 2-12. The dogbone is stretched to ~105% of its free length, so from 30mm to 31.5mm, and then held at that specific length for a set period of time. This is similar to the ID- and relaxation phases of the SRPS method. The constants $\alpha_0 - \alpha_5$ and $\tau_1 - \tau_5$ are called Prony constants describing at what specific time what a specific amount of decay has occurred. What this means is that the experimental data from a tensile stress relaxation test can be directly used to curve fit in order to determine the viscoelastic behaviour of the material.

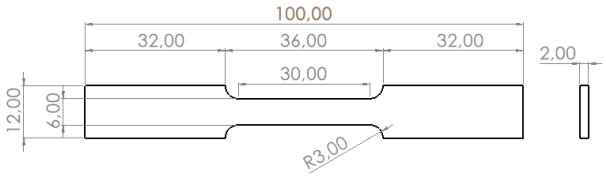


**Figure 2-12:** Dogbone dimensions

Another important concept in the realm of viscoelasticity is the
William-Landel-Ferry shift function (WLF). The function relies on the TTS that states that temperature works as a catalyst for relaxation time. More simply stated, with regards to a given reference temperature, if the temperature deviates by a specified amount, it can tell how much faster or slower the material relaxes, with faster being at a higher temperature. The WLF is stated as

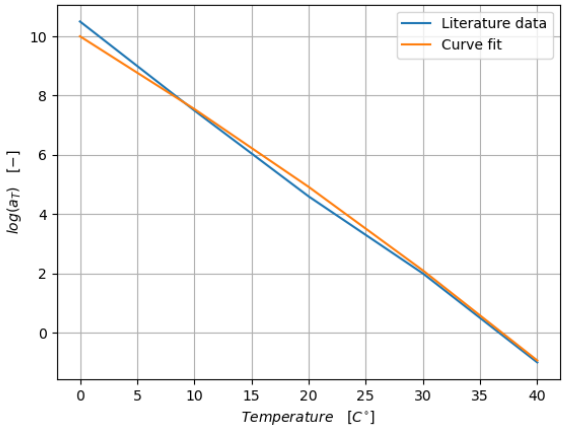


**Figure 2-13:** WLF shift function of PLA from curve fit versus data from the literature [19].

$$\log(a_T) = -\frac{C_1(T - T_{ref})}{C_2 + (T - T_{ref})}, \tag{2-3}$$

in which $log(\alpha_T)$ is the shift function, $C1$ and $C2$ are material constants determined from repeated testing at different temperatures, T is the operating temperature for the simulation and $T_{ref}$ is the chosen reference temperature from which your current temperature deviates. The material used for the experiment of the linear guide is PLA. PLA is chosen for the linear guide as material as it is very susceptible to viscoelastic effects, due to the room temperature already being close to its glass transition temperature, $T_g$, amplifying the effect of stress relaxation [18]. For the material properties used in the model, see table 2-1. The WLF of PLA has been found in the literature, and the constants C1 and C2 have been derived from this data. A curve fit has been made to see if for the same reference temperature, the literature data and curve fit actually coincide, see figure 2-13. The use of the WLF is only valid when the material is thermorheologically simple, or more simply stated, adheres to the TTS.

The boundary conditions of the system consist of both imposed displacement and a body force load in the form of an imposed temperature. The imposed temperature highly influences the degree of stress relaxation and is therefore used to match the experimental and numerical results. All nodes in the model are given a body force load of 14°C. Figure 2-14 gives the von Mises stress in the undeformed

**Table 2-1:** Material properties linear guide

| Parameter | Value | Unit |
|---|---|---|
| E | 5.3e9 | Pa |
| v | 0.35 | - |
| refT | 19 | °C |
| C1 | 8.14e1 | - |
| C2 | 2.64e2 | °C |
| $\alpha_0$ | 0.710 | - |
| $\alpha_1$ | 0.272 | - |
| $\alpha_2$ | 0.334 | - |
| $\alpha_3$ | 0.128 | - |
| $\alpha_4$ | 0.542 | - |
| $\alpha_5$ | 0.430 | - |
| $\tau_1$ | 3.22 | s |
| $\tau_2$ | 1.17e2 | s |
| $\tau_3$ | 9.98e2 | s |
| $\tau_4$ | 1.00e4 | s |
| $\tau_5$ | 1.00e5 | s |

configuration (a), after the ID phase (b), and after the RD phase (c). For all the sharp tips of the mechanism, the nodal displacements are 0, except for a rotation around the z-axis as can be seen in the figure. The central hole's in plane axis, where the red arrow attaches, is constrained in the y-direction and then displaced in the x-direction. The displacement is imposed in 4 time steps for both the ID and RD phases. Two types of simulation are being performed. Firstly, a constant displacement of $2 \cdot d_o$ with a variation in relaxation time of 1000s - 4000s is simulated from the start of the ID phase to the end of the RD phase. Then, a constant relaxation time of 2000s with a variation in displacement of $2 \cdot d_o \cdot D_f$ is simulated, in which $D_f$ is varied from 0.8 - 1.0, from the start of the ID phase to the end of the RD phase. $D_f$ stands for the displacement factor, which is a percentage of the total displacement to create a mirror image. Again, $d_o$ is 2mm. To solve the iterative numerical scheme Ansys utilized the Newton-Rhapson method.

### *B. Experimental Validation Linear Guide*

Validating the numerical model of the linear guide requires a reproduction of the imposed boundary conditions, in the form of an experimental test setup. A combination between an aluminium frame, in

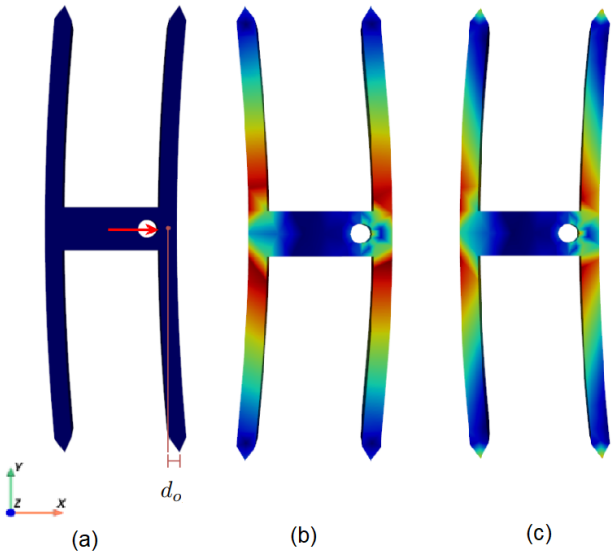


**Figure 2-14:** Numerical model in undeformed state (a), deformed state (b) and final state (c).

which the linear guide is suspended, attached to a heavy base via aluminium profiles and a linear precision stage, attached to a heavy base with a load cell, are utilized to measure the force and displacement during deformation, see figure 2-15. The linear precision stage, M-505.4DG, from Physik Instrumente (PI) is placed in series with a Futek LSB205 load cell. Attached to the load cell is a metal rod with a hook on the end. The linear guide was inserted into a solid aluminium block, the frame, with v-shaped grooves, in order to emulate the pinned constraints from the simulation (solely rotation around the contact line). The frame is slightly, ~0.1mm, shorter than the linear guide in order to ensure contact throughout the full displacement. The frame was elevated using aluminium extrusion profiles in order to align with the PI stage. The hook protruding from the load cell is inserted into the hole in the middle of the linear guide. During a displacement of the PI stage, the force-deflection curve of the linear guide can now be measured.

The experiments for the linear guide include, in the same fashion as the simulation, a variation in relaxation time, from 1000s to 4000s, and a variation in displacement, of $2 \cdot d_o^* \cdot D_f$ with a $D_f$ of 0.8 - 1.0. In the experiments, $d_o^* = 3mm$ will be used, as there was a large discrepancy between results from tests with $d_o = 2mm$ and the simulation. It is good to note that the mechanism is oriented so that the PI stage pulls during the ID phase. The precision stage has a speed of 0.5mm/s, so in the time tests 12s are needed to abridge the 6mm ($2 \cdot d_o^*$) displacement and in the displacement tests 10.8s and 9.6s to abridge 5.4mm and 4.8mm displacements, respectively.

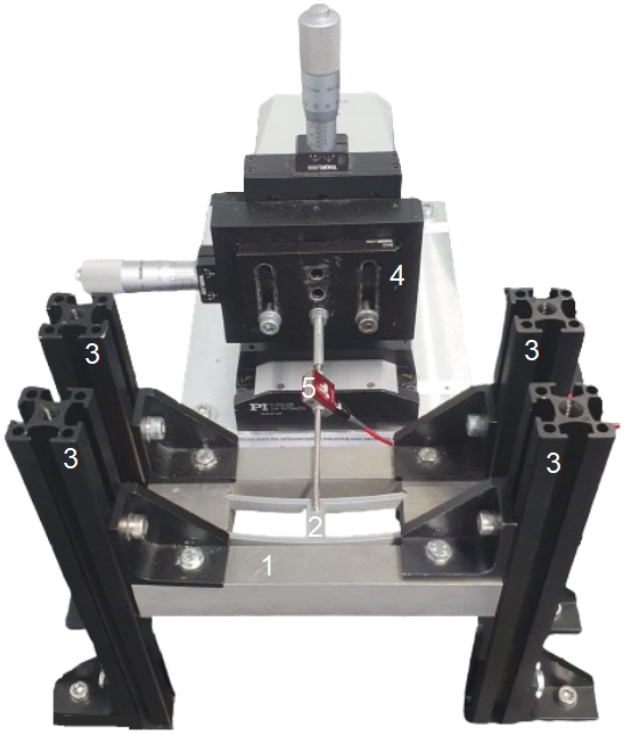


**Figure 2-15:** Linear guide testing setup with aluminium frame (1), linear guide mechanism (2), aluminium extrusion profiles (3), precision stage (4) and load cell (5).

The linear guide prototypes have been modelled using the Solidworks 2023 CAD software, and manufactured from polylactic acid (PLA) using the Prusa i3 MK3S+ fused deposition modelling (FDM) printer, using a 90% infill. The frame which constrains the linear guide has been watercut out of aluminium.

### C. *Numerical Model Helicoid*

The geometry of the helicoidal shell was drawn using Solidworks 2023, and imported in Ansys Mechanical APDL 2022 R2, using the Parasolid command. Again, a static structural analysis was performed on the geometry. For numerical efficiency purposes, the helicoid's numerical model has been reduced to a single flange, instead of the 6-flanged physical sample. The geometry adapts a four node SHELL181 element type. Due to the high levels of deformation in the material, a different material was chosen for the helicoid with regards to the linear guide. The material properties therefore differ from the ones of the linear guide, see table 2-2. The same material model as before with different parameters, linear elastic combined with viscoelastic, has been utilized in this simulation. The tensile test data for the Prony series has been gathered from the same type of test as in the linear guide's model. The Young's modulus (E) and poisson ratio (v) have been adopted from Radaelli's paper [12], since the helicoid has been made at the same manufacturer using the same material and manufacturing process. The WLF shift function data has been found in the literature [20]. In the same fashion as for the linear guide, a curve fit has been made on the literature data to acquire the shift function constants, see figure 2-16.

**Table 2-2:** Material properties helicoidal shell

| Parameter | Value | Unit |
|---|---|---|
| E | 1.8e9 | Pa |
| v | 0.38 | - |
| refT | 20 | °C |
| C1 | 60 | - |
| C2 | 280 | °C |
| $\alpha_0$ | 0.9 | - |
| $\alpha_1$ | 0.85 | - |
| $\alpha_2$ | 0.71 | - |
| $\alpha_3$ | 0.63 | - |
| $\alpha_4$ | 0.55 | - |
| $\alpha_5$ | 0.508 | - |
| $\tau_1$ | 10 | s |
| $\tau_2$ | 1.00e2 | s |
| $\tau_3$ | 1.00e3 | s |
| $\tau_4$ | 1.00e4 | s |
| $\tau_5$ | 2.40e4 | s |

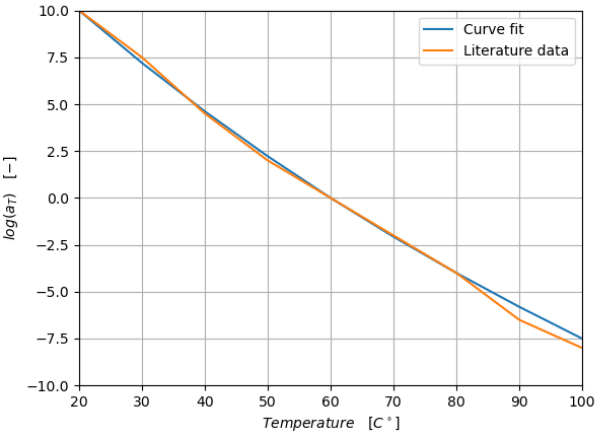


**Figure 2-16:** WLF shift function Nylon (PA12) curve fit versus data from the literature [20].

In the simulation shown in figure 2-17, the line at the far end on the left (green) is constrained in all degrees of freedom (DoF)s. The line on the far end

of on the right (red) is constrained in translation along the x- and z-axis, and in rotation around the x- and z-axis. The symmetry axis (blue) is constrained in rotation around the x-axis and z-axis. A body force load in the form of a temperature of 18°C, has been applied to all nodes. A distorting moment has also been applied near the top line (double arrow) in order to initiate buckling at a specific location. In the physical model this occurs as well due to manufacturing asymmetries. Not including the buckling moment would result more simulation difficulty due to the arising of a singularity. In ~10 time steps, the top line (red) is rotated around the symmetry axis (blue), held for a specific relaxation time, and rotated back, again in 10 time steps. Similar to the linear guide, the helicoid has been simulated for a variation in time and a variation in angular rotation, also referred to as twist. The time variation test was performed for relaxation times from 1000s to 4000s, whilst keeping the rotation at a twist factor, $t_f$, of 1.0, which equates to 360°, or exactly mirrored around the symmetry axis. The twist variation tests were all performed at a relaxation time of 2000s, varying the total twist by $t_f \cdot 360°$, in which $t_f$ is a percentage of the exact mirrored amount, from 0.95 to 1.05.

### D. Experimental Validation Helicoid

In order to validate the numerical results of the helicoidal shell model, a torque test has been performed utilizing a rotating clamp, attached to a cardan axis in which a helicoid is clamped, attached to a PLA block which is attached to a stationary load cell, see figure 2-18. The hardware includes a ZwickRoell torque test and tensile test bench combination with a HBM T20WN load cell.

The experiments for the helicoid include, again to mimic the simulation, a variation in relaxation time, from 1000s to 4000s, while keeping the rotation at ·360°, and a variation in $t_f$, $0.95 - 1.05$, while keeping the relaxation time at 2000s. The upper clamped part, attached to the cardan axis, is rotated around its longitudinal axis in the ID phase, held during the relaxation phase and then rotated back in the RD phase. The torque bench rotated the upper attachment with an angular speed of 36°/s.

The helicoid prototypes have been modelled using the Solidworks 2023 CAD software, and are manufactured from PA12 using a multi jet fusion (MJF) printer. The reason for using PA12 is that it has a very high elongation before yield, meaning that even for large deformation the material behaves (visco)elastically.

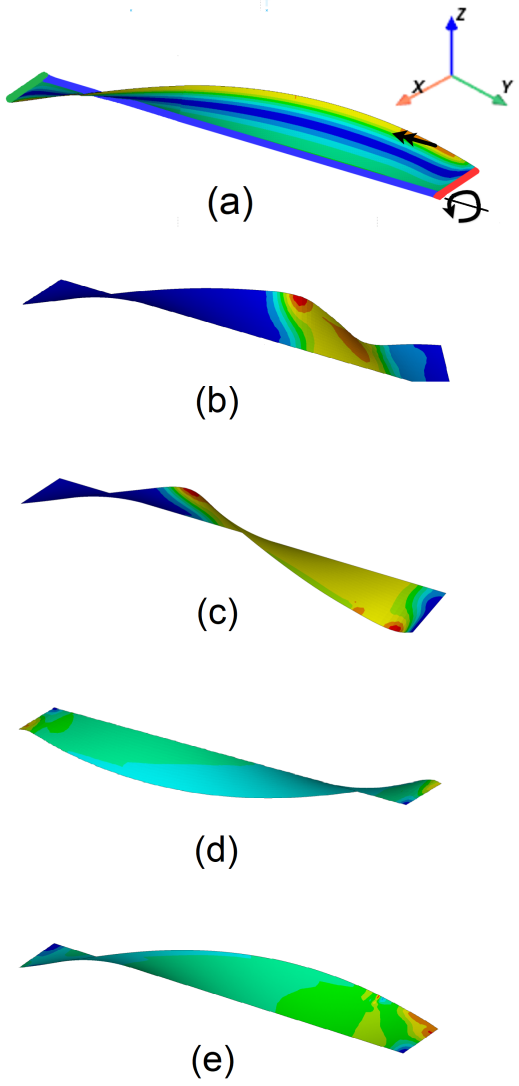


**Figure 2-17:** Helicoidal shell simulation fully undeformed (a), to partially deformed (b)(c), to fully mirrored (d) and back (e).

## IV Results

In this section, the experimental results are presented to see if, firstly, the tested mechanisms indeed do become neutrally stable. And secondly, to gauge the predictive value of the numerical simulation. The results are presented in the form of force-deflection curves, for both the time test and deflection test, which include both the numerical and experimental results. In each of the subsections, the results of the tests and simulations, for that specific mechanism, will be addressed. Where necessary, discrepancies between simulation and experiment will be clarified. In short, after this section it will be clear if both relaxation time and the increase in stress levels by means of deformation, regardless of type of stress, will result in a higher degree of stress relaxation. It is again good to note that temperature is not directly taken into account as a testing variable, but merely as a model param-

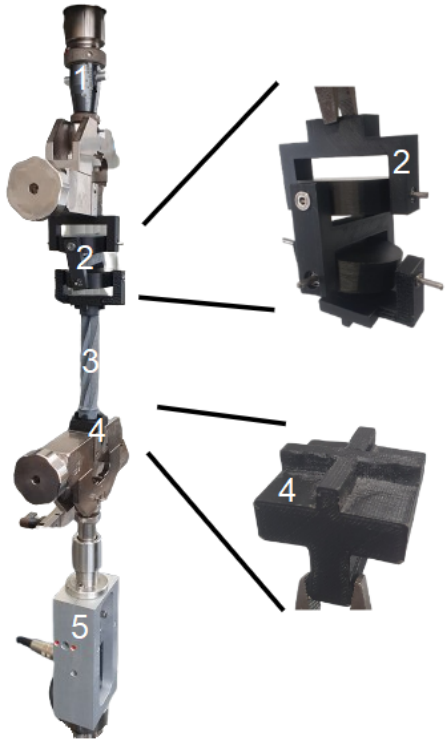


**Figure 2-18:** Torque test setup with rotating clamp (1), attached to cardan axis (2), clamped to helicoid (3), on top of a PLA block (4) in a clamp attached to a load cell (5).

eter taken from the environment. Performing an experiment in which the temperature could be varied would require a more sophisticated experimental setup with a climate chamber.

### A. *Linear Guide: Time*

Figure 2-19 shows the force-displacement diagram as measured using the setup as given in section III.B. and the numerical model as described in section III.A.. An obvious discrepancy is immediately noted: the numerical model predicts a force-displacement diagram in which the displacement is almost exactly $\frac{2}{3}$ of that of the experiment. As mentioned in section III.B., a correction on $d_o$. In an attempt to show the close resemblance between a scaled version of the numerical model and the experimental results, a correction factor of $d_o = \frac{d_o^*}{1.5} = 2mm$ has been applied to the experimental model's displacement values, see figure 2-20. As can be seen in the figure, the numerical model and the experimental results now match quite well. The discrepancy presented here holds for all experimental results of the linear guide, hence it is to be noted that all deflection values in the experimental data are scaled by the correction factor. Zooming in on this figure shows that the scaled version of the experimental data reasonably resembles the numerical model during both the RD phase, see figure 2-21.

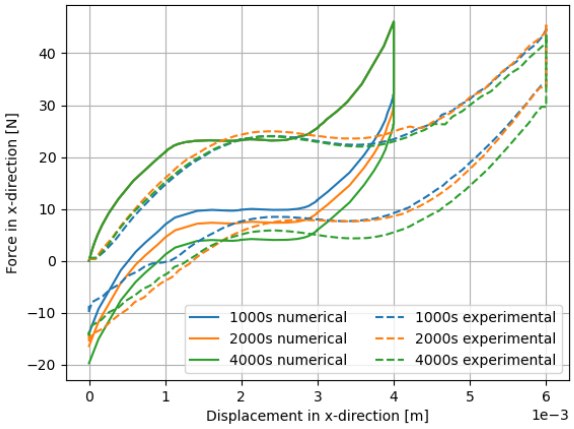


**Figure 2-19:** Uncorrected force-deflection curve linear guide for a variation of time.

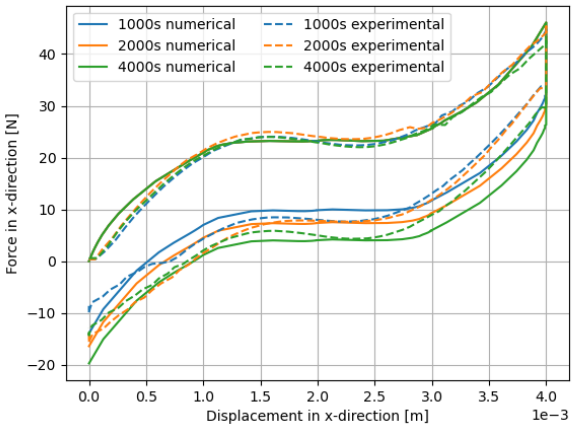


**Figure 2-20:** Corrected force-deflection curve linear guide for a variation of time.

Taking only into account the measured data from the aforementioned figures, it is visible that as predicted, with an increase in relaxation time comes an increased drop off of the level of force in the zero-stiffness part of the RD phase of the movement. The force difference between the ID and the RD phase for a relaxation time of 4000s, is $\frac{F_{back}}{F_{forth}} = \frac{5.0N}{23.0N} = 0.22$.

This shows that the linear guide can indeed be made neutrally stable using the SRPS method. At 4000s the force at the the zero-stiffness portion of the movement was reduced by close to a factor 5.

### B. *Linear Guide: Displacement*

Next to varying time as a parameter to influence relaxation of the mechanism, the displacement in the

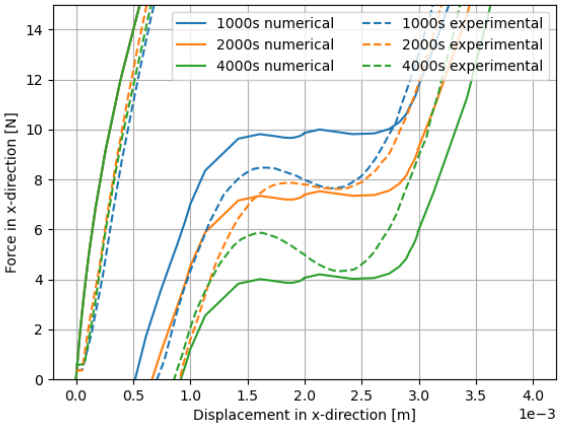


**Figure 2-21:** Corrected and zoomed force-deflection curve linear guide for a variation of time.

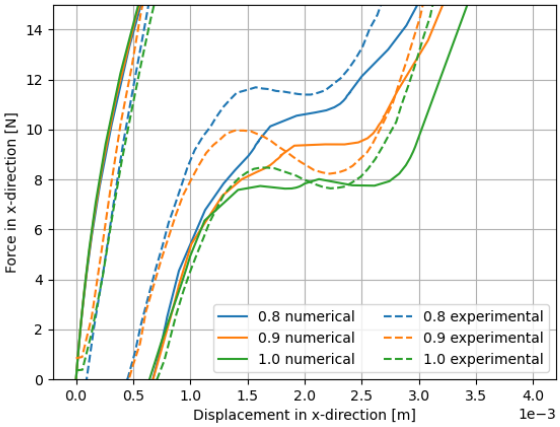


**Figure 2-23:** Corrected and zoomed force-deflection curve linear guide for a variation of displacement.

x-direction was considered as a means of increasing stress. The reasoning behind this was that as mentioned, an increase in stress levels, increases the amount of polymer fibres that become mobile and thus increases the amount of relaxation. In figure 2-22, the numerical data versus the measurements have been shown in a force-displacement diagram, again scaled. It can be seen that again, the models match quite reasonably, but especially on the zoomed version, figure 2-23, there is a visible difference. The slope of the force-displacement diagram on the way back, in the model, seems to become slightly more resembling of a classic snap-through buckling beam. That is, in the model, the force deflection curve during the RD phase from a $D_f$ of 0.8-1.0 becomes decreasingly sloped, whereas in the experiment seems unaffected.

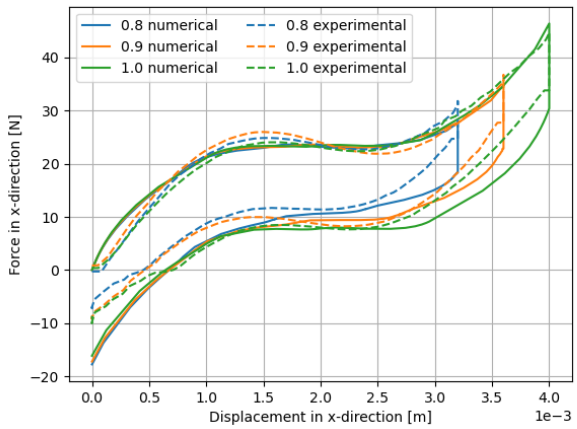


**Figure 2-22:** Corrected and zoomed force-deflection curve linear guide for a variation of displacement.

The measurements seem to not match the model as closely as just varying time would, but it seems as if increasing the amount of displacement does increase the level of relaxation in the mechanism. Adding an increase of displacement on top of the prescribed relaxation time is therefore seemingly a valid tactic for speeding up the process of shifting the ZS line in this mechanism.

### C. *Helicoidal Shell: Time*

The experimental results of the varying time test of the helicoid can be found in figure 2-24. As can be seen in the figure, the model and the experiment match relatively closely, but the height of the second peak on the ID phase seems to be lower in the measured samples. In a zoomed version of the previous figure, figure 2-25, a close match between the numerical and experimental data can be observed. Thus, for a variation in relaxation times, the numerical model for the helicoidal shell seems to be a good predictor of the stress relaxation behaviour when the helicoid is deformed.

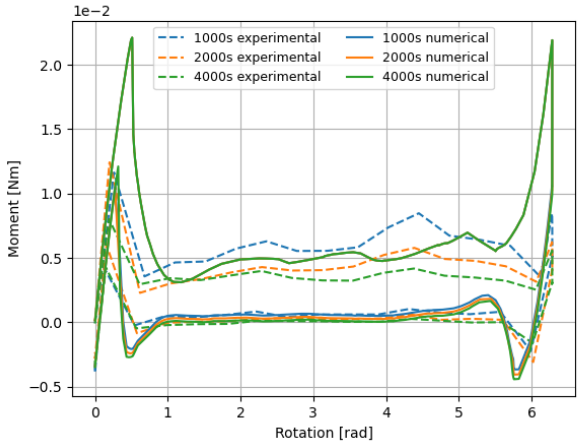


**Figure 2-24:** Moment-angular deflection curve helicoidal shell for a variation of time.

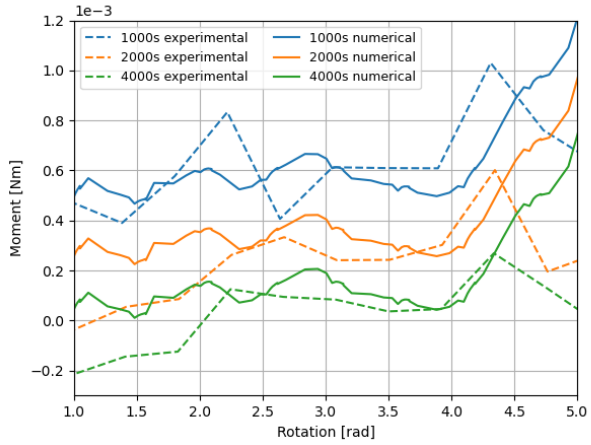


**Figure 2-25:** Moment-angular deflection curve helicoidal shell for a variation of time.

Besides the close match between theoretical and physical results, it is clear as well that there is a major difference in reaction torque between ID and RD phase. For a relaxation time of 4000s, the torque level in the ZS region of the RD phase is a fraction $\frac{M_{back}}{M_{forth}} = \frac{0.1Nmm}{4.0Nmm} = 0.025$ of the torque in the ID phase. Thus, the constant moment-level during the RD phase is reduced by about a factor 40. This model is therefore indeed capable of predicting the required time to make the helicoidal shell mechanism neutrally stable.

The result of this experiment can also be witnessed physically, see figure 2-26, in which the helicoidal shell mechanism no longer has a preferred configuration.

### *D. Helicoidal Shell: Twist*

The data displayed in this section is that of the twist-varying tests for the helicoidal shell. The twist factor has been varied, at a constant relaxation time of 2000s, from 0.95 - 1.05. The results of this series of tests can be found in figure 2-27, in the form of a moment-angular deflection curve. The ID phase seems to reasonably follow the simulation results. The RD phase, seems like an even better match. Taking a look at 2-28 it can bee seen that a variation in the twist angle seems to have limited effect in the lowering of the force deflection curve on the way back.

A thing to note is that the temperature on this test day was higher than the other test days. Hence all values of the RD phase lie below the 0Nmm value.

## V Discussion

This section will reflect on the results of section IV. Some limitations to this research will be addressed along with a list of recommendations for future research. To start of, both the linear guide and helicoidal shell, with zero-stiffness behaviour for completely different reasons, have been made neutrally stable using the SRPS method. It is clear from the test results that increasing relaxation time results in a further shifted force level in the RD phase. An explanation for this would be that since the monomers have a longer time to untangle and shear, the level of relaxation will increase. Increasing the stress levels in the mechanism by overstretching or overtwisting the mechanism is however still disputed. In the linear guide, it seemes as if increasing the displacement from a $D_f$ of 0.8 to 1.0 results in a higher degree of relaxation. In the helicoidal shell, this shift is not as clear. It may be due to the fact that the linear guide was not stretched beyond its mirrored position by increasing the $D_f$ to values of >1. This was not possible due to the force limits on the precision stage. It can however not be claimed that the direction of the stresses (tension or compression) has no significant impact on the way in which the deformed mechanisms relax. Another reason that overstretching or overtwisting might be a valid method for increasing the relaxation in zero-stiffness examples is that the symmetry can be compromised. When overstretching, the linear guide will look increasingly c-shaped. When overtwisting, the helicoid will have an increased pitch angle and shorter flanges.

The model for the linear guide and the helicoid seem to reasonably match the test results, albeit for the linear guide with a correction factor applied to the linear displacement. There is however a mismatch between the simulation and experiment for the linear guide. Some reasons for this discrepancy have been thought of, but none were conclusive. Firstly, displacing the linear guide too much might induce a lot of bending and therefore a loss of contact with the v-grooves, invalidating the emulation of a pinned connection. Shortening the frame might also have pronounced the C-shape of the linear guide in a way that in its travel will exceed the prescribed 4mm. A comparison of the software to the hardware of the precision stage has also been done to see if there was no software issue. Furthermore, the grooves in the frame might be too narrow, resulting in a loss of contact when over-displaced. A misalignment between the precision stage and the linear guide might have resulted in the measurement of a component of the force of the linear guide

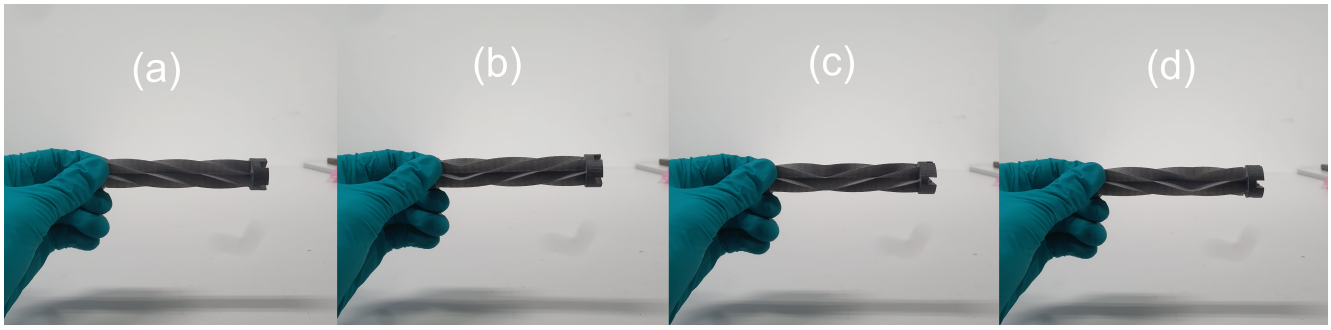


**Figure 2-26:** Neutrally stable helicoid in multiple positions.

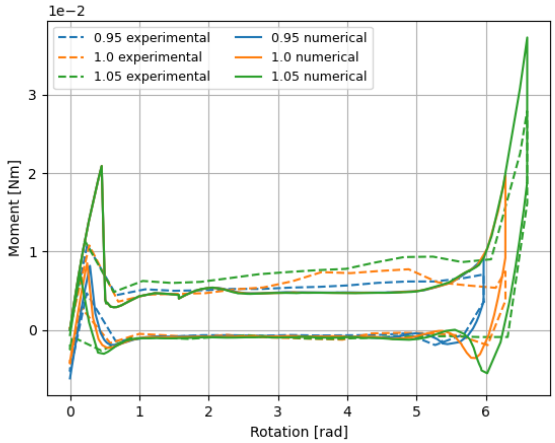


**Figure 2-27:** Moment-angular deflection curve helicoidal shell for a variation of twist.

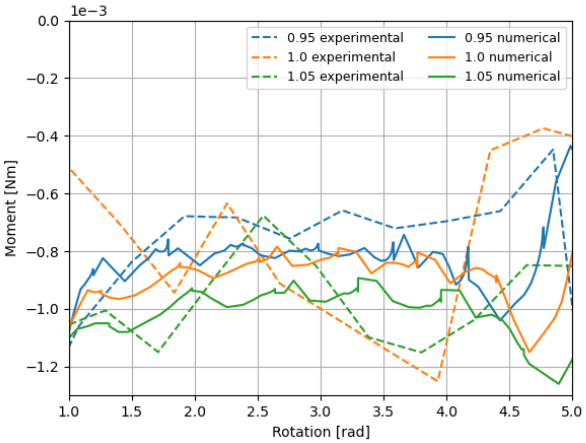


**Figure 2-28:** Moment-angular deflection curve helicoidal shell for a variation of twist.

instead of the full force of the linear guide, creating a more spread out displacement path. Finally, an asymmetric shrinkage of the 3D print material might have resulted in a more pronounced C-shape of the guide as well, creating the same issues as an increase in $d_o$.

### A. *Limitations*

One of the limitations of this research is the fact that the Prony series data is limited. As mentioned before, a test setup in which the test temperature could be controlled was too complex for the purposes of this research. As a result, the Prony series data could only be gathered for a single temperature, a room temperature of 18°C. Recalling the WLF, a slight increase in temperature at deformation can lead to a major increase in stress relaxation. If the experiments are to be done on a day warmer than about 25°C, the accelerated relaxation would saturate the simulation.

Another important point to make that is only implicitly addressed is the fact that all experiments and simulations take a finite amount of time to perform, ergo strain rate was not taken into consideration. The amount of time steps it took to complete the simulations was mostly dependent on the convergence needs and not precisely the same as in the experiment. This might lead to some slight deviations in the results.

The final point to make here is the fact that only two types of ZS mechanisms have been tested. There might be a specific example of a ZS mechanism in which the SRPS method does not work. A more extensive research on classifying ZS mechanisms and their ability to be made NS using this method should be done to emphasize the claims from this work.

### B. *Recommendations*

To give some leads for further research concerning the use of stress relaxation for prestressing, a few suggestions will be made. Firstly, investigation of the potential of metals instead of polymers is recommended. Using polymers in this study was mostly done for the practicality of viscoelastic behaviour at room temperature. Metals only exhibit this behaviour at a when being stressed at high temperatures [21]. What this means is that if the SRPS method is applied for metals at a high temperature,

letting it relax at this temperature, and the metal cools down again to room temperature, the neutrally stable behaviour might be eternalized. This would expand the practical use of compliant mechanisms tenfold.

Another idea comes from the simulation of the linear guide, varying the displacement. It could be seen, in simulation, that increasing the $D_f$ lead to an increasing undulating shape of the RD phase. If indeed this is possible, then not only ZS compliant mechanisms can be subjected to the SRPS method to create neutrally stable mechanisms, but most snapping mechanisms. If the linear guide was deformed far beyond its mirrored configuration, it would get more of a C-shape, emphasizing its snapping behaviour during the RD phase. If the ID phase of the deformation now however would be more of a straight line due to lack of curvature or high thickness, the increase of undulating shape during the RD phase might compensate and make the mechanism neutrally stable. In other words, if both the symmetry deformation condition and the zero-stiffness condition are dropped, the SRPS could be extended to still make mechanisms neutrally stable.

An improvement on this research would be finding out if a v-groove linear guide setup can be improved upon. Scaling the mechanism up would diminish the influence of manufacturing tolerances, but the load cell would have to be rated for a higher force as well.

A further expansion of this research logically would be to do the mentioned types of tests for a different temperature. The choice of what polymer to use would then not be limited to the glass transition temperature of the material.

## VI Conclusion

In this work a novel prestressing method was presented to create neutrally stable mechanisms from complex monolithic structures. The broad group of compliant mechanisms for which this method would be viable needs only to have a zero-stiffness region in its intended deformation direction along with the ability to configure as a mirror image of its original configuration in this deformation direction.

The results section compares the numerical simulation and experimental results of the linear guide and helicoidal shell. It was clear that in both the linear guide and the helicoidal shell, neutral stability could be achieved by extending the relaxation phase of the SRPS method. An increase in displacement for the linear guide also works as a catalyst for the relaxation, whereas for the helicoidal shell this is inconclusive.

## Bibliography

[1] M. Schenk and S. D. Guest, "On zero stiffness," *Proceedings of the Institution of Mechanical Engineers, Part C: Journal of Mechanical Engineering Science*, vol. 228, no. 10, pp. 1701–1714, 2014.

[2] T. Murphey and S. Pellegrino, "A novel actuated composite tape-spring for deployable structures," in *45th AIAA/ASME/ASCE/AHS/ASC Structures, Structural Dynamics & Materials Conference*, p. 1528, 2004.

[3] L. L. Howell, S. P. Magleby, B. M. Olsen, and J. Wiley, *Handbook of compliant mechanisms*. Wiley Online Library, 2013.

[4] K. A. Seffen and S. D. Guest, "Prestressed morphing bistable and neutrally stable shells," 2011.

[5] R. S. Lakes, *Viscoelastic materials*. Cambridge university press, 2009.

[6] S. P. Marques and G. J. Creus, *Computational viscoelasticity*. Springer Science & Business Media, 2012.

[7] R. Roy and L. Qi, "Stress relaxation study of paper and plastic film based packaging material," 2009.

[8] W. Harris, R. Kohrumel, and D. C. C. M. M. P. DEPT, "Calculating creep and stress relaxation from long term data," 1992.

[9] C. Henderson, "The application of boltzmann's superposition theory to materials exhibiting reversible $\beta$ flow," *Proceedings of the Royal Society of London. Series A. Mathematical and Physical Sciences*, vol. 206, no. 1084, pp. 72–86, 1951.

[10] Y. Lou, Q. Lei, and G. Wu, "Research on polymer viscous flow activation energy and non-newtonian index model based on feature size," *Advances in Polymer Technology*, vol. 2019, no. 1, p. 1070427, 2019.

[11] S. Palathingal and G. Ananthasuresh, "Design of bistable arches by determining critical points in the force-displacement characteristic," *Mechanism and Machine Theory*, vol. 117, pp. 175–188, 2017.

[12] G. Radaelli, "Reverse-twisting of helicoidal shells to obtain neutrally stable linkage mechanisms," *International Journal of Mechanical Sciences*, vol. 202, p. 106532, 2021.

[13] L. Lee, "Creep and time-dependent response of composites," in *Durability of Composites for Civil Structural Applications*, pp. 150–169, Elsevier, 2007.

[14] J. S. Bergstrom, *Mechanics of solid polymers: theory and computational modeling*. William Andrew, 2015.

[15] M. Grasso, L. Azzouz, P. Ruiz-Hincapie, M. Zarrelli, and G. Ren, "Effect of temperature on the mechanical properties of 3d-printed pla tensile specimens," *Rapid Prototyping Journal*, vol. 24, no. 8, pp. 1337–1346, 2018.

[16] J. Ferry, *Viscoelastic Properties of Polymers*, vol. 264. Wiley, 1980.

[17] S.-H. Chae, J.-H. Zhao, D. R. Edwards, and P. S. Ho, "Characterization of viscoelasticity of molding compounds in time domain," in *International Electronic Packaging Technical Conference and Exhibition*, vol. 43598, pp. 435–441, 2009.

[18] M. T. Shaw and W. J. MacKnight, *Introduction to polymer viscoelasticity*. John Wiley & Sons, 2018.

[19] H. Chen, Z. Pan, D. Yuan, G. S. Sulley, R. N. Oosterbeek, C. K. Williams, and L. Brassart, "Shear yielding and crazing in dry and wet amorphous pla at body temperature," *Polymer*, vol. 289, p. 126477, 2023.

[20] H. Amel, *Investigating the Cyclic Performance of Laser Sintered Nylon 12*. PhD thesis, University of Sheffield, 2015.

[21] M. Kassner, *Fundamentals of creep in metals and alloys*. Elsevier/Academic Press, 2015.

# Appendix A

# Literature study

# Abstract

This paper consists of two chapters. On the one hand an overview of the modelling of creep and viscoelasticity in compliant mechanisms is given. The paper starts with basic concepts such as viscous dampers and Hookean springs and progresses to integer order derivative and integral models, and even fractional order models. It is advised for most applications to use the Prony series to curve fit data for a specific relevant time range. Considerations such as whether the model should be combined with a hyperelastic model are also addressed.

The second part of this paper is a literature survey on the application of elastic, plastic and viscoelastic prestress as a means of generating bistability, multistability or neutral stability in compliant mechanisms. For each category a few examples are given, except for the regions in which no literature has been found. It is shown that in for elastic bistability and multistability, buckling is one of the most common used phenomena. For elastic neutral stability, the mechanisms are fabricated in a way that deformations cancel eachother. For plastic bistability and multistability, manufacturing techniques such as rolling are often involved in altering the Gaussian curvatures of structures. Thermal stresses are also a significant contributor to plastic bistability and multistability in composite laminates due to a discrepancies in expansion coefficients. Only a few examples for viscoelastic bistability have been found, two of which were only temporarily stable. No viscoelastically prestressed multistable of neutrally stable mechanisms have been found. Theoretically, these structures should be possible however.

# Table of Contents

# Chapter 1

# Acknowledgements

This literature survey is written in the template of Delft Center for Systems and Control (DCSC).

Delft, University of Technology M. Blaakman
October 9, 2024

# Chapter 2

# Creep and Stress relaxation

## 2-1 Introduction

In this chapter the concepts of creep and viscoelasticity will be discussed. Creep is the more relevant term when dealing with metals and viscoelasticity better encapsulates the behaviour of polymers. In this chapter, first some fundamental concepts will be addressed along with some simple models describing these concepts. Secondly, the underlying mechanisms of creep will be explained. Both metallic and polymeric creep will be discussed, be it more briefly for metals since metals are a bit simpler in their creep dynamics. Thirdly, an introduction to viscoelasticity and hyperelasticity will be given. The basic existing models will be explained and their limitations will be addressed. All of the information given here is in the context of modelling compliant mechanisms.

## 2-2 Basic Mechanical Concepts

In this section the two main concepts for getting a feeling for viscoelastic behaviour, creep and stress relaxation are given: Hookean elasticity and Newtonian viscosity. These concepts lay the foundation for the understanding of viscoelastic behaviour and most simple models describing this behaviour.

### 2-2-1 Hookean Elasticity

The Hookean model describes a 1D linear-elastic spring which when extended by an applied force F, has an instantaneous elongation u, which scales dependent on the spring constant k. This is called Hooke's law. The governing equations for the force necessary to provide a required elongation are given as follows:

$$F = k \cdot u \tag{2-1}$$

The stress-strain relationship is given as:

$$\sigma = E \cdot \epsilon \tag{2-2}$$

In this equation E is the Young's modulus of the material and $\epsilon$ is the strain of the spring. Do note that even though u and $\epsilon$ have a different symbol, they represent essentially the same deformation of a linear spring. However, the strain is the normalized or called relative deformation, with regard to a reference point or datum, and displacement is the absolute deformation with regard to that same reference. This model assumes that an instantaneous displacement results in an instantaneous force. It is therefore incapable of modelling time-dependent material behaviour.

### 2-2-2 Newtonian Viscosity

Viscosity is the resistance of a fluid to deformation and flow. In the most simple case one could compare the pouring of syrup vs water in a bowl. Syrup would flow less easily than water. We would say that syrup has a higher viscosity. A Newtonian fluid is a fluid in which the amount of force exerted by the fluid is proportional to the velocity with which it gets deformed. Specifically the shear stress-shear velocity diagram would show a constant slope.

In a Newtonian fluid, the governing equation for exerted force by a damper is given as follows:

$$F = c \cdot \dot{u} \tag{2-3}$$

In this equation, c stands for the damping coefficient and $\dot{u}$ is the velocity. The stress strain relationship is given as:

$$\sigma = \eta \cdot \frac{d\epsilon}{dt} \tag{2-4}$$

In this equation $\eta$ is the viscosity of the material, and $\frac{d\epsilon}{dt}$ is the strain rate of the damper. The Newtonian damper model is a time dependent anelastic model. As a result it is unable to describe linear elastic behaviour with its governing equations. In viscoelastic materials, a combination of linear-elastic and viscous behaviour can be seen. This phenomenon will be addressed later on in this chapter, as most viscoelastic models rely foundationally on combining dampers and springs. The schematic model for these components is given in Figure 2-1. On the other hand, creep in metals is often dependent on an Arrhenius type equation involving a measure called activation energy, which describes the energy barrier a material needs to overcome in order to start creeping.

## 2-3 Creep

Creep is essentially the deformation of a material at a constant load, or the decrease of internal stress in a pre-loaded material at a constant deformation. The latter of these two descriptions has also been called stress relaxation. The working principles for these two phenomena are the same [2],[3],[4],[5],[6],[7],[8] and are sometimes used interchangeably [9]. Whilst creep

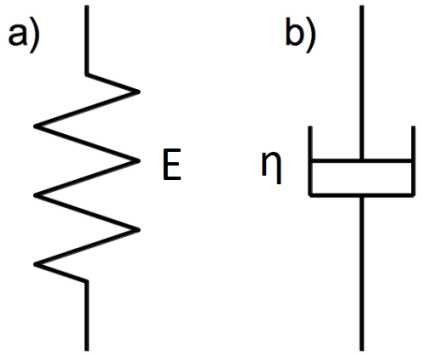


**Figure 2-1:** Hookean spring (a), Newtonian damper (b) [1]

deformation has different microscopic working principles for crystalline, amorphous, composite and aggregate based (concrete) materials, all constitutive models are dependent on time, temperature and load. The key takeaway from the concept of creep, is that the specific point in time at which a material behaves a certain way, is temperature- and stress-dependent, not only for the present, but also in its entire history.

Materials which are typically susceptible to creep and stress relaxation are for example polymers, experiencing material behaviour which can be described as viscoelastic. Viscoelastic material, is a type of material which is highly influenced by the phenomenon of creep. This type of material exhibits viscous, or flow, behaviour as well as elastic behaviour, hence the name. The viscous behaviour of this type of material means that there is a delay in its response when loaded, and that the rate at which the material is loaded influences its reaction. Viscoelasticity also means that there is not a threshold of stress which will cause creeping behaviour. Instead, at any stress level will the material experience some kind of creep deformation. This highly contrasts the creep behaviour of metals, which mostly only starts at a certain temperature in combination a certain stress. More on viscoelasticity can be found in section 2-6.

## 2-4 Time-Temperature-Stress Superposition principle

As mentioned earlier in this chapter, the process of creep is influenced by time, temperature and stress. Whilst the behaviour of the material will always follow the same path in the stress-time plot, the former two of the aforementioned factors will make the strain-time curve shift along the time axis. In other words, both the temperature and the stress on the material will influence over what time range the creep behaviour is seen. This phenomenon is what we call the Time-Temperature-Stress Superposition Principle (TTSSP). In figure 2-2a, the effect of temperature on stress relaxation can be seen and figure 2-2b depicts the effect of stress on creep.

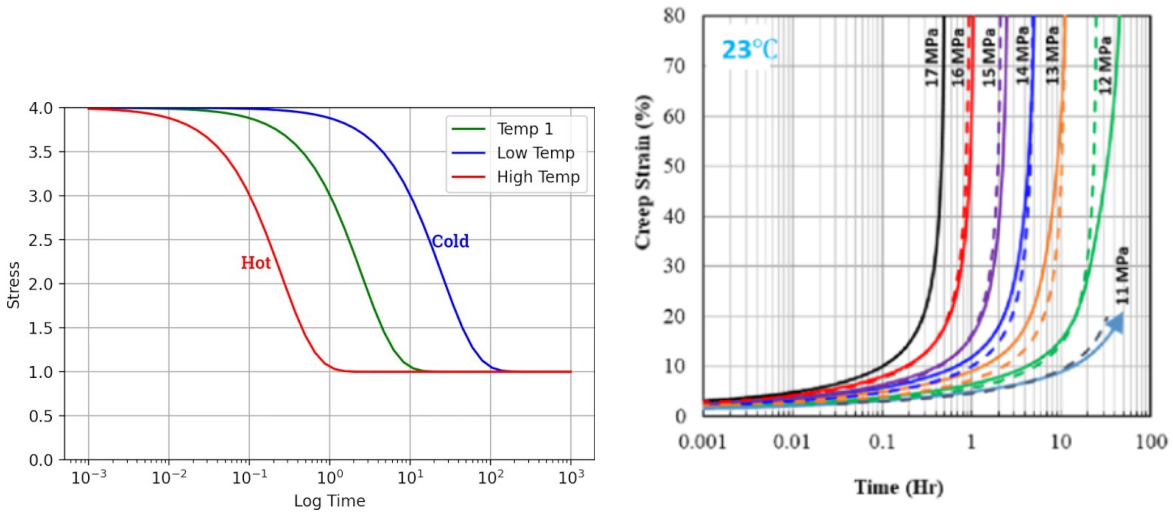


**(a)** Time-Temperature Superposition [10] **(b)** Time-Stress Superposition [11]

**Figure 2-2:** Time-Temperature and Time-Stress superposition separately

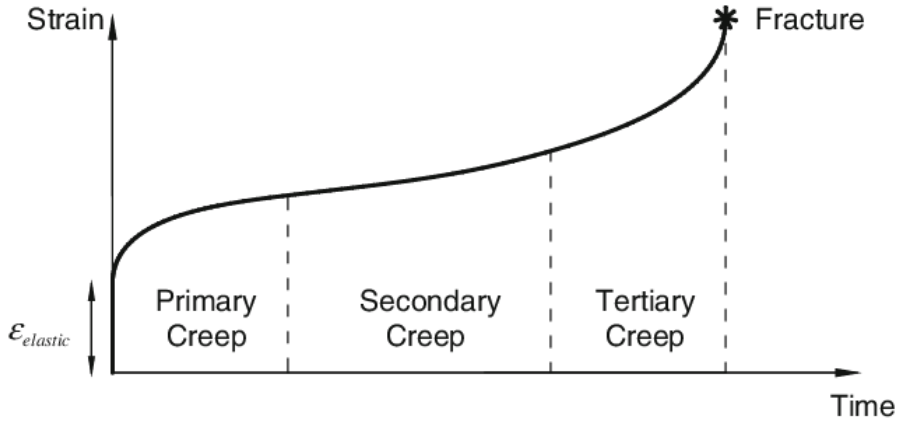


**Figure 2-3:** Strain-time curve for stages of creep [13]

## 2-5 Creep in Metals

Creep in metals in literature is defined as plastic flow at temperatures as low as upward of half the absolute melting temperature of the material [12]. It consists of three different stages, primary, secondary and tertiary creep. In the first stage, the strain rate is decreasing until it reaches a certain constant strain rate. The zone in which this strain rate remains constant is what we call the secondary creep stage. After this stage the strain rate starts to increase again ending in the rupture of the material. For illustration see figure 2-3. In polymers, the same stages can be seen, but different physical mechanisms are at play. More on that can be read in the next section.

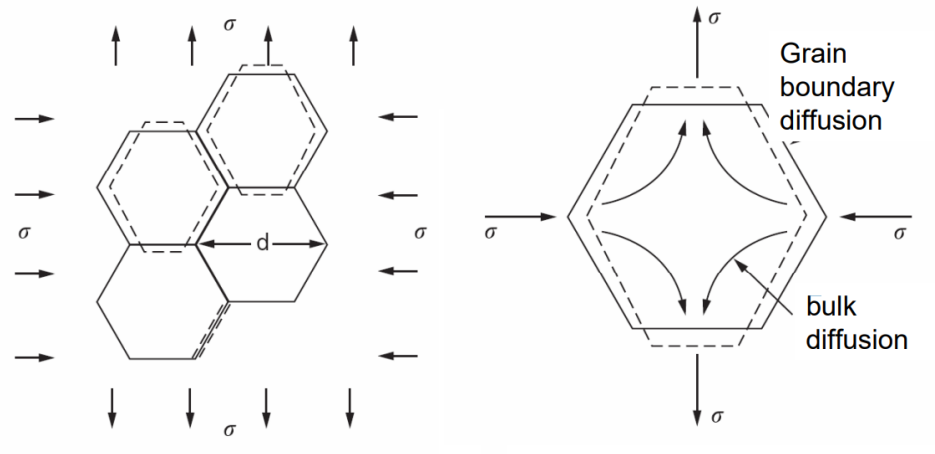


**Figure 2-4:** Overview diffusional dreep mechanisms [15]

### 2-5-1 Creep Resistance in Metals

The strengthening of metals for creep resistance is quite similar to the improvement of general material characteristics. In the book Introduction to Aerospace Materials by Mouritz [14], some methods for improving creep resistance of metals are given. The only added factor when compared to regular strengthening of metals is the temperature resistance. Alloying metals with elements with a high melting temperature drastically increase their creep strength. By introducing alloying element into interstitial sites of crystal lattices, the climb and glide of dislocations is inhibited. Metals which adapt precipitates in their lattice structure have similar improved qualities, especially if the precipitates are once again more stable at higher temperatures. Finally, contrary to the normal strengthening of metals, the increase of grain size can increase the creep resistance of metals which suffer most from grain boundary sliding, due to there being fewer grain boundaries.

### 2-5-2 Diffusional creep

Diffusional creep is the phenomenon in which atoms and vacancies in crystal material lattices move in alignment with an applied load. This form of creep is mostly prevalent at higher temperatures and lower stresses, but it also occurs at a slower rate at lower temperatures. Diffusional creep is subdivided into bulk diffusion and grain boundary diffusion. Bulk diffusion is the movement of vacancies in crystals itself and grain boundary creep is the diffusion of vacancies along the grain boundaries of crystals, see figure 2-4.

#### Bulk diffusion

Bulk diffusional creep, also known as Nabarro-Herring Creep, is the diffusion of atoms in a material at low stress and elevated temperatures. It occurs in both amorphous and crystalline materials. It occurs due to the diffusion of vacancies in a material, from high chemical potential regions, subjected to tensile stress, normal to the material or grain boundaries. The latter obviously only happens in crystalline metals.

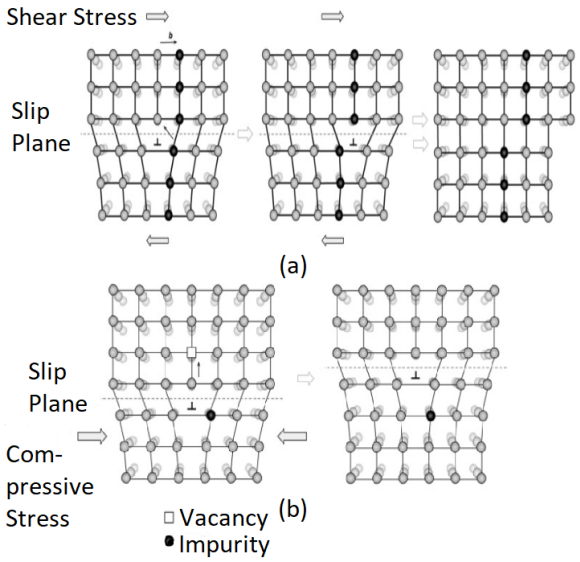


**Figure 2-5:** (a) Glide controlled dislocation creep, (b) Climb controlled dislocation creep [16]

#### Grain boundary diffusion

Whereas bulk diffusion moves vacancies within metal grains itself, grain boundary diffusional creep, also known as Coble creep, describes the movement of vacancies along the grain boundaries due to diffusion. This form of creep is also most prevalent at low stresses and low to medium temperatures.

### 2-5-3 Dislocation creep

Dislocation creep is the movement of dislocations through a crystal lattice. Dislocation creep can either be driven by higher stresses or higher temperatures, or both, dependent on the material structure. Dislocation creep can be subdivided into glide controlled dislocation creep, the slipping of whole planes in a lattice, or climb controlled dislocation creep, in which dislocations can 'climb' over obstacles due to diffusion of vacancies. For a schematic of dislocation controlled creep, see figure 2-5

#### Glide controlled dislocation creep

Glide controlled dislocation creep is the creep planes of atoms in the crystal lattice. If it meets any imperfections such as stray atoms of a different material or other dislocations, the glide plane will not be able to move any further. If this is not the case, such as for very pure materials, it will be easier for a dislocation to shear its way to the grain boundary. Glide controlled creep in metals occurs at highers stresses.

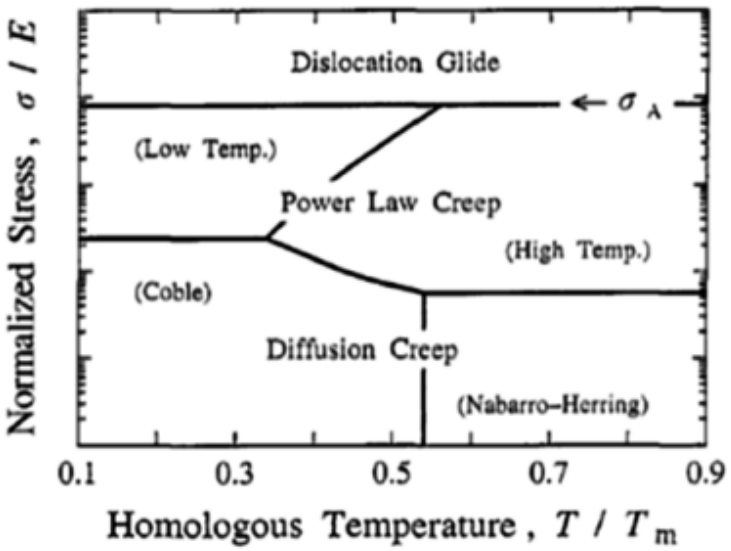


**Figure 2-6:** Deformation mechanism map for a 2.25 Cr-1Mo steel [17]

### Climb controlled dislocation creep

If in glide controlled dislocation creep a dislocations meets an obstacle which impairs it from moving any further, it will stop in its tracks. It can however 'climb' over some obstacles when a vacancy diffuses into the spot where the dislocation is stuck. Do note that this type of creep is thus also influenced by the diffusion of vacancies through crystal structures. This results in climb controlled creep in metals to occur at high stresses and high temperatures.
The main takeaway from this section is that metals do not behave viscoelastic but rather elastic-viscoplastic, meaning that after a certain yield stress, material will start to deform rate-, time-, stress- and temperature-dependently instead of elastically. Before this yield stress, the material will exhibit linear elastic behaviour.

### Power law creep

Power law creep, also referred to as five-power-law creep, is the region inbetween low and high stresses over the full temperature range at which creep occurs. The five stands for the value of the exponent of the stress factor in this creep region. Sometimes power law creep is referred to as dislocation climb controlled creep, but this is not entirely accurate as climb controlled creep dominates in other regions [12]. For an overview of the dominant creep mechanisms for different temperatures and stresses, see figure 2-6. The x-axis represents the normalized temperature, in which $T_m$ is the melting temperature, and the y-axis represents the normalized stress. The boundaries of each region specify what the dominant physical creep phenomenon is under the given circumstances.

## 2-6 Creep in Polymers

Polymeric creep strain is normally viscoelastic. In other words, instantaneous load results in a time dependent deformation combined with instantaneous deformation. When the load is taken away, only a part of the strain can be recovered elastically. This behaviour stems from the structure of polymers at an atomic level. Polymers are made up out of long strands of fibre (monomers). These monomers are randomly (amorphous) or semi-randomly (semi-crystalline) entangled. Next to this entanglement, sometimes the monomers are linked together with what are called covalent bonds. Such polymers are called cross-linked polymers. The covalent bonds are formed by atoms sharing electron pairs with each other, creating a more stable structure. This connection of different stands of monomers is called cross-linking. It gives polymers a higher strength, stiffness and creep resistance [18],[19]. When a load is applied, the bonded monomers are first aligned and untwisted from their random orientation to the orientation of the load (primary creep). As more monomers are fully aligning, the strain rate decreases, until it reaches a steady state in which these monomers stretch elastically and reform covalent bonds or cross-links (secondary creep), see figure 2-7. The internal friction is limiting the ease of movement along with the level of entanglement. If the material is now stretched until the yield strength of the monomers, the strain rate will increase exponentially, as the material starts breaking (tertiary creep). The last phase is called viscoplasicity. If at some point in the steady state regime, before the yield stress, the load is removed (recovery phase), the fibres will still keep having a certain degree of alignment with the initially applied load see figure 2-8. As a result, when releasing the tension, not the full deformation is recovered, see figure 2-9(a). Here it can be seen that for an instantaneous stress, held constant over a prolonged timespan, a level of strain will remain when the stress is removed. This remaining strain in some cases increases the crystallinity of material. The non-recoverable strain in viscoelastic materials is essentially a loss of energy in the system. This dissipative process results increased temperature or generation of sound [20],[21].

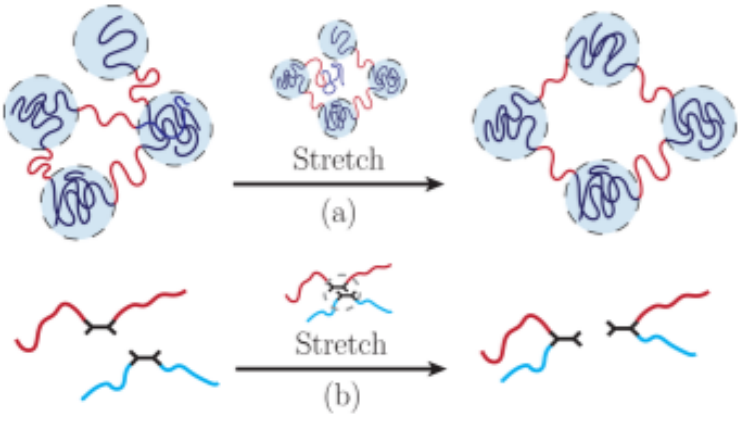


**Figure 2-7:** Reforming of cross-links [22]

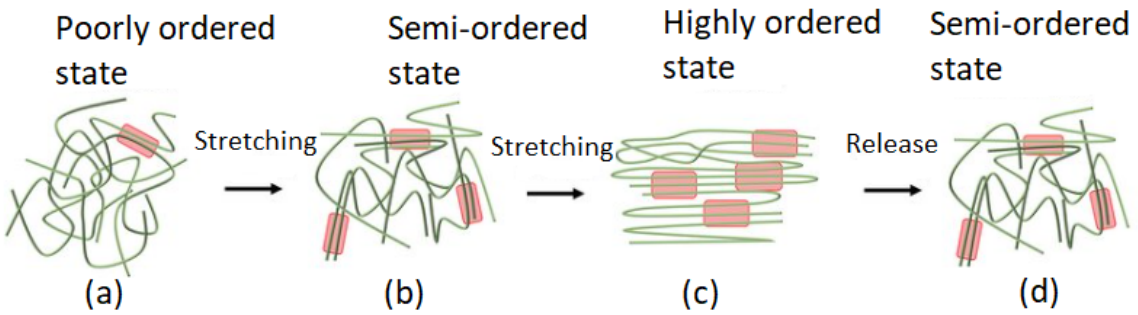


**Figure 2-8:** (a) Randomly ordered state, (b) Loading leads to alignment, (c) Fully aligned, (d) Release of tension [23]

It is important to note that as mentioned for metals, creep and stress relaxation only start to occur after a certain stress level has been imposed, whereas in polymers this happens at any and all imposed stress levels. A second thing to note is the fact that plastic deformation in metals refers to the dislocations of atoms or grains in the material, whereas in polymers plastic deformation refers to the breaking of monomers themselves. Non-recoverable deformation on the other hand is the rearrangement of monomers within the polymer structure. In this sense, non-recoverable deformation in polymers can be seen as plastic deformation in metals and plastic deformation of polymers is the actual breaking of the material.

### 2-6-1 Time Dependent Deformation

As mentioned in 2-3, when a viscoelastic material gets loaded, its response (eg. deformation) is time-dependent, instead of instantaneous. When designing machines this is a factor that highly complicates the design as now not only your actuators have certain performance limitations, but also everything in between the input and output of the the machine will depend on how fast the actuator is moving. This is one of the main reasons why engineering plastics are hardly used structurally (although they are being used).

### 2-6-2 Polymer states

Polymers have essentially two different states of behaviour: The glassy state and the rubbery state. Most polymers behave like rubbers at room temperature. Below a certain temperature, polymers become very stiff and brittle. This is what we call the glass transition temperature. Figure 2-10 shows the young's modulus of amorphous, semi-crystalline and cross-linked polymers versus temperature. Amorphous polymers have randomly ordered polymeric chains, semi-crystalline polymers have amorphous patches but also structured patches of polymeric chains and cross-linked polymers have either

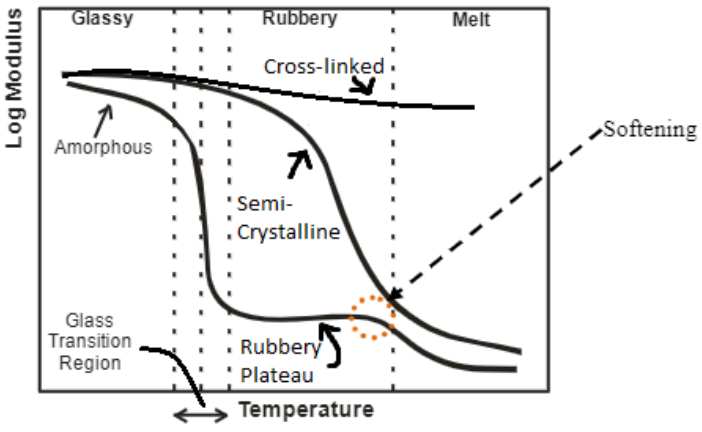


**Figure 2-10:** States rubber [25]

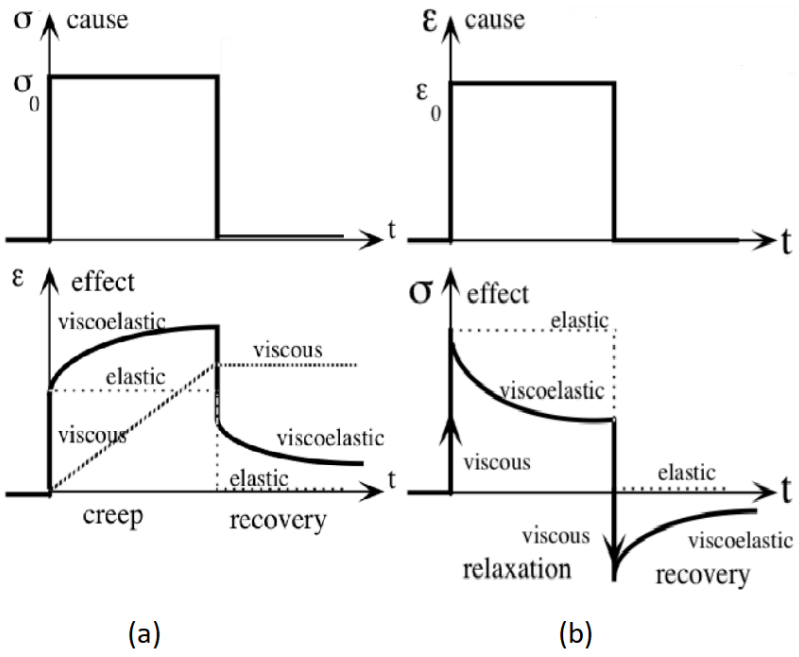


**Figure 2-9:** Viscoelastic creep and stress relaxation response to instantaneous stress (a), viscoelastic creep and stress relaxation response to instantaneous strain (b) [24]

a lot of covalent bonds, or a lot of physical entanglement, or both. Due to evenly spread randomness in the polymeric chains in amorphous material, the glass transition temperature is very steep: all monomers go from reasonably immobile to very mobile in an instant. In semi-crystalline polymers this happens more gradually due to the coexistence of multiple arrangements: crystalline and amorphous structures. The crystalline structures are more resilient to slipping due to the existence of large ordered structures. The same goes for cross-linked polymers. Cross-linking has a significantly higher impact on retaining structural strength than crystallinity however. A better overview of this is given in figure 2-11. In this research we are mainly interested in working with viscoelastic materials which are in the rubbery phase at room temperature, due to their application in compliant mechanisms.

### 2-6-3 Boltzmann Superposition Principle

Many linear models for viscoelasticity rely on what is called the Boltzmann Superposition Principle (BSP). The BSP states that in case that there is a linear relationship between stress and strain, and their time derivatives, that the resulting strain from a combination of stresses is the same as the sum of all strains induced by the individual components of that stress combination [28]. This is a reciprocating phenomenon, meaning that the linear combination of all strains also will result in a linear combination of all stresses induced by this strain, see figure 2-12.

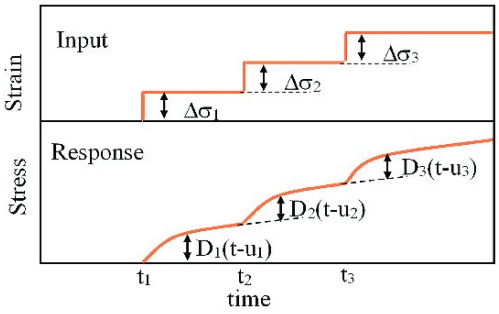


**Figure 2-12:** Boltzmann superposition principle [27]

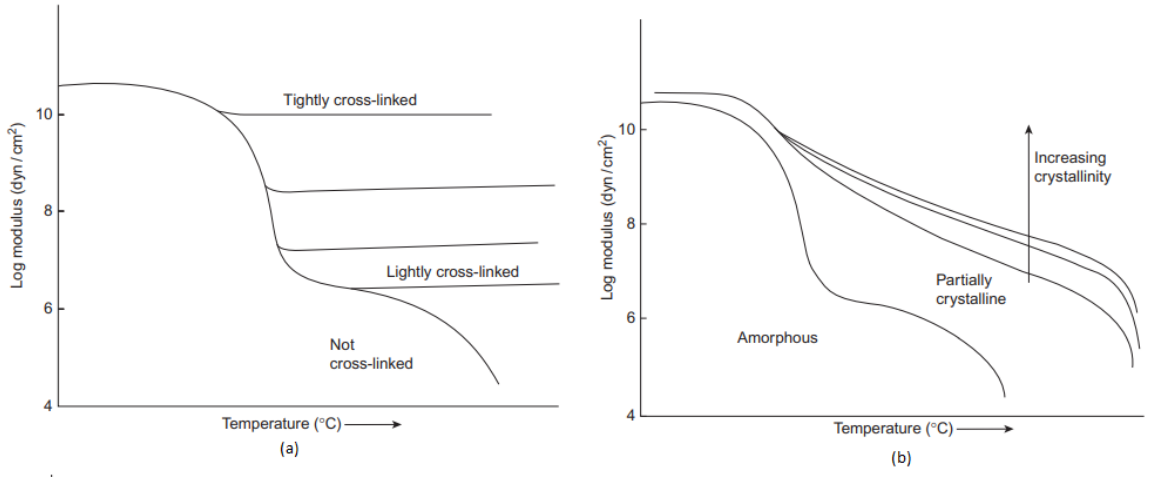


**Figure 2-11:** (a) Infuence cross-linking on Young's modulus, (b) Influence crystallinity on Young's modulus [26]

### 2-6-4 Creep Resistance in Polymers

In the book of Mouritz, as mentioned before, creep of polymers is also addressed. For polymers, creep is reduced by factors which prevent the untangling and aligning of polymeric chains. Two of the main factors reducing creep in polymers are increasing crystallinity and cross-linking. Cross-linking seems like an obvious factor due to the increase of connections within the material preventing sliding and twisting motions. Crystallinity in alignment with the load direction results in the fibres in the lattice structure being elastically stressed, whereas randomly oriented structures also involve untangling, resulting in more non-recoverable strain when loaded.

## 2-7 Derivative Based Viscoelastic Models

In order to describe creep or stress relaxation behaviour of a viscoelastic materials, different models have been created. This section will list the most important models. The use of the most simple derivative based models will be explained, along with the limitations.

### 2-7-1 Maxwell model

As mentioned in section 2-2, most analytical creep models for viscoelasticity are based on a linear Hookean spring and a Newtonian dashpot. The simplest model for viscoelasticity is called the Maxwell model, see figure 2-13(a). This model shows a single spring and dashpot in series. The Maxwell model describes that, in viscoelastic materials, an instantaneous stress does not immediately result in a proportional strain. This is due to the strain being dependent on the time-dependent behaviour of the dashpot. From section 2-2 we gather the stress strain relationships of the individual components.

Due to the series placement of the damper and the spring in the Maxwell model, the stress in the damper is equal to the stress in the spring, but the strains add up, giving the following stress strain relationship:

$$\sigma = \eta(\cdot\frac{d\epsilon}{dt} - \frac{1}{E}\frac{d\sigma}{dt}) \tag{2-5}$$

The simple Maxwell model is not too often used to model creep behaviour, as it only describes the decoupled linear elastic and viscous flow of materials.

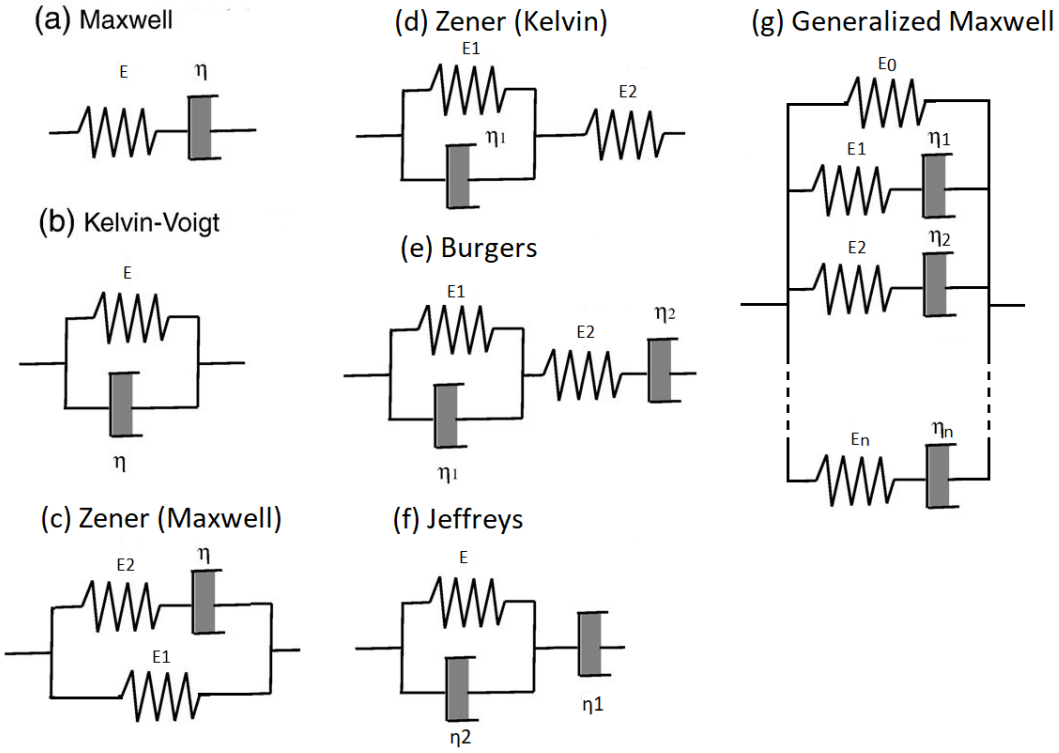


**Figure 2-13:** (a) Maxwell model, (b) Kelvin-Voigt model, (c) Zener model (Maxwell representation), (d) Zener model (Kelvin representation), (e) Burgers model, (f) Jeffreys model, (g) Generalized Maxwell model [29],[30],[31],[32]

### 2-7-2 Kelvin-Voigt model

A model that better describes the coupled viscosity and elasticity is the Kelvin-Voigt model. The Kelvin-Voigt model is similarly simple as the Maxwell model. In is model, a dashpot and a spring are put in parallel, see figure 2-13(b). The Kelvin-Voigt model describes the anelastic part of viscoelasticity. Due to the parallel placement of the spring and the damper, the stresses in each component add up giving a stress strain relationship as follows:

$$\sigma = E \cdot \epsilon + \eta \cdot \frac{d\epsilon}{dt} \tag{2-6}$$

One of the drawbacks is of the Kelvin-Voigt model is its inability to describe the recovery of viscoelastic materials. Recovery is what happens when you load a viscoelastic material for a while, and then suddenly remove the load. This sudden decrease in load normally results in a sudden elastic spring-back movement of the material. The Kelvin-Voigt material however would show a very gradual decrease in strain.

### 2-7-3 Zener model

The Zener model also called the Standard Linear Solid model (SLS), is a model which either places a Maxwell element in parallel with another linear spring (Maxwell representation), figure 2-13(c), or places a Kelvin-Voigt element in series with a linear spring (Kelvin representation), figure 2-13(d). The constitutive stress-strain relationship for the Maxwell and Kelvin representation, respectively, are stated as follows, in dot notation:

$$\sigma + \frac{\eta}{E_2}\dot{\sigma} = E_1\epsilon + \frac{\eta(E_1+E_2)}{E_2}\dot{\epsilon}, \quad \sigma + \frac{\eta}{E_1+E_2}\dot{\sigma} = \frac{E_1E_2}{E_1+E_2}\epsilon + \frac{E_1\eta}{E_1+E_2}\dot{\epsilon} \tag{2-7}$$

The Kelvin representation highlights the immediate elastic and delayed viscous response, making it suitable for describing creep and stress relaxation while the Maxwell model emphasized an initial viscous respone followed by an elastic response making it suitable for materials that show both instantaneous and delayed responses simultaneously.

### 2-7-4 Burgers model

Another famous model for viscoelasticity is the Burgers model. This is one of the most widely used models for modelling creep deformation according to Dolz et al. [33]. Again, the Burgers model has two different representations, but the most widely used one is the Kelvin representation. The Kelvin representation adds a viscous damper to the SLS model in series to the already existing spring and spring-damper components, see figure 2-13(e), giving it an even better ability to model stress relaxation. The constitutive stress strain relationship for the Burgers model is given as follows:

$$\sigma + (\frac{\eta_1}{E_1} + \frac{\eta_2}{E_1} + \frac{\eta_2}{E_2}) \cdot \dot{\sigma} + \frac{\eta_1\eta_2}{E_1E_2} \cdot \ddot{\sigma} = \eta_2\dot{\epsilon} + \frac{\eta_1\eta_2}{E_1}\ddot{\epsilon} \tag{2-8}$$

### 2-7-5 Jeffreys model

The Jeffreys model is another model used to describe viscoelastic behaviour. It removes the spring in series with the viscous damper and the spring-damper component, see figure 2-13(f). The stress-strain relationship of the Jeffreys model is given by, according to D.D. Joseph [32], the following equation:

$$\frac{\eta_1+\eta_2}{E}\frac{d\sigma}{dt} + \sigma = \eta_1(\frac{d\epsilon}{dt} + \frac{\eta_2}{E}\frac{d^2\epsilon}{dt^2}) \tag{2-9}$$

The Jeffreys model, also called Anti-Zener model (AZM) has a major drawback and that is its inability to model solid-like behaviour. What is meant by that, is the fact that an instantaneous deformation results in a viscous (read: time-dependent response). Hence there is no immediate elasticity.

### 2-7-6 Generalized Maxwell

The Generalized Maxwell model, also known as the Maxwell-Wiechert model, consists, surprisingly, of some of the same components as the the preceding models. It is built up from a parallel set of components, the first of which is always a single Hookean spring, followed up by n Maxwell elements, in which n is the order of the Generalized Maxwell model, see figure 2-13(g). The Generalized Maxwell model is capable of describing material with different relaxation times very well, enabling it to model materials with a range of creep activation energies [34]. The constitutive equations of the Generalized Maxwell model, when solved for initial conditions t=0, are given by the following differential equation [30]:

$$\sigma(t) = \epsilon_0[E_\infty + \Sigma_{i=1}^{N} E_i \cdot e^{\frac{-E_i}{\eta_i}t}] \tag{2-10}$$

Here, $\epsilon_0$ is the initial strain, $E_\infty$ is the Young's modulus of the i-th element of the model, $\eta_i$ is the viscosity of the i-th element of the model and t is the time. By simplifying $E_\infty\epsilon_0$ to $\sigma_0$ and $\frac{\eta_i}{E_i}$ to $\tau_i$, the relaxation time, the equation can be rewritten to:

$$\sigma(t) = \sigma_0(1 + \Sigma_{i=1}^{N} E_i \cdot e^{-\frac{t}{\tau_i}}) \tag{2-11}$$

The resulting equation is what we call the Prony series. This series is often being used to curve fit stress relaxation data for a set number of Generalized Maxwell parameters in order to create an analytical stress strain relationship.

The aformentioned models give an intuitive meaning to parameters for creep and stress relaxation. Most of them are not computationally heavy. They are mostly useful for simple, 1D behaviour since complex geometry shows more anisotropic behaviour, especially in fibre reinforced materials [35]. Curve fitting might make the models better for more advanced geometries. Especially the Prony series is generally used for this. For large deformations the Prony series is usually combined with a hyperelastic model, as is done by Pouriyayevali et al. [36]. More on this can be found in section 2-10.

## 2-8 Integral Based Viscoelastic Models

The models of the previous section describe, behaviour of pure solids, pure liquids and anything inbetween. A factor which these models do however not explicitly take into account, is the history-dependent behaviour of viscoelastic material. For this, the hereditary integral was introduced, first by Boltzmann [37]. The hereditary integral relies on the BSP in the sense that an adding different stress inputs gives a cumulative strain output. By superposing the input output relationship over time, the hereditary integral describes the cumulative time- and history-dependent stress strain relationship of materials. It does so by including a

**Table 2-1:** Memory functions for different types of decay

| Model | Memory function |
|---|---|
| Maxwell model | $Ee^{\frac{t}{\tau}}$ |
| Kelvin-Voigt model | $E\tau e^{\frac{t}{\tau}}$ |
| Generalized Maxwell model | $\Sigma_{i=1}^{N} \frac{E_i \tau_i}{1+(\frac{t}{\tau})^{\beta_i}}$ |
| Prony series | $\Sigma_{i=1}^{N} \frac{E_i \tau_i}{1+(t\tau_i)^{\beta_i}}$ |

convolution function in the integral, with the convoluted function being called the memory function. The hereditary integral is formulated as,

$$\sigma(t) = \int_0^t G(t-\tau)\frac{d\epsilon(\tau)}{d\tau}d\tau \tag{2-12}$$

in which G(t-$\tau$) is the memory function, representing past deformations. This function is now in a general form. Dependent on the type of material behaviour, the memory function may change. The memory function expresses the combined relaxation times of the sum of components used. An overview in memory functions for simple models is given in Table 2-1.

In the table, E is the relaxation modulus, $\tau$ is the relaxation time and $\beta$ is a dimensionless parameter. On of the most widely used models is the Schapery integral, which uses the Prony series as a memory function for its hereditary integral to calculate the creep compliance. Creep compliance a is time dependent metric of how under constant load a material deforms over a time span. It is given as:

$$J(t) = \frac{\epsilon(t)}{\sigma} \tag{2-13}$$

An important note is the fact that in both the derivative and integral based models, the Prony series is used often to model behaviour. The reason for this is that the Prony series is essentially an empirical curve fit which will be 'good enough' when it satisfies a certain tolerance. For the curve fitting coefficients of the Prony series, we need to measure the shear modulus, or the bulk modulus, of the material versus time. The need for knowledge on the shear modulus stems from the fact that the assumption is made that all of the relaxation in viscoelastic material stems from the shearing of monomer strands [38]. In other words, the Poisson ratio is constant. If this is not a valid assumption, eg the poisson ratio changes with deformation, the bulk modulus is also required for an accurate material description [39]. We will need either different datasets for a multitude of temperatures, or an isochronous master curve.

### 2-8-1 Relaxation Modulus

The relaxation modulus, which is similar to the Young's modulus, but changes over time, can be calculated as follows:

$$E(t) = \frac{\sigma(t)}{\sigma_0} \tag{2-14}$$

In order to model viscoelastic materials using the Prony series in modelling software, not the relaxation modulus, but the shear relaxation modulus is required along with the time dependent bulk modulus. The shear relaxation modulus and bulk modulus can be formulated as follows:

$$G(t) = \frac{E(t)}{2(1+\nu)}, \quad K(t) = \frac{E(t)}{3(1-2\nu)} \tag{2-15}$$

The relaxation modulus is not to be confused with the memory function. Although both are related to time dependent response of viscoelastic material, the relaxation modulus assumes a direct time dependent response of stress to varying strain, whereas the memory function takes strains from the past into account.

Integral based models take history-dependence into account giving a more complete image of the process. The convolution integral does however add a level of computational complexity to problems, which can be an issue for simple examples.

## 2-9 Fractional Calculus Based Viscoelastic Methods

Next to integer order derivative- and integral based models, there exist also fractional based viscoelastic models. Fractional calculus enables for capturing non-integer order derivatives and integrals. Where most traditional viscoealstic models are based on integral or derivative models with integer order components, fractional models use fractional order components. Fractional order models have the power to fit model parameters better than their integer counterpart to describe viscoelastic behaviour more accurately [42].

One of these fractional order components is called the fractional order dashpot, or the Abel Dashpot, see figure 2-14(a). Without going into too much detail on the mathematics behind this, the stress strain relationship of the Abel dashpot [43] is given by,

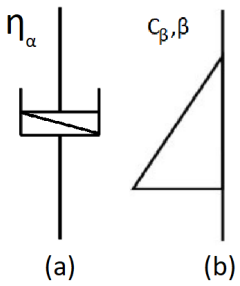


**Figure 2-14:** (a) Fractional order dashpot [40], (b) Scott-Blair element [41]

$$\sigma(t) = \eta \frac{d^\alpha \epsilon(t)}{dt^\alpha}, \quad 0 < \alpha \leq 1 \tag{2-16}$$

in which $\sigma$ is the time-dependent stress, $\eta$ is the viscosity of the material, $\alpha$ is the non-integer order for the derivative, and $\epsilon$ is the time-dependent strain. A schematic of what models using the Abel dashpot would look like are given in figure 2-15.

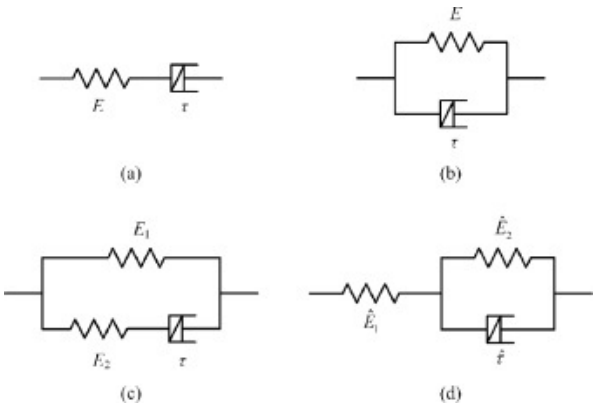


**Figure 2-15:** Fractional Maxwell model (a), Fractional Kelvin-Voigt model (b), Fractional Zener model (c), Fractional Poynting-Thomson model (d) [44]

Another basic fractional element is the springpot or the Scott-Blair element, see figure 2-14(b). The stress strain relationship of this component is given as follows:

$$\sigma(t) = G(t)\epsilon_0, \quad G(t) = \frac{c_\beta}{\Gamma(1-\beta)} t^{-\beta} \tag{2-17}$$

In eq. 2-17, $\Gamma$ stands for the gamma function as described by Artin [45], and $\beta$ is a power-law exponent. $c_\beta$ does not have a well defined physical meaning, but is often referred to as the *firmness* of the material [46]. The Scott-Blair element behaves as a mixture of a viscous damper and a linear spring. Component $\beta$ determines how much the element represents one or the other, see figure 2-16. In the same fashion as the Abel dashpot, the Scott-Blair element can be used as an individual component in linear models. Both the Scott-Blair and the Abel elements are constant order fractional models.

Fractional order models are generally well suited for describing viscoelastic models. The requirement of fewer parameters to describe viscoelastic behaviour gives them an advantage over integer order models [47]. The advantages of fractional order models do however come with a cost. Fractional models are computationally heavier than integer order models [48]. Another disadvantage of fractional calculus models is that they are not yet widely implemented in Finite Element Method (FEM) software. Efforts of implementing fractional calculus into FEM software are however being made [49].

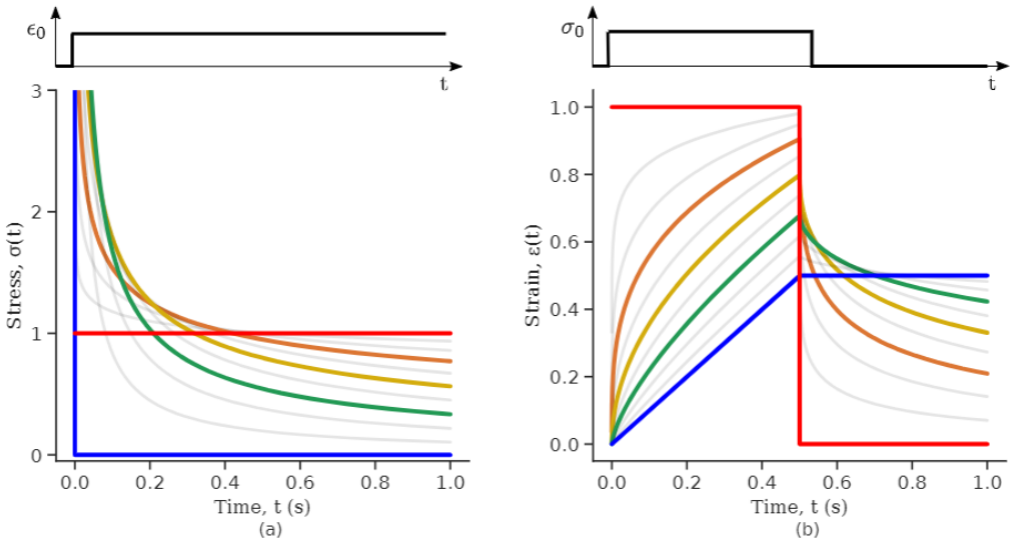


**Figure 2-16:** Scott-Blair response to constant strain (a) or constant stress (b). If $\beta = 0$ the element behaves like a spring. If $\beta = 1$ the element behaves like a damper [46].

## 2-10 Hyperelasticity

As mentioned before, viscoelasticity can be combined with hyperelasticity for large deformation problems. There are generally 2 different types of hyperelastic behaviour: Totally incompressible and nearly incompressible and compressible models. Most polymers fall into the near- or totally incompressible category. Most foams fall into the compressible category.

Table 2-2, gives an overview for the capabilities of the most general hyperelastic models. The number of datasets needed refers to how many experiments (uniaxial, equibiaxial, shear, etc) you need to do in order to have reliable results. Hyperelastic materials are subdivided into 4 categories: elastomer, rubber, bio tissue and foams. The table shows which model is typically used for each type of hyperelastic material. The deformation category has "Range dependent" entries. This essentially means that for these models, their accuracy depends on their fit. If they are fitted for a specific Range of Motion (RoM), they will most likely be accurate within that RoM, but not necessarily very far outside of those bounds. From table 2-2 it seems as if, if computational time plays no role, that the Arruda-Boyce model will be the best choice for modelling elastomeric compliant mechanisms, since it's unconditional stability, and ability to give good results for a specified RoM.

## 2-11 Other models

A few other models which are not included in the 3 main sections, but are interesting for further reading are the non-stationary nonlinear viscoealstic model for shale [59], the nonlinear Newton body model [60], the extended Schapery model [61] and the microdamage model [62]. There are also some analytical models for aggregates, since a substance such as concrete

**Table 2-2:** Hyperelastic Models and their limitations [50],[51],[52],[53],[54],[55],[56],[57],[58]

| Model | Deformation (%) | # of Datasets | Load Instability | Material |
|---|---|---|---|---|
| Neo-Hookean | <100 | 1 | None | Elastomers, Bio |
| Mooney-Rivlin | <200 | 2 | Biaxial | Elastomer, Rubber |
| Ogden | Full RoM | >3 | Parameter dependent | Rubber, Elastomer, Bio |
| Arruda-Boyce | Range dependent | 3 | None | Elastomer, Rubber |
| Yeoh | Range dependent | 3 | None | Elastomer, Foams |
| Blatz-Ko | <100 | 1 | Conditionally stable | Rubber, Foams |

behaves somewhere in-between an ideal solid and an ideal fluid [63].

## 2-12 Summary

In this chapter, the basic concepts of creep, stress relaxation and viscoelasticity for metals and polymers respectively, are explained. Some of the limitations of types of models are addressed along with some recommendations for modelling of compliant mechanisms. For metals, the conditions for the dominant type of creep are explained. The time-temperature-stress superposition and Boltzmann superposition principles are addressed. Afterwards, first some simple viscoelastic models and concepts are discussed, and then some more complex models are explored. For viscoelastic models, since it is difficult to describe the stress-strain relationship analytically, test date need to be curve-fitted in order to create a reliable range wherein the mechanism's deformations can be predicted. If the compliant mechanism modelled is using polymers, there is a need for combining viscoelasticity and hyperelasticity. For modelling viscoelasticity, curve fitting the Prony series will be an essential step. For our pick of a hyperelastic material we needed to look at the deformation, number of experiments needed in order to gain reasonable data, loading stability, and if time plays a role, computational time will also matter. The most logical pick would be, as mentioned, the Arruda-Boyce model, if computational time does not play a role. The caveat that comes with curve fitting a model however is that curve fits highly depend on the used software and that the model used therefore might change from our initial pick.

It has been shown that creep and stress relaxation in metals and polymers are slightly different. There is not a hard separation between which phenomenological models to use for which type of material, but under certain circumstances, one of the models may outperform the others. Metals seem to only behave exert flow behaviour at a certain threshold temperature and stress whereas polymers show this behaviour at any stress and temperature level. As a result, in theory, it would be possible to alter the characteristic properties of a metal by heating it and then 'lock' this behaviour into place, by cooling it again. For viscoelastic materials this would be slightly less intuitive since there will always be some form of relaxation behaviour.

# Chapter 3

# Preload and Type of Stability in Compliant Mechanisms

## 3-1 Introduction

When a mechanism is in equilibrium, the net forces and moments are zero. While it may seem like nothing is happening in the background, a variety of factors are balancing in order for the system to behave as if it is unaffected in this state of being. Geometric factors, gravity, interplay between components, material stiffness, etc. are all competing in order for the mechanism to be configured in a specific way. If an equilibrium of the sort occurs we are speaking of *static equilibrium*.

When a mechanism is in static equilibrium, its potential energy versus displacement, of one of its spatial degrees of freedom, would have at least one, and possibly multiple, local minima. This means that when a mechanism is in equilibrium position, in case of a conservative system, it takes energy to remove it from this preferred position. In a force-displacement graph, at the same displacements, in the same directions, as the local minima of the potential energy graph, the force would be equal to zero. The energy needed to move a mechanism from an equilibrium point can be subdivided in potential gravitational energy and potential strain energy. These energies can be interchanged from configurations. In the case of mechanisms with moving parts, kinetic energy also needs to be taken into account. The kinetic energy in a system transfers back into strain and gravitational energy when a system is back at rest however. Hence we do not look at the influence of kinetic energy on a system in this paper.

As mentioned, the reaction force of a mechanism is directly related to its energy. In fact, the reaction force of a system is equal to the time derivative of its energy with respect to its spatial degrees of freedom. Taking the derivative of the reaction force again with regards to its spatial degrees of freedom, we end up with the *stiffness*. Stiffness is a measure of how the force and moment balance changes as a system is reconfigured. In a perfectly rigid world,

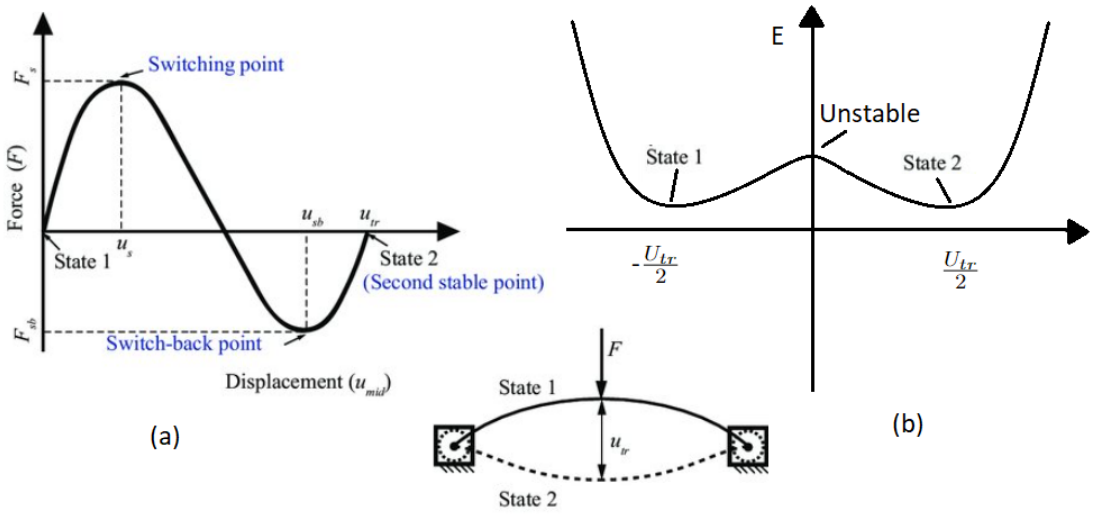


**Figure 3-1:** (a) Force-displacement graph of buckling clamped beam, (b) Strain energy-displacement graph of buckling clamped beam[64]

these instantaneous factors would give perfect information on the mechanical arrangement of a system. While stiffness is a useful measure for predicting the morphing of a structure under load, it can become problematic when dealing with bifurcations in deflection paths. Take for example a buckling of a column. If a force is compressing the column in its axial direction, its stiffness orthogonal to the load direction will become zero. In short, this means that the stiffness matrix can no longer describe which way the column will move. When a slight imperfection in the structure exists this will favour buckling towards a specific direction. This makes the stiffness an unpredictable metric in some cases.

The number of equilibrium configurations of a mechanism are leading in its stability classification. A discernment between three types of stability is made here: bistability, multistability and neutral stability. A system is called bistable when it has two distinct stable equilibrium points. It would take energy to get the system from one to the other stable state. A typical example of a bistable mechanism is the post-buckling beam of figure 3-1. If the beam in the given example has a force pressing down the middle, at first an increasing force is needed to deform the material, leading to an increasing strain energy. After a certain displacement, there is a point of no-return after which the force decreases again, and changes direction, pulling the material towards a new equilibrium. If at the point of no-return, we would have stopped deforming the material we would have what we call an unstable equilibrium point. A slight disturbance would make the mechanism snap to either stable points. For a schematic of an unstable equilibrium in a generic energy-deflection profile, see figure 3-3(a). It is important to note that the type of stability as defined here is dependent on a mechanism's *stable* equilibrium points, figure 3-3(b), and not the total equilibrium points.

The second type of stability is *multistability*, meaning that the system has more than two stable equilibrium points. In the same fashion as bistability, multistability is often a result of buckling. One of the typical ways to achieve multistability is to stack bistable elements with

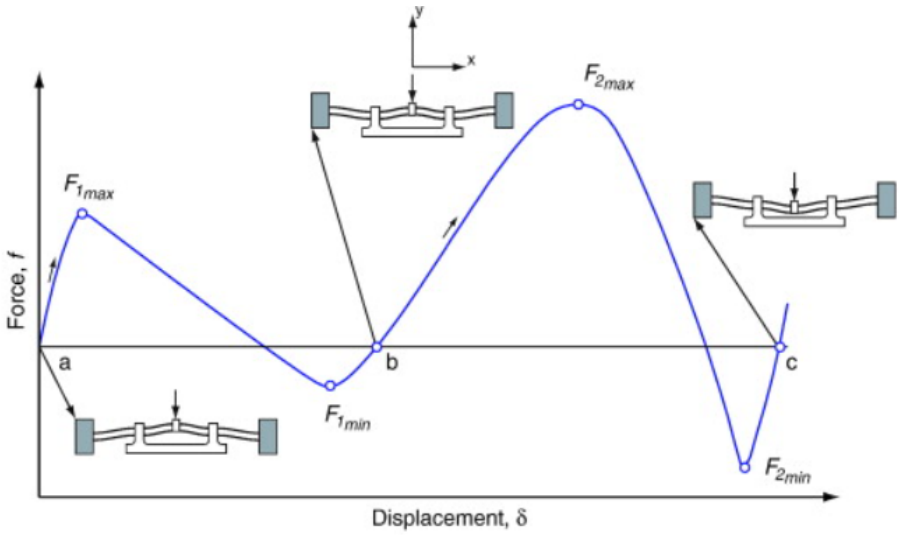


**Figure 3-2:** Force-deflection curve of tristable compliant mechanism [66]

asymmetric force-displacement curves in series [65]. When the mechanism's parameters are properly tuned, the system can have almost completely decoupled modes of behaviour due to energy barriers. An example of the force-deflection curve of a tristable compliant mechanism making use of stacked bistable components can be seen in figure 3-2

The third and final type of stability discussed in this paper is *neutral stability*. To fully understand the concept of neutral stability, the concept of 'zero-stiffness' will first have to be explained. In the literature, zero-stiffness and neutral stability are more often than not used interchangeably, but there is a nuance to it. A mechanism is said to have zero-stiffness if over a certain deflection path its force remains constant. In the the force-displacement curve of a mechanism you would see a range in which there exists a horizontal line. This indicates the requirement of an actuation force for the mechanism. In the case of neutral stability this horizontal line would be positioned at zero, meaning that there is a constant zero-force range in which the mechanisms can move. In terms of energy this would mean that there is zero work required to make the mechanism move between configurations, thus rendering the mechanism indifferent of its configuration. This would show a horizontal line in the energy-deflection profile. The working principle for this is an exchange between sources of potential energy. Elegant and intuitive examples on neutral stability have been given by Schenk [67], but many more exist. To reiterate, neutral stability rests on the foundation of zero-stiffness and zero net work. For the schematic of how this would look in an energy-deflection graph, see figure 3-3(c).

In order to achieve the aforementioned states of stability, compliant mechanisms get preloaded or prestressed. The terms differ in the sense that applying a preload will impose a deformation of the mechanism, be it elastic, plastic, or viscoelastic, resulting in a prestress. This stress alters the strain energy (distribution) of the mechanism and can therefore influence its stability. A distinction between the two terms will not be made in this survey. Preload or prestress in this paper is defined as an addition of energy to the system before it is being operated. For elastic materials this might be the compression or extension of a spring. In

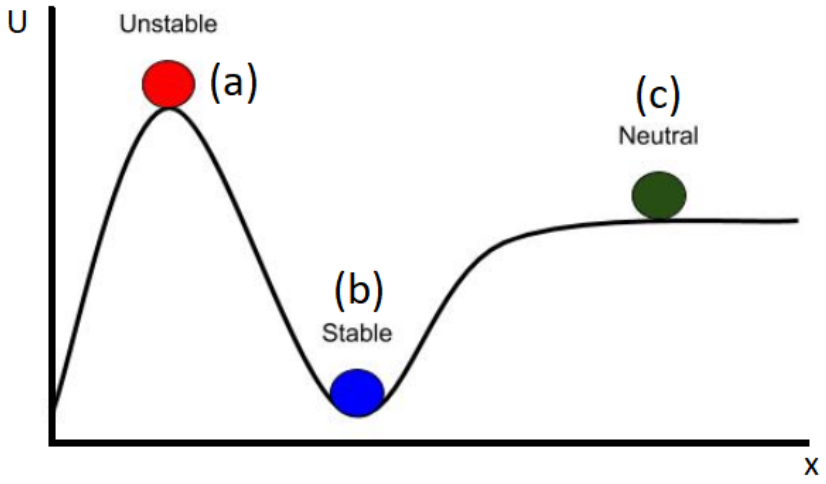


**Figure 3-3:** Schematic energy-deflection profile for an (a) unstable equilibrium point, (b) stable equilibrium point and (c) neutrally stable equilibrium range

terms of plastic deformation this might mean the asymmetric stretching or compressing of a plate in order to increase internal stresses. Finally, viscoelastic prestressing can be achieved using viscoelastic recovery to create tension.

In this paper an overview of the application of prestress by means of elastic, plastic and viscoelastic preload, with regard to type of stability will be given. The most prevalent methods for each type of stability will be highlighted. A vacancy in the literature will be exposed on the topic of viscoelastic prestress. More on this can be found in section 3-3. An argument on why this vacancy might exist in the first place, and a possible solution, are made in section 3-4.

## 3-2 Method

In order to find a literature gap, types of prestress will be plotted against types of stability. The types of prestress are, as mentioned before, elastic, plastic and viscoelastic prestress. These types of prestress induce bistability, multistability or neutral stability.

The search string for this literature survey has been sorted with the **and** function for synonyms for prestress + type of equilibrium + type of prestress + type of machanism. As mentioned by Kok [68], the term neutral stability is often overshadowed by one of its characteristics: zero-stiffness. A variety of synonyms for neutral stability have therefore been added in the search string as well. Due to the term viscoelasticity, a lot of results were from the field of fluid mechanics. The **not** function was used to restrict searches to the discipline of compliant mechanisms. Finally, since there exist a number of conjugates of the terms neutral and stable, the asterisk function * has been used. For the complete search string and its variants, see table 3-2.

**Table 3-1:** Type of Prestress and Stability

| | **and** | | | | **not** |
|---|---|---|---|---|---|
| | Synonyms preload | Type of equilibrium | Type of prestress | Type of mechanism | |
| **or** | Prestress | Bistab* | Elastic | Compliant mechanism | Fluid* |
| | Pre-stress | Multistab* | Elastic deformation | Metamaterial | Convection |
| | Preload | Neutral* stab* | Plastic | Composite | |
| | Pre-load | Neutral* elastic | Plastic Deformation | Shell | |
| | Self stress | Zero-stiffness | Viscoelastic | | |
| | Self-stress | Zero stiffness | Viscoelastic deformation | | |
| | Pretension | Continuous equilibrium | | | |
| | Buckling | Static* balanc* | | | |
| | Prestrain | Tristab* | | | |
| | Pre-strain | Energy invariant | | | |

### 3-2-1 Overview

An overview of the types of the existing types of prestress versus the type of stability this achieves is constructed in table 3-2. This is the categorization that the next section will follow, starting with elastically prestressed bistable structures, and ending with viscoelastically prestressed neutrally stable structures.

**Table 3-2:** Literature survey of stability and prestress in compliant mechanisms

| | **Type of Prestress** | | |
|---|---|---|---|
| **Stability** | **Elastic** | **Plastic** | **Viscoelastic** |
| **Bistable** | [69], [70], [71], [72], [73], [74] | [75], [76], [77], [78], [79] | [80], [81], [82] |
| **Multistable** | [65], [83], [84] | [85], [86] | |
| **Neutrally stable** | [67], [87], [88], [84], [89], [90], [91], [92] | [76], [93] | |

## 3-3 Results: Occurrences and Classification

In the introduction the topics of stability and prestress have been introduced. This section will give an overview of methods for achieving prestress, along with their use cases, through examples. The examples stated in this survey have been condensed to a single table. For this see table 3-2.

### 3-3-1 Elastic Bistable

To reiterate on the previous section, in order to call a structure or mechanism prestressed, a load has to be applied to alter its enery profile. In the case of elastically prestressed bistable structures either the material itself can be deformed, or elastic components (read: springs, elastic bands, etc.) can be deformed to alter the energy profile.

A first example is the tensegrity structure presented first by Calladine [70] and later adopted to make a bistable mechanism by Micheletti [71] and by Vangelatos [69] to create a nano metamaterial. The latter's principle relies on a 3-revolutionary joint system connected by wires, attached on two ends to the base, see figure 3-4(a). If the wires together are longer than the distance between the attachment points to the 'base', the system experiences a bifurcation. It can be stable in either the up or down position. If it transitions from one to the other position, it will at some point in the transition quickly 'snap' beyond the instable equilibrium point. This is what we call snap-through. This principle is used in a larger tensegrity structure as can bee seen in figure 3-4(b). The same principle applies the other way around when the system does not consist of wires but elastic bands. This form has been adapted by Shimura [72], in which the elastic bands create a pretension favouring one of two other stable positions, 3-6(b). Another phenomenon which often occurs within the elastic bistable prestress domain is the occurrence of snap-through buckling, which is essentially the same as normal snap-through only with the addition of a buckled beam.

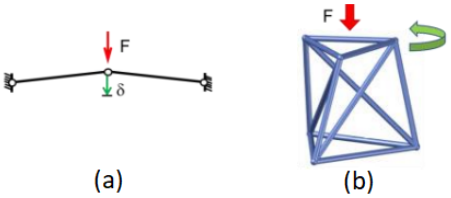


**Figure 3-4:** (a) Schematic, (b) Tensegrity structure [69].

Another example found in the literature is the bistable jumping robot produced by Jung [73]. It consistst of two rigid links connected by a rotational joint and by an axial spring, see figure 3-5. In the figure it can be clearly seen that there are two stable configurations for this mechanism. Its working principle relies on using a snap-through instability to go from one stable position to another at a very high pace, inducing a jump.

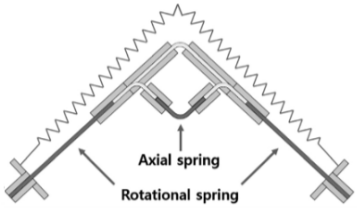


**Figure 3-5:** Snap-Through jumping robot [73].

### 3-3-2 Elastic Multistable

Multistability has mainly been achieved elastically by stacking bistable components with an asymmetric force-displacement curve for their spatial degree of freedom. Examples such as the octostable buckled mechanism of Gou [83] and the tristable gripper of Jo [65] depict this form of prestressing very well, see figures 3-7 and 3-8.

The tristable gripper designed by Jo has unlike most bistable grippers, next to an open and closed state a holding state as well. The mechanism works as follows: When in the closed configuration as can be seen in figure 3-7(a), the gripper's vertical driving part is fully retracted. When it gets protracted as can be seen in 3-7(c), the mechanism fully opens. So far there is very little difference from ordinary grippers. When however now the gripper retracts the driving pin halfway

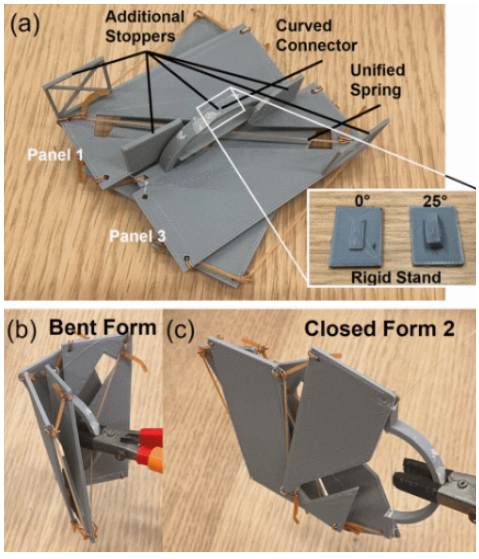


**Figure 3-6:** (a) Full mechanism, (b) First stable equilibrium, (c) Second stable equilibrium [72].

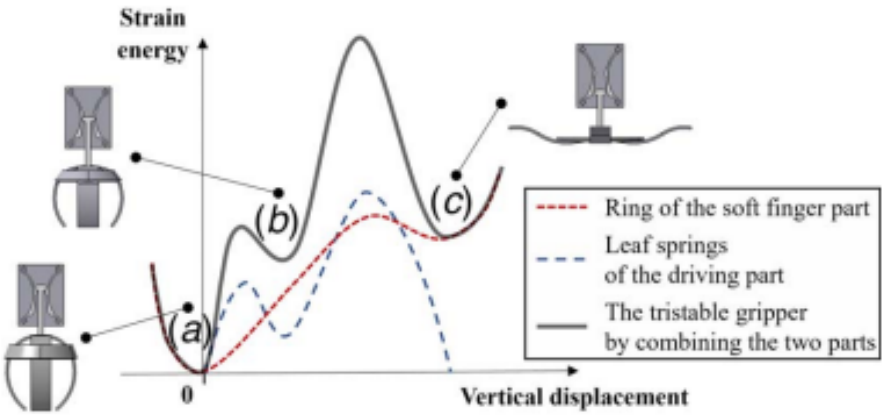


**Figure 3-7:** Tristable gripper in with all its stable states [65].

back, 3-7(b) the gripper closes and gets mechanically
locked in the vertical driving shaft. The gripper claws are attached to a ring which gets held in place as the claws buckle up, inducing a prestress.

The octostable buckled mechanism of Gou [83] uses a a single bistable element as a means of prestress, and a multitude of end-effectors to create a mechanism stable in eight different positions, see figure 3-8. They use the Pseudo-Rigid Body Model (PRBM) to describe the mechanism's Equations of motion (EoM) and to find the force-displacement relationships. The paper's focusses on the tradeoff between stiffness and flexibility of the attachments to the end-effectors. If the flexures are too flexible there will not be any distinct stability, too rigid might however lead to yielding.

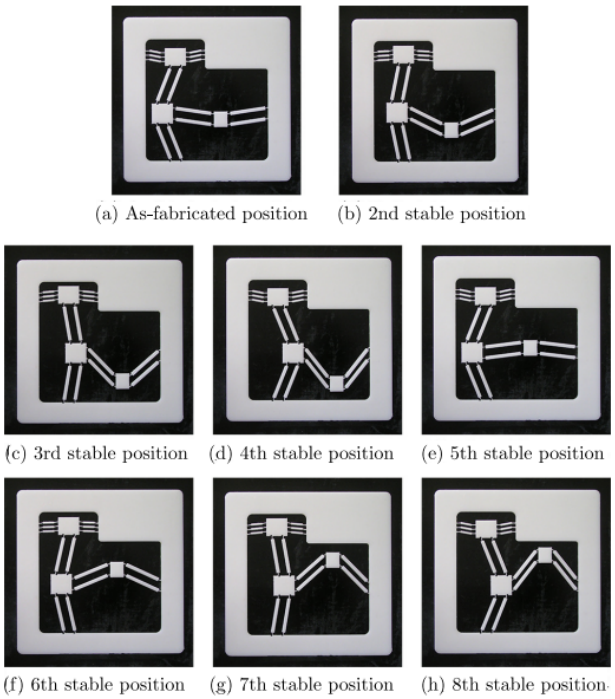


**Figure 3-8:** Octostable mechanism in all its stable positions [83].

A more interesting example can be found in the multistable polygon configuration of Risso [84]. Risso uses a biaxially prestressed membrane attached to N-sided polygon-shaped Fibre Reinforced Polymer (FRP) frames to create multistable structures. In the study,

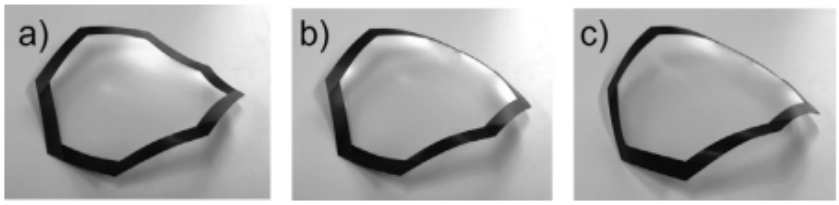


**Figure 3-9:** 8-sided prestressed polygon with its 3 unique stable configurations [84].

Risso categorizes the relationship between inflection point on the structure and its stability. In the study, it is found that 3 main stable equilibrium configurations can be found for any polygon with N $>$ 4, a saddle shape, half saddle/half cylinder shape and full cylinder shape. Per side extra, the system will increase by 3 non-unique similar stable states, see figure 3-9.

### 3-3-3 Elastic Neutrally Stable

Examples of neutrally stable mechanisms using elastic deformation to balance the stiffness of structures is widespread. Elegant examples such as the Anglepoise lamp as mentioned by Guest and Schenk [67] and the end-to-end attached rod as first mentioned by Thomson and Tait [87], see figures 3-10 and 3-11, have been known for many years. This subsection will give some more state of the art examples and their working principles.

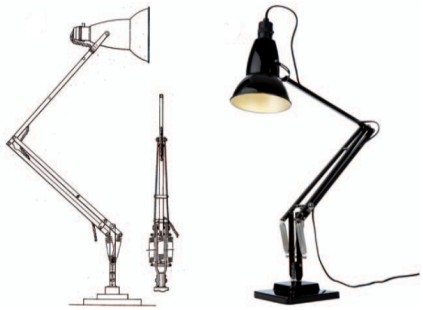

**Figure 3-10:** Anglepoise lamp [67].

The polygon structure of subsection 3-3-2 is one of the state of the art examples of elastically prestressed multistability. The study, after successfully creating multistable elastically prestressed sttructures argues that in the boundary case where the number of sides of the polygon goes to infinity, the system has an infinite amount of stable states and therefore becomes neutrally stable. The resulting structure is a neutrally stable ring, see figure 3-12.

An extension on the simple Anglepoise lamp has been given by Chaudhary et al. [88] in the form of a totimorphic structure. This term means infinitely maleable and describes a neutrally stable tensegrity structure. In figure 3-13(a), a schematic can be seen. The system works as follows, it has springs attached to pulleys in order to be able to emulate free length springs, enabling the springs

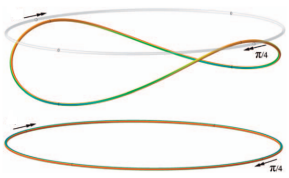

**Figure 3-11:** Thomson and Tate ring [87].

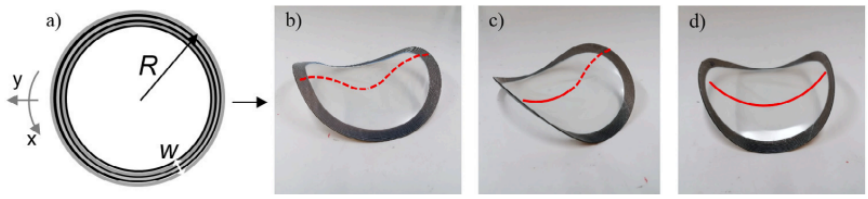


**Figure 3-12:** $\infty$-sided prestressed polygon with its 3 unique stable configurations [84].

to perfectly balance a lever. This balanced unit cell can then be stacked in order to create more complex neutrally stable structures. Figure 3-13(b), shows one of the use cases for the totimorphic structure: a zero Poisson ratio structure.

Wang et al. [89] even went one step further. They attached an inextensible rope to one of the ends of the spring, enabling the pulley to give the springs some more slack and therefore undoing the neutral stability, see figure 3-13(c). Now this sounds like a downgrade, but the reality is that they achieved the ability to switch between neutrally stable and elastic behaviour, by lengthening and shortening a wire. A schematic of the elastic and plastic behaviour of the structure created by Wang can be seen in figures 3-13(d) and 3-13(e), respectively. Only the schematics of the structure are shown since the real world example has too many different parts to give a clear image.

Another strategy for achieving elastically prestressed neutral stability in structures is by creating designing structures in a way that local deformation patterns are anti-symmetric. Two examples of this are the the curved crease mechanism designed by Kok [91] and the reverse twisting helicoidal shell by Radaelli [90]. In the first example it can be seen that over the full deformation there always exists an axis, the inflection axis, that experiences no force. Figure 3-14(a) shows that for a single full deflection, the curved crease mechanism ends in the same configuration as it started in, only moved to the right. This is the same principle as the end-to-end attached rods by the Thomson and Tate.

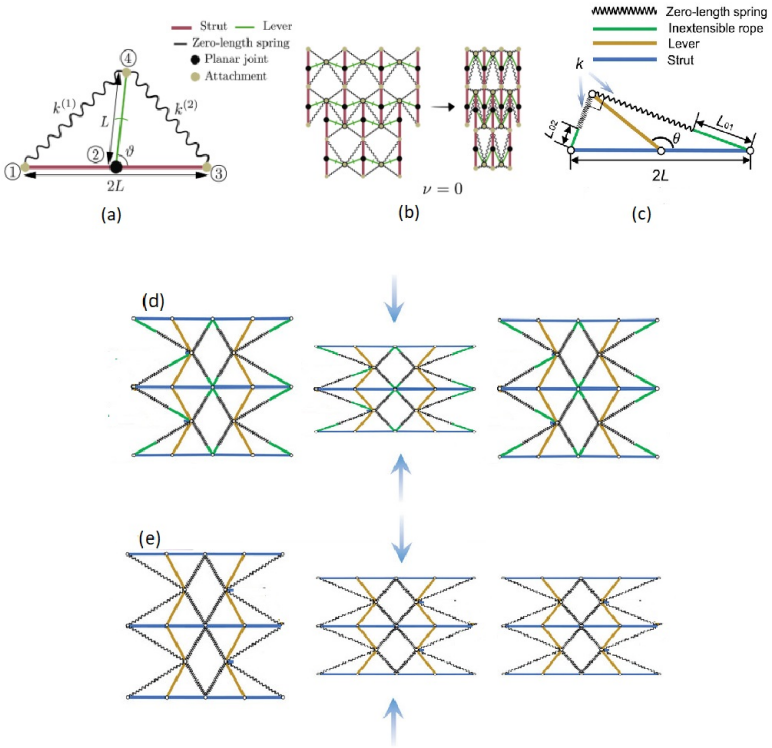


**Figure 3-13:** (a) Totimorhpic structure, (b) Zero-Poisson ratio configuration [88], (c) Tensegrity with inextensible rope, (d) Elastic configuration, (e) Neutrally stable configuration [89].

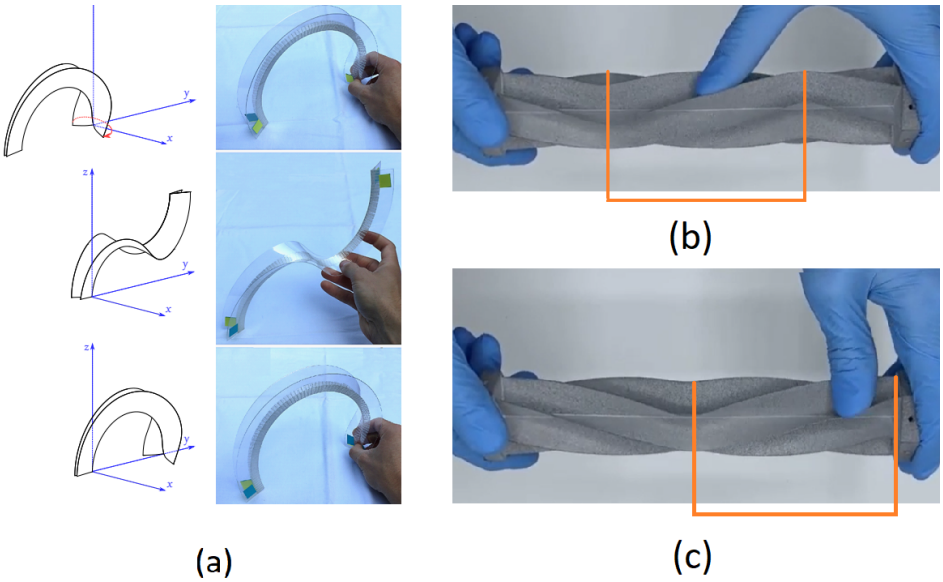


**Figure 3-14:** (a) Curved crease mechanism [91], (b) Reverse-twist mechanism, (c) Reverse-twist mechanism with moved deformation region [90].

In the second example, the helicoidal shell of Radaelli is reverse twisted, creating an anti-symmetrically buckled region. This region can exist anywhere on the structure since the buckled flanges of the helicoid counter each other's pull. As a result, the reverse twisted region can slide along the longitudinal axis, see figure 3-14(b)(c).

The final method that is often used in literature to achieve elastically prestressed neutral stability, is the use of composite shells with perpendicular same-sense curvature. One example is that of the composite boom of Liuyi [92]. In this paper, a deployable boom, or tape spring, has been manufactured by curing two pieces of fabric with resin around a cylindrical rod, and then attaching them with perpendicular curvatures. Attaching the opposing laminates creates a structure which is indifferent to its position, see figure 3-15.

**Figure 3-15:** Neutrally stable tape spring [92].

### 3-3-4 Plastic Bistable

So far we have seen the use of buckling and the use of springs to create bistable elastic mechanisms. Creating bistable plastically prestressed mechanisms is most often more a more difficult task due to the complexity of distributing stress through a mechanism. It occurs as a result of remaining stress from to manufacturing processes, either mechanical or thermal. Logically, shell structres are often vulnerable to these types processes due to their slender nature. Two of the most famous examples are the bistable tape spring analyzed by Kebadze et al. [75] and the bistable disc of Seffen and Guest [76], see figures 3-16(a) and 3-16(b). Both of

these structures gained their prestress by being cold rolled in two orthogonal directions with the opposite surface up during both rolls. This last detail is important, because swapping the rolling surface can result in neutral stability. This method, is also used by Hamouche et al. [77] to create a bistable disc, see figure 3-16(c). Hamouche flipped one of the rolling surfaces around and rolled the disc in the same-sense. The bistable disc of Hamouche is special in the sense that, in theory, the disc should have been neutrally stable, but due to small imperfections in geometry neutral stability was not achieved.

Not just mechanical manufacturing processes leave residual stresses that can influence the stability of structures. Thermal stress is also a big factor in unwanted deformation after forming structures, due to asymmetric cooling of bodies with different shapes, materials or thicknesses. The research group of J.P. Stacey [78] uses this to their advantage. Instead of using mechanical rolling techniques, they employed a composite two-layer tape spring, with "mismatched" thermal expansion coefficients in order to create a prestress, see figure 3-17.

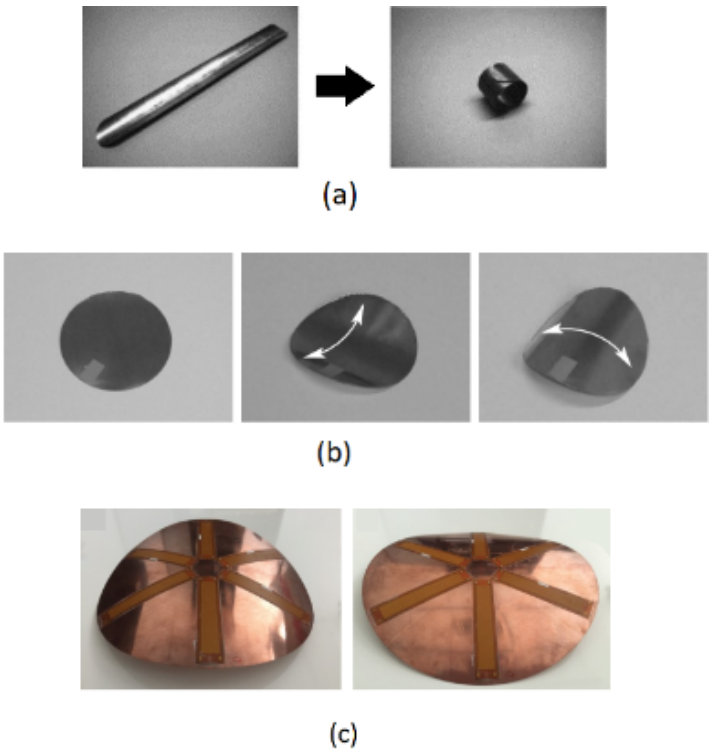


**Figure 3-16:** (a) Bistable tape spring [75], (b) Bistable disc [76], (c) Bistable disc by Hamouche [77].

A final example of plastically prestressed bistable structures is the composite tape-spring designed by Xu et al. [79]. It relies on two thermally prestressed tape springs which are attached by pin spokes to eachother. The tape springs form a helical shape due to their plastic deformation. When attaching the helices to eachother using pin spokes, a helical composite is created, see figure 3-18.

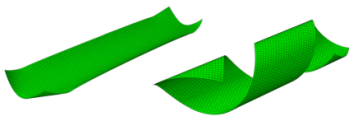

**Figure 3-17:** Bistable composite tape spring in its stable states [78].

It is good to note that in this section, many of the listed single element examples are shell structures. One of the composites is using shell structures as well for its type of stability. The fact that many of the produced structures feature shells, stems mainly from the fact that thinner structures are just plainly less challenging to form and influence with manufacturing or thermal stresses due to the thinner features.

### 3-3-5 Plastic Multistable

In the same fashion as in the previous subsection, techniques for creating bistability can also be used to generate multistable structures. An example of this is shown by the Norman et al. [85], see figure 3-19. In this paper the technique of rolling is used to coil the shell structures. The shell is then corrugated plastically as well. The resulting structure behaves tape-spring-esque, in the sense that it has a coiled up and rolled out stable state. The rolled out state in this example is however split into two seperate stable twisting modes.

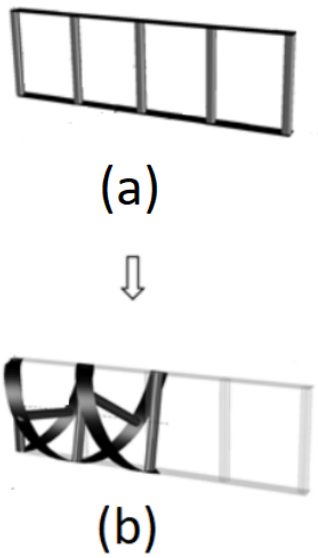


**Figure 3-18:** (a) Helical composite first stable position, (b) Helical composite second stable position [79].

Another intriguing example is based on a Kirigami "cutting and folding" technique, proposed by Lele et al. [86]. In this paper a quadstable building block for more sophisticated Kirigami structures is fabricated and tested. The building block consists out of a 3-laminate carbon fibre reinforced structure with different fibre orientations as can be seen in figure 3-20(b). The patches which are attached to the slit structure are bistable and curved the antisymmetrically. This creates initially 3 different stable configurations. The slit connection also creates another bistability generating an overall quadstable mechanism. The bistability of the two patches is induced by the thermal stresses that remain from the curing process at elevated temperature.

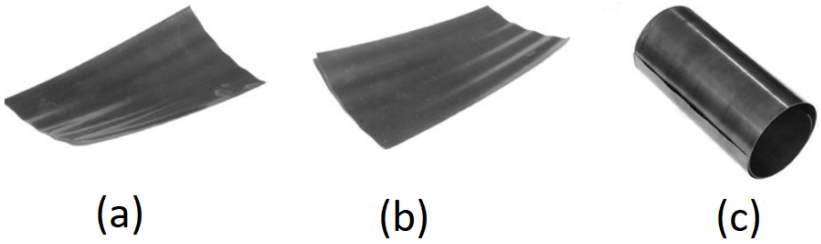


**Figure 3-19:** Stable modes of tristable corrugated shell [85].

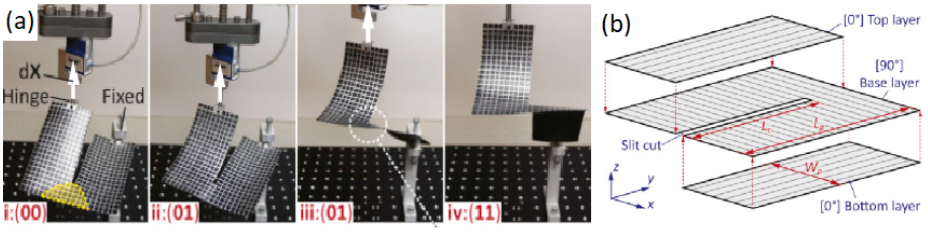


**Figure 3-20:** Quadstable Kirigami composite laminate structure [86].

### 3-3-6 Plastic Neutrally Stable

Neutral stability in plastically deformed structures is often achieved using the same stiffness altering principles that are used for bistability and multistability. Firstly, an example by Seffen and Guest [76] is shown in figure 3-21. They took a strip and rolled it across and along its length in order to make it neutrally stable. It is notable that this is one of the few monolithic examples of neutrally stable shell structures. As Seffen and Guest [76] stated, when applying same-sense rolling techniques, isotropy is important as otherwise the structure becomes monostable.

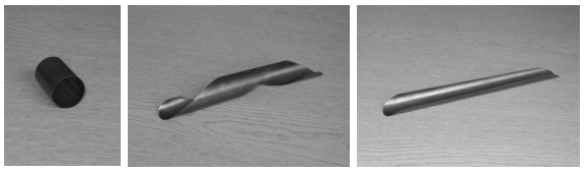

**Figure 3-21:** Neutrally stable coiled strip [76].

A technique that has been used in the creation of elastically prestressed neutrally stable mechanisms can also be used for plastically prestressed structures. Recall that for composite tape springs with pependicular anti-symmetric laminate curvatures neutral stability has been achieved. In subsection 3-3-3, this has been done by wrapping the laminates around a cylinder and then curing it in order to get the stress-free curvatures. In the study of Murphey and Pellegrino [93], instead of curing for stress-free laminates, the study revolves around the rolling of laminates and then attaching, generating a plastic prestress. The resulting structure and its stable configurations can be seen in figure 3-22.

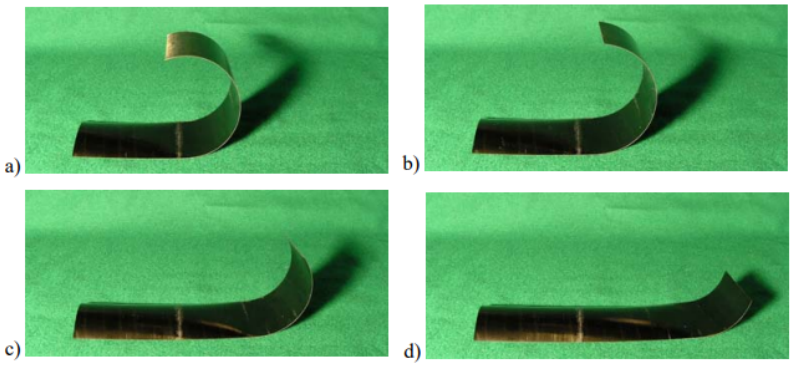


**Figure 3-22:** Neutrally stable tape spring [93].

### 3-3-7 Viscoelastic Bistable

A lot of research has been done on the viscoelastic prestressing of structures, especially in the context of structural engineering [94],[95]. Yet only a handful of studies have achieved non-mono equilibrium. This is unsurprising as altering the energy profile of viscoelastic materials permanently is a rather difficult task when taking into account the fact that stress relaxation will occur at any stress level. Despite this, two authors have managed to achieve pseudo-bistability using viscoelastic prestressing, and another has achieved actual bistability.

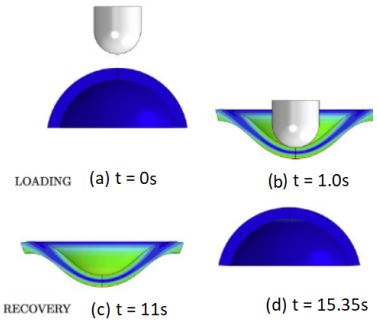


**Figure 3-23:** Pseudo-bistabe dome [80].

The pseudo-bistable dome created by Brinkmeyer et al. [80], is a dome shaped structure which when deformed along its symmetry axis takes on a pseudo stable state. Due to the viscoelastic effect of as stress relaxation, the dome does not immediately snap back but experiences a delay. Gomez et al. [81] noticed the same for a similar structure, figure 3-24 and also concluded that there was a large discrepancy between expected and measured snap-back times. The delay in snap-back gives a false sense of stability. It is noted that the longer the initial deformation takes, the longer the snap-back will take, again due to stress relaxation.

The final example of viscoelastic prestress for bistability is the creation of Viscoelastically Prestressed Polymer Matrix Composites (VPPMC), by Wang et al. [82]. In this example VPPMC beams are constructed by asymmetrically spreading Nylon fibres in a resin, stretching the fibres, releasing them, and then curing the resin. The fibres will experience viscoelastic recovery and curve the beam in the direction of the more densely packed side. Two pairs of these beams are then attached to the edges of a fibreglass sheet perpendicular to eachother and also with the reciprical of the other pair's curvature. For a more detailed schematic, see figure 3-25. The resulting structure is a bistable plate.

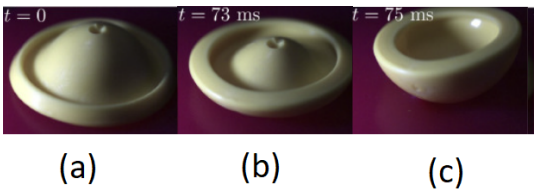


**Figure 3-24:** (a) Popper toy after initial deformation, (b) Delay in snap-back, (c) Snapped-back state [81].

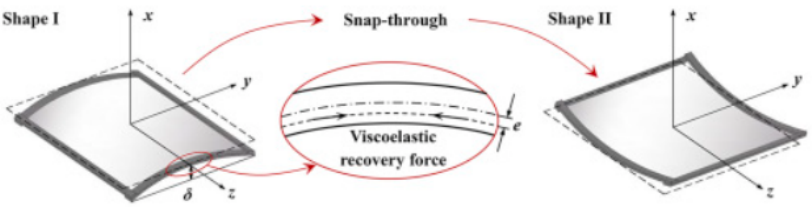


**Figure 3-25:** Bistable VPPMC plate [82]

.

### 3-3-8 Viscoelastic Multistable

Multistable viscoelastically prestressed structures have, thus far, not been created. Fact is however, that in the same fashion as previous subsections, viscoelastically prestressed structures can be stacked in series in order to create a multistable structure. However, no such structures have been constructed to the knowledge of the author.

### 3-3-9 Viscoelastic Neutrally Stable

As for the previous subsection, the same goes for this subsection. Essentially, neutral stability for viscoelastically prestressed structures should be possible, at least temporarily, as strain energy can be stored in viscoelastic structures for at least some time. However, no such structures have been constructed to the knowledge of the author.

## 3-4 Discussion and Conclusion

The objective of this literature review is to give an overview of types of stability in compliant mechanisms, of how different prestressing techniques achieve these types of stability, and of the literature vacancy in the domain of viscoelastic prestress. A distinction between the imposing of boundary conditions is included in the definition of prestress in this paper, since prestress has been defined as an addition of energy to the system prior to its functioning. Assembled structures can have their individual components (such as springs) tweaked to adjust their full superposed stiffness, in contrast to single element structures, which have to be (topology) optimized to create a specific stiffness profile and, in turn, a specific type of stability.

In elastically prestressed mechanisms, regular buckling, snap-through buckling and regular snap-through structures are mainly used to create bistability and mulitstability. Neutral stability is mostly generated by creating antisymmetric deformation patterns, cancelling out induced energy barriers. This type of stability is of a more delicate type than the other types of stability since slight discrepancies in geometry and load can highly influence the deformation pattern.

The type of stability in plastically prestressed mechanisms is mainly dictated by either residual stresses due to thermal or mechanical manufacturing processes. Rolling techniques are the first and foremost methods for creating altercations in energy profiles of structures, whether they are being used for creating bistable, multistable or neutrally stable mechanisms. Thermal stress induced stabilities also scarcely in the literature. Plastically prestressed mechanisms are almost always shell structures. A logical reason for this is the fact that shells are more vulnerable to deformation due to residual manufacturing stresses, and can therefore be used to demonstrate different types of stability.

Viscoelastically prestressed mechanisms are consistently able to produce pseudo-bistable mechanisms due to the viscoelastic recovery from which these mechanisms 'suffer'. A first of its kind

has been the research of Wang [82], in which viscoelastic recovery is used to generate a permanently bistable mechanism. This paves the way for achieving multistability in viscoelastically prestressed mechanisms. Theotretically, neutral stability as a result of viscoelastic prestress should be possible. Even though energy dissipates from viscoelastic systems, the rearrangement of the internal structure should be possible in a way that the system acts neutrally stable, for at least a single motion.

# Bibliography


[1] L. Halloran, "A rheological study of stress relaxation in elastomers for «in situ» x-ray diffraction measurements," 2011.

[2] R. Roy and L. Qi, "Stress relaxation study of paper and plastic film based packaging material," 2009.

[3] R. Lakes and R. Vanderby, "Interrelation of creep and relaxation: a modeling approach for ligaments," 1999.

[4] A. Zanj, F. He, and P. C. Breedveld, "Energy-based viscoelastic model: a physical approach for material an elastic behavior by the bond graph approach," *Simulation*, vol. 96, no. 1, pp. 111–127, 2020.

[5] J.-H. Zheng, Y. Jin, L. Xu, C. Fan, W. Song, and Y. Chen, "Comparative study of creep and stress relaxation behaviour during ageing of 7050 aluminum alloy," *Metals*, vol. 13, no. 4, p. 778, 2023.

[6] Y. Zong, P. Liu, B. Guo, and D. Shan, "Investigation on high temperature short-term creep and stress relaxation of titanium alloy," *Materials Science and Engineering: A*, vol. 620, pp. 172–180, 2015.

[7] S. Huč, T. Hozjan, and S. Svensson, "Rheological behavior of wood in stress relaxation under compression," *Wood Science and Technology*, vol. 52, pp. 793–808, 2018.

[8] W. G. Hu and H. Y. Guan, "Study on compressive stress relaxation behavior of beech based on the finite element method," *Maderas. Ciencia y tecnología*, vol. 21, no. 1, pp. 15–24, 2019.

[9] W. Harris, R. Kohrumel, and D. C. C. M. M. P. DEPT, "Calculating creep and stress relaxation from long term data," 1992.

[10] J. Bergstrom, "*What is time-temperature-superposition (TTS)?*." https://polymerfem.com/what-is-time-temperature-superposition-tts/, May 2023. [Accessed: 19-02-2024].

[11] M. Amjadi and A. Fatemi, "Creep behavior and modeling of high-density polyethylene (hdpe)," *Polymer Testing*, vol. 94, p. 107031, 2021.

[12] M. Kassner, *Fundamentals of creep in metals and alloys*. Elsevier/Academic Press, 2015.

[13] C. Pellegrino and J. Sena-Cruz, "Design procedures for the use of composites in strengthening of reinforced concrete structures," *State-of-the-art Report of the RILEM Technical Committee*, p. 392, 2015.

[14] A. P. Mouritz, *Introduction to aerospace materials*. Elsevier, 2012.

[15] M. F. Ashby and D. R. Jones, *Engineering materials 1: an introduction to properties, applications and design*, vol. 1. Elsevier, 2012.

[16] V. F. Cormier, M. I. Bergman, and P. L. Olson, *Earth's core: geophysics of a planet's deepest interior*. Elsevier, 2021.

[17] J. Larsson, "Evaluation of current methods for creep analysis and impression creep testing of power plant steels," 2012.

[18] F. M. Uhl, G. F. Levchik, S. V. Levchik, C. Dick, J. J. Liggat, C. Snape, and C. A. Wilkie, "The thermal stability of cross-linked polymers: methyl methacrylate with divinylbenzene and styrene with dimethacrylates," *Polymer degradation and stability*, vol. 71, no. 2, pp. 317–325, 2001.

[19] A. X. Chen, J. D. Hilgar, A. A. Samoylov, S. S. Pazhankave, J. A. Bunch, K. Choudhary, G. L. Esparza, A. Lim, X. Luo, H. Chen, *et al.*, "Increasing the strength, hardness, and survivability of semiconducting polymers by crosslinking," *Advanced Materials Interfaces*, vol. 10, no. 3, p. 2202053, 2023.

[20] G. Ligia and R. Deodato, "Viscoelastic behaviour of polymers," *Physicochemical behavior and supramolecular organization of polymers*, pp. 43–162, 2009.

[21] A. Rudin and P. Choi, *The elements of polymer science and engineering*. Academic press, 2012.

[22] F. Meng, R. H. Pritchard, and E. M. Terentjev, "Stress relaxation, dynamics, and plasticity of transient polymer networks," *Macromolecules*, vol. 49, no. 7, pp. 2843–2852, 2016.

[23] B. Schmuck, G. Greco, T. B. Pessatti, S. Sonavane, V. Langwallner, T. Arndt, and A. Rising, "Strategies for making high-performance artificial spider silk fibers," *Advanced Functional Materials*, p. 2305040, 2023.

[24] R. S. Lakes, *Viscoelastic materials*. Cambridge university press, 2009.

[25] L. E. van den Berg, *Development of 2nd generation proteinous bioplastics*. PhD thesis, The University of Waikato, 2009.

[26] A. Rudin and P. Choi, "Mechanical properties of polymer solids and liquids," *The elements of polymer science & engineering*, vol. 3, 2013.

[27] X. Wang, K. Zhao, and H. Zhao, "Finite element simulation of biofilm viscoelastic behavior under various loadings," *Journal of Mechanics in Medicine and Biology*, vol. 18, no. 05, p. 1850056, 2018.

[28] C. Henderson, "The application of boltzmann's superposition theory to materials exhibiting reversible $\beta$ flow," *Proceedings of the Royal Society of London. Series A. Mathematical and Physical Sciences*, vol. 206, no. 1084, pp. 72–86, 1951.

[29] S.-i. Karato, "Rheology of the earth's mantle: A historical review," *Gondwana Research*, vol. 18, no. 1, pp. 17–45, 2010.

[30] S.-H. Chae, J.-H. Zhao, D. R. Edwards, and P. S. Ho, "Characterization of viscoelasticity of molding compounds in time domain," in *International Electronic Packaging Technical Conference and Exhibition*, vol. 43598, pp. 435–441, 2009.

[31] K. Wilkie, C. Drapaca, and S. Sivaloganathan, "Aging impact on brain biomechanics with applications to hydrocephalus," *Mathematical medicine and biology: a journal of the IMA*, vol. 29, no. 2, pp. 145–161, 2012.

[32] D. D. Joseph, *Fluid dynamics of viscoelastic liquids*, vol. 84. Springer Science & Business Media, 2013.

[33] M. Dolz, M. Hernández, and J. Delegido, "Creep and recovery experimental investigation of low oil content food emulsions," *Food Hydrocolloids*, vol. 22, no. 3, pp. 421–427, 2008.

[34] J. Liu, G. Liao, Z. Xie, B. Li, L. Cui, and Y. Liu, "Investigation on the rheological behavior of pa6 film during biaxial stretching," *Materials Today Communications*, vol. 38, p. 107616, 2024.

[35] H. Ghazisaeidi, "A description of the anisotropic material behaviour of short glass fibre reinforced thermoplastics using fea.," 2006.

[36] H. Pouriayevali, Y. Guo, and V. Shim, "A visco-hyperelastic constitutive description of elastomer behaviour at high strain rates," *Procedia Engineering*, vol. 10, pp. 2274–2279, 2011.

[37] H. F. Brinson, L. C. Brinson, *et al.*, "Polymer engineering science and viscoelasticity," *An introduction*, pp. 99–157, 2008.

[38] J. Bergstrom, "*Volumetric Relaxation in a Prony Series*." https://polymerfem.com/volumetric-relaxation-in-a-prony-series/, October 2022. [Accessed: 28-02-2024].

[39] R. S. Lakes and A. Wineman, "On poisson's ratio in linearly viscoelastic solids," *Journal of Elasticity*, vol. 85, pp. 45–63, 2006.

[40] L.-J. Shen, "Fractional derivative models for viscoelastic materials at finite deformations," *International Journal of Solids and Structures*, vol. 190, pp. 226–237, 2020.

[41] M. Paggi, A. Sapora, *et al.*, "An accurate thermoviscoelastic rheological model for ethylene vinyl acetate based on fractional calculus," *International Journal of Photoenergy*, vol. 2015, 2015.

[42] Q. Ma, X. Lin, and H. Li, "A comparative teaching of fractional calculus and integer calculus," in *2018 International Conference on Social Science and Education Reform (ICSSER 2018)*, pp. 94–97, Atlantis Press, 2018.

[43] H. Zhou, T. Su, H. Deng, R. Wang, J. Zhao, X. Sun, and L. An, "Characterizing three-dimensional creep of beishan granite by the variable-coefficient abel dashpot," *Mechanics of Time-Dependent Materials*, vol. 25, pp. 85–100, 2021.

[44] J. Long, R. Xiao, and W. Chen, "Fractional viscoelastic models with non-singular kernels," *Mechanics of Materials*, vol. 127, pp. 55–64, 2018.

[45] E. Artin, *The gamma function*. Courier Dover Publications, 2015.

[46] A. Bonfanti, J. L. Kaplan, G. Charras, and A. Kabla, "Fractional viscoelastic models for power-law materials," *Soft Matter*, vol. 16, no. 26, pp. 6002–6020, 2020.

[47] A. Krusser and M. Shitikova, "Classification of viscoelastic models with integer and fractional order derivatives," in *IOP Conference Series: Materials Science and Engineering*, vol. 747, p. 012007, IOP Publishing, 2020.

[48] K. Adolfsson, M. Enelund, and P. Olsson, "On the fractional order model of viscoelasticity," *Mechanics of Time-dependent materials*, vol. 9, pp. 15–34, 2005.

[49] J. I. S. Lustosa, F. de Campos Bannwart, and E. C. de Oliveira, "Fractional calculus applied to evaluate stress concentration and shear effects in simply supported beams," *CQD-Revista Eletrônica Paulista de Matemática*, 2022.

[50] J. Bergstrom, "*Blatz-Ko Model*." https://polymerfem.com/blatz-ko-model/, May 2023. [Accessed: 19-02-2024].

[51] A. Harish, "*How to choose a hyperelastic material model for your fea?*." https://polymerfem.com/all-about-the-arruda-boyce-hyperelastic-model/, Jun 2023. [Accessed: 19-02-2024].

[52] F. T. Stumpf and R. J. Marczak, "Constitutive characterization of hyperelastic materials considering the baker-ericksen inequalities,"

[53] F. Peyraut, "Loading restrictions for the blatz–ko hyperelastic model—application to a finite element analysis," *International Journal of Non-Linear Mechanics*, vol. 39, no. 6, pp. 969–976, 2004.

[54] S. Xiao and T. Belytschko, "Material stability analysis of particle methods," *Advances in Computational Mathematics*, vol. 23, pp. 171–190, 2005.

[55] J. Bergstrom, "*5 common mistakes when using hyperelasticity*." https://polymerfem.com/5-common-mistakes-when-using-hyperelasticity/, May 2023. [Accessed: 19-02-2024].

[56] S. K. Melly, L. Liu, Y. Liu, and J. Leng, "A review on material models for isotropic hyperelasticity," *International Journal of Mechanical System Dynamics*, vol. 1, no. 1, pp. 71–88, 2021.

[57] J. Bergstrom, "*All about the arruda-boyce hyperelastic model.*" https://polymerfem.com/all-about-the-arruda-boyce-hyperelastic-model/, May 2023. [Accessed: 19-02-2024].

[58] S. Sharma, "*Critical comparison of popular hyper-elastic material models in design of anti-vibration mounts for automotive industry through FEA.*" https://polymerfem.com/polymer_files/external/shacco.pdf. [Accessed: 19-02-2024].

[59] S.-Q. Yang and L. Cheng, "Non-stationary and nonlinear visco-elastic shear creep model for shale," *International Journal of Rock Mechanics and Mining Sciences*, vol. 48, no. 6, pp. 1011–1020, 2011.

[60] Q. Xu, B. Engquist, M. Solaimanian, and K. Yan, "A new nonlinear viscoelastic model and mathematical solution of solids for improving prediction accuracy," *Scientific reports*, vol. 10, no. 1, p. 2202, 2020.

[61] T. Zink, L. Kehrer, V. Hirschberg, M. Wilhelm, and T. Böhlke, "Nonlinear schapery viscoelastic material model for thermoplastic polymers," *Journal of Applied Polymer Science*, vol. 139, no. 17, p. 52028, 2022.

[62] M. Basso, L. Pupure, M. Simonato, R. Furlanetto, L. De Nardo, and R. Joffe, "Nonlinear creep behaviour of glass fiber reinforced polypropylene: Impact of aging on stiffness degradation," *Composites Part B: Engineering*, vol. 163, pp. 702–709, 2019.

[63] C. Zhang, Z. Zhu, S. Zhu, Z. He, D. Zhu, J. Liu, and S. Meng, "Nonlinear creep damage constitutive model of concrete based on fractional calculus theory," *Materials*, vol. 12, no. 9, p. 1505, 2019.

[64] S. Palathingal and G. Ananthasuresh, "Design of bistable arches by determining critical points in the force-displacement characteristic," *Mechanism and Machine Theory*, vol. 117, pp. 175–188, 2017.

[65] S. M. Jo and H.-S. Yoon, "Energy-efficient tristable soft gripper using shape memory alloy wires for gripping convex and concave objects," *Journal of Mechanisms and Robotics*, vol. 16, no. 2, p. 021013, 2024.

[66] D.-A. Wang, J.-H. Chen, and H.-T. Pham, "A tristable compliant micromechanism with two serially connected bistable mechanisms," *Mechanism and Machine Theory*, vol. 71, pp. 27–39, 2014.

[67] M. Schenk and S. D. Guest, "On zero stiffness," *Proceedings of the Institution of Mechanical Engineers, Part C: Journal of Mechanical Engineering Science*, vol. 228, no. 10, pp. 1701–1714, 2014.

[68] S. Kok, "Literature review of occurrences and working principles of elastic neutral stability," 2020.

[69] Z. Vangelatos, I. Farina, A. Micheletti, N. Singh, C. Grigoropoulos, and F. Fraternali, "On the fabrication and mechanical modelling microscale bistable tensegrity systems," in *IOP Conference Series: Materials Science and Engineering*, vol. 999, p. 012002, IOP Publishing, 2020.

[70] C. R. Calladine, "Buckminster fuller's "tensegrity" structures and clerk maxwell's rules for the construction of stiff frames," *International journal of solids and structures*, vol. 14, no. 2, pp. 161–172, 1978.

[71] A. Micheletti, "Bistable regimes in an elastic tensegrity system," *Proceedings of the Royal Society A: Mathematical, Physical and Engineering Sciences*, vol. 469, no. 2154, p. 20130052, 2013.

[72] K. Shimura, N. Iwamoto, and T. Umedachi, "Bistable tensegrity robot with jumping repeatability based on rigid plate-shaped compressors," in *2023 IEEE/RSJ International Conference on Intelligent Robots and Systems (IROS)*, pp. 8324–8330, IEEE, 2023.

[73] S.-P. Jung, G.-P. Jung, J.-S. Koh, D.-Y. Lee, and K.-J. Cho, "Fabrication of composite and sheet metal laminated bistable jumping mechanism," *Journal of Mechanisms and Robotics*, vol. 7, no. 2, p. 021010, 2015.

[74] C. Aza, A. Pirrera, and M. Schenk, "Multistable morphing mechanisms of nonlinear springs," *Journal of Mechanisms and Robotics*, vol. 11, no. 5, p. 051014, 2019.

[75] E. Kebadze, S. Guest, and S. Pellegrino, "Bistable prestressed shell structures," *International Journal of Solids and Structures*, vol. 41, no. 11-12, pp. 2801–2820, 2004.

[76] K. A. Seffen and S. D. Guest, "Prestressed morphing bistable and neutrally stable shells," 2011.

[77] W. Hamouche, C. Maurini, S. Vidoli, and A. Vincenti, "Multi-parameter actuation of a neutrally stable shell: a flexible gear-less motor," *Proceedings of the Royal Society A: Mathematical, Physical and Engineering Sciences*, vol. 473, no. 2204, p. 20170364, 2017.

[78] J. P. Stacey, M. P. O'Donnell, and M. Schenk, "Thermal prestress in composite compliant shell mechanisms," *Journal of Mechanisms and Robotics*, vol. 11, no. 2, p. 020908, 2019.

[79] B. Xu, B. Wang, K. S. Fancey, S. Zhong, C. Zhao, and X. Chen, "A bistable helical structure based on composite tape-springs," *Composites Communications*, vol. 43, p. 101723, 2023.

[80] A. Brinkmeyer, M. Santer, A. Pirrera, and P. Weaver, "Pseudo-bistable self-actuated domes for morphing applications," *International Journal of Solids and Structures*, vol. 49, no. 9, pp. 1077–1087, 2012.

[81] M. Gomez, D. E. Moulton, and D. Vella, "Dynamics of viscoelastic snap-through," *Journal of the Mechanics and Physics of Solids*, vol. 124, pp. 781–813, 2019.

[82] B. Wang, C. Ge, and K. S. Fancey, "Snap-through behaviour of a bistable structure based on viscoelastically generated prestress," *Composites Part B: Engineering*, vol. 114, pp. 23–33, 2017.

[83] Y. Gou, G. Chen, and L. Howell, "A design approach to fully compliant multistable mechanisms employing a single bistable mechanism," vol. 49, pp. 1–24.

[84] G. Risso and P. Ermanni, "Multi-stability of fiber reinforced polymer frames with different geometries," *Composite Structures*, vol. 313, p. 116958, 2023.

[85] A. Norman, K. Seffen, and S. Guest, "Multistable corrugated shells," *Proceedings of the Royal Society A: Mathematical, Physical and Engineering Sciences*, vol. 464, no. 2095, pp. 1653–1672, 2008.

[86] A. Lele, V. Deshpande, O. Myers, and S. Li, "Snap-through and stiffness adaptation of a multi-stable kirigami composite module," *Composites Science and Technology*, vol. 182, p. 107750, 2019.

[87] W. Thomson and P. G. Tait, *Treatise on natural philosophy*. CUP Archive, 2022.

[88] G. Chaudhary, S. Ganga Prasath, E. Soucy, and L. Mahadevan, "Totimorphic assemblies from neutrally stable units," *Proceedings of the National Academy of Sciences*, vol. 118, no. 42, p. e2107003118, 2021.

[89] X. Wang, Z. Meng, and C. Q. Chen, "Robotic materials transformable between elasticity and plasticity," *Advanced Science*, p. 2206637, 2023.

[90] G. Radaelli, "Reverse-twisting of helicoidal shells to obtain neutrally stable linkage mechanisms," *International Journal of Mechanical Sciences*, vol. 202, p. 106532, 2021.

[91] S. Kok, "Towards neutrally stable compliant shells," 2020.

[92] Y. Liuyi, T. Huifeng, and C. Zongsheng, "Numerical and experimental investigations of thin-walled neutrally stable deployable composite booms,"

[93] T. Murphey and S. Pellegrino, "A novel actuated composite tape-spring for deployable structures," in *45th AIAA/ASME/ASCE/AHS/ASC Structures, Structural Dynamics & Materials Conference*, p. 1528, 2004.

[94] X. Lin, B. Wang, C. Zhao, W. Nsengiyumva, S. Zhong, H. Chen, and D. Liu, "Durability of viscoelastic fibre prestressing in a polymeric composite," *Polymers*, vol. 15, no. 4, p. 811, 2023.

[95] K. S. Fancey, "Viscoelastically prestressed polymeric matrix composites–potential for useful life and impact protection," *Composites Part B: Engineering*, vol. 41, no. 6, pp. 454–461, 2010.

# Glossary

## List of Acronyms

| | |
|---|---|
| **TTSSP** | Time-Temperature-Stress Superposition Principle |
| **RoM** | Range of Motion |
| **SLS** | Standard Linear Solid model |
| **AZM** | Anti-Zener model |
| **BSP** | Boltzmann Superposition Principle |
| **FEM** | Finite Element Method |
| **EoM** | Equations of motion |
| **PRBM** | Pseudo-Rigid Body Model |
| **FRP** | Fibre Reinforced Polymer |
| **VPPMC** | Viscoelastically Prestressed Polymer Matrix Composites |

**Figure A-1:** Tensile test setup

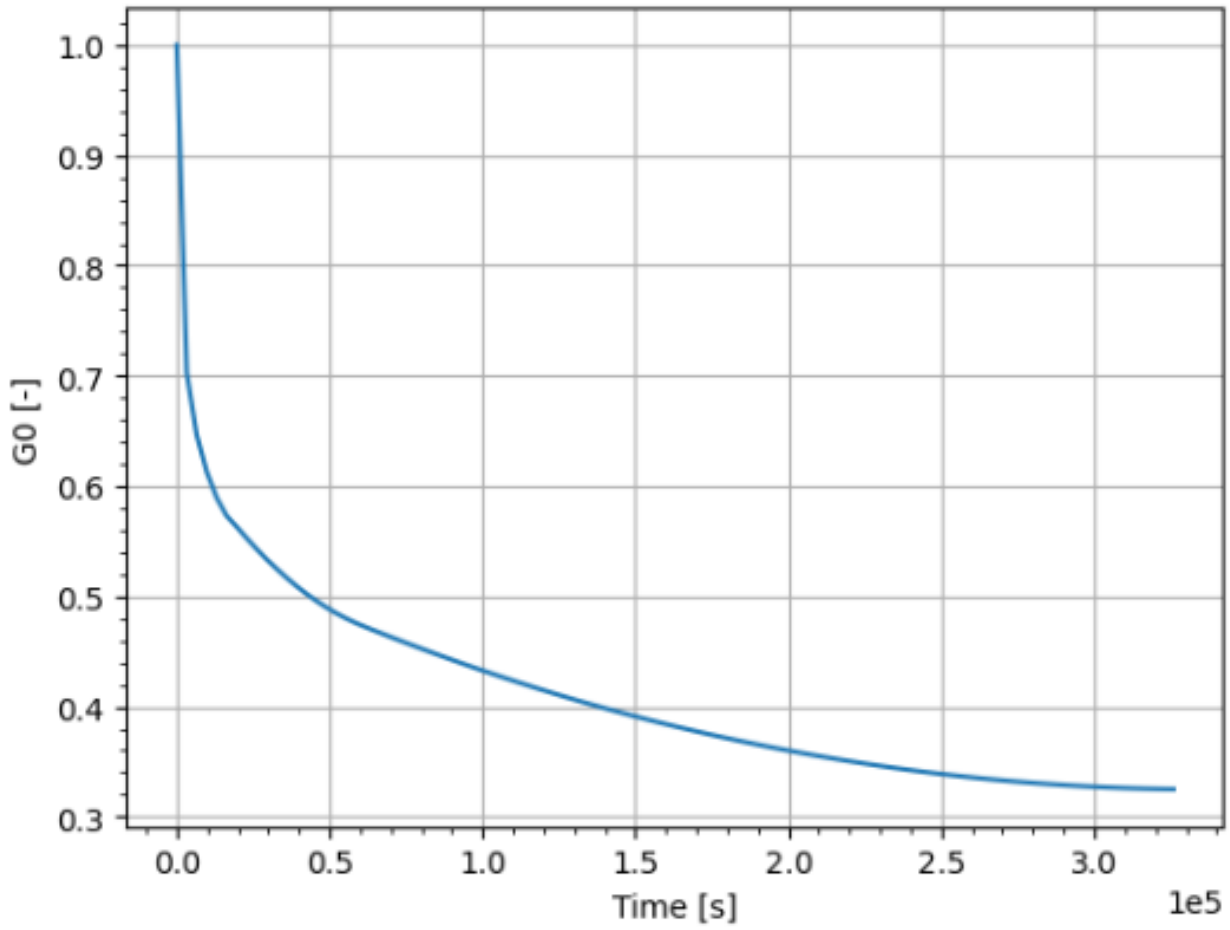


**Figure A-2:** Stress relaxation test data PLA

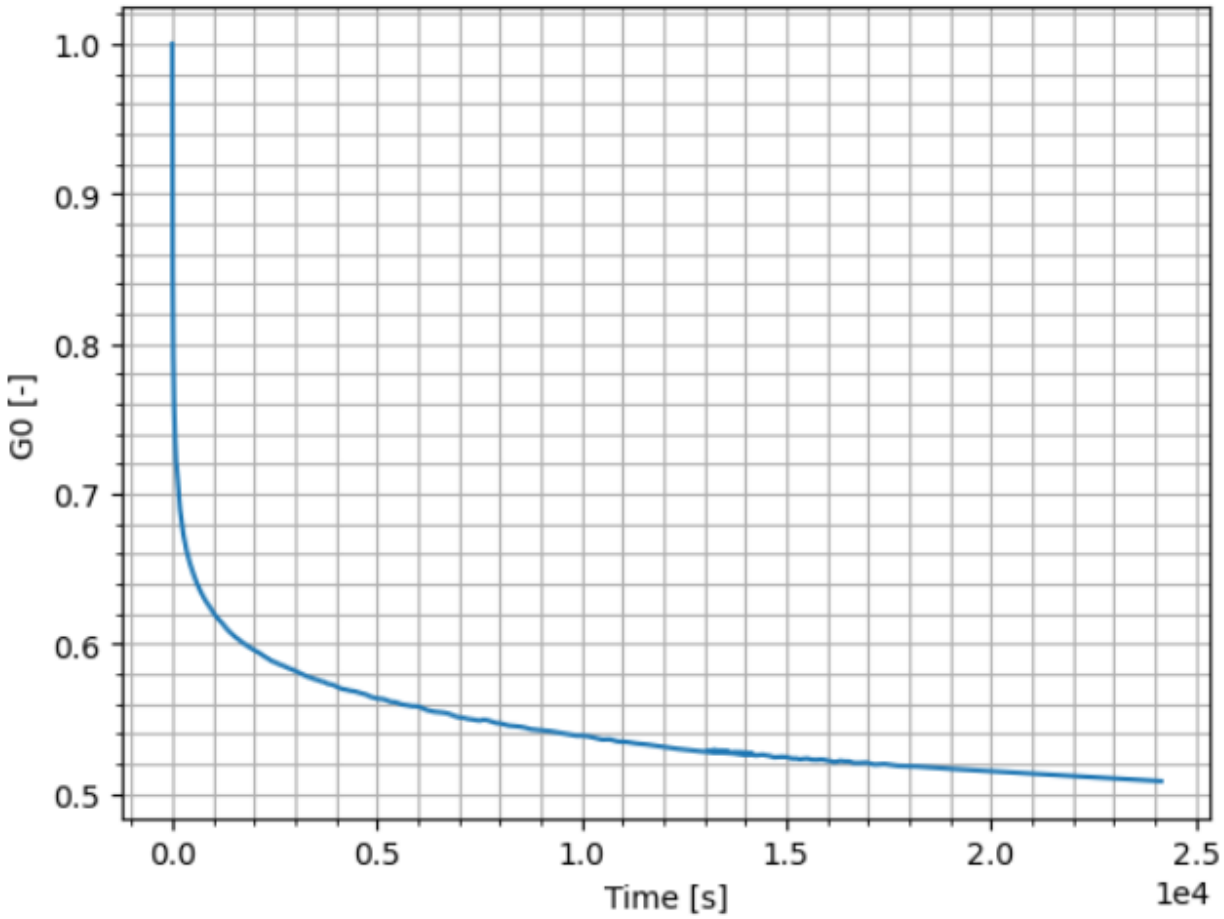


**Figure A-3:** Stress relaxation test data PA12

# Appendix B

# Torque test

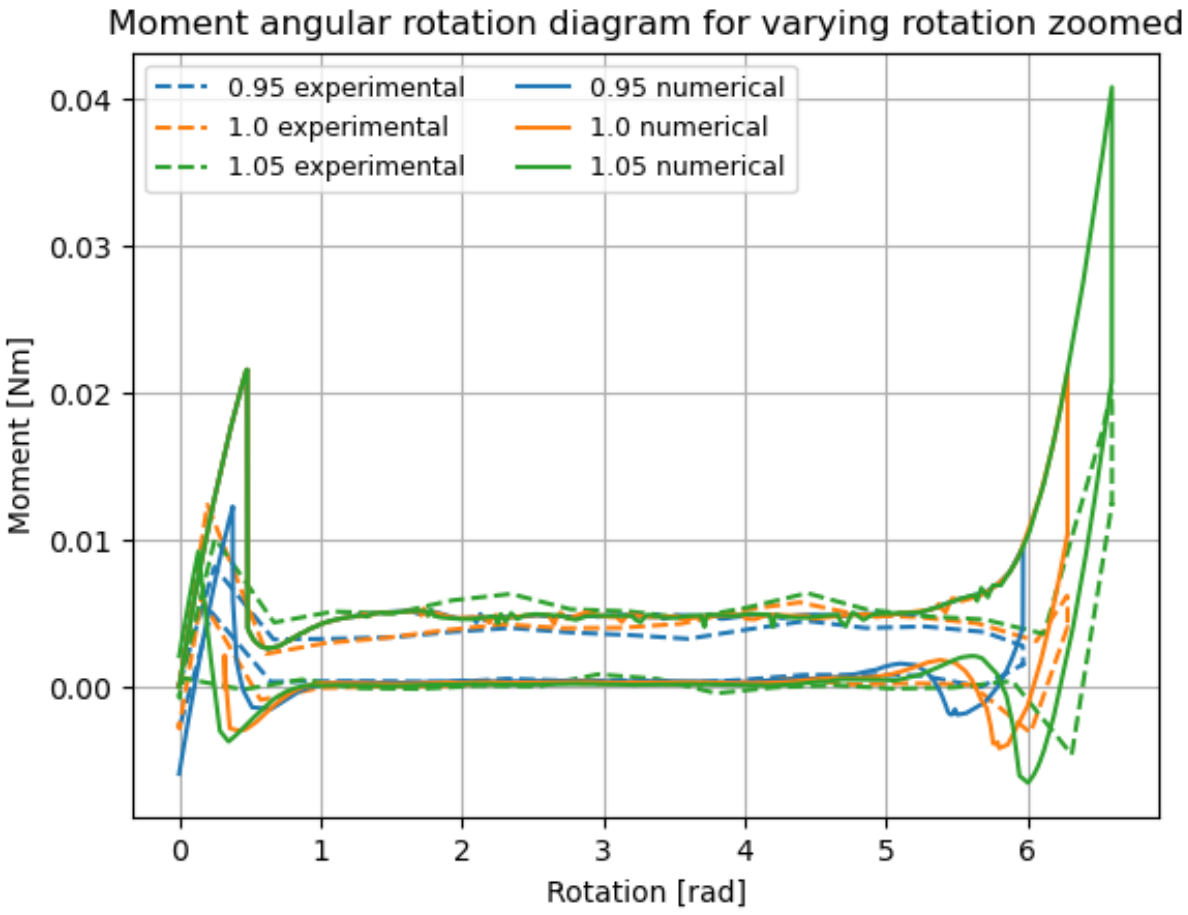


**Figure B-1:** Stiffness shift for varying twist factors helicoid

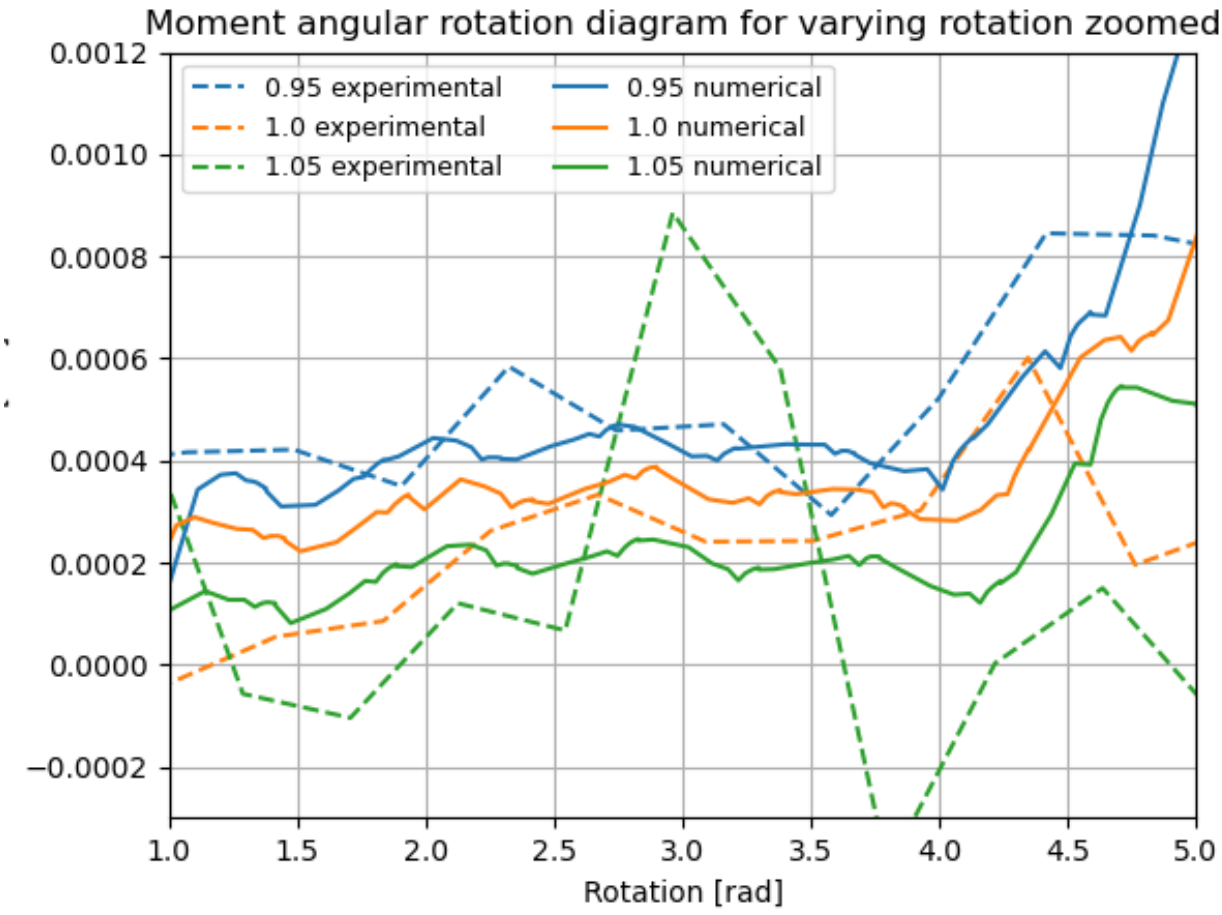


**Figure B-2:** Stiffness shift for varying twist factors helicoid

# Appendix C

# CODE

## I APDL code linear guide

```
FINISH          !some commands to clear the workspace
/CLEAR
/OUTPUT

!!!!parameters!!!!
E = 5.3e9             ! Young's modulus (Pa)
v = 0.35            ! Poisson ratio (-)


Trelax = 2000
Temprel = 14
DispFactor = 1
refT = 19           ! Reference temperature (K)
C1 = 570/7            ! WLF constant  (-)
C2 = -1850/7            ! WLF constant  (C)


disp_0 = 0.00001        ! Buckling displacement y-direction
tot_disp = 4/1000

!Import geometry
~PARAIN,'ProtoConst8','x_t','.\Documents\TU Delft\Solidworks\Helicoid\',SOLIDS
ALLSEL,ALL


!!!!preprocessi!ng!!!!

/PREP7      !enter preprocessor menu

!Define element type
ET,1,SOLID187 !element type 1

lsel,s,,,2

!Define material model
MP,EX,1,E   !set Young's modulus of mat 1
MP,PRXY,1,v   !set Poisson ratio of mat 1



/com,Curve Fitting Experimental Data Written To Twist_SDEC_1.exp
```

```
! PLA

TBFT,EADD,1,SDEC,Twisting_SDEC_1.exp
TBFT,FCASE,1,NEW,PVHE,myfit
TBFT,FADD,1,VISCO,PSHEAR,5
TBFT,FADD,1,VISCO,PBULK,5
TBFT,FADD,1,VISCO,SHIFT,NONE
TBFT,FCASE,1,FINI
TBFT,SET,1,CASE,myfit,,1,0.709915956744
TBFT,SET,1,CASE,myfit,,2,0.271659625458
TBFT,SET,1,CASE,myfit,,3,3.21582456034
TBFT,SET,1,CASE,myfit,,4,0.334455409177
TBFT,SET,1,CASE,myfit,,5,117.031325819
TBFT,SET,1,CASE,myfit,,6,0.128104732879
TBFT,SET,1,CASE,myfit,,7,997.816269103
TBFT,SET,1,CASE,myfit,,8,0.542162079753
TBFT,SET,1,CASE,myfit,,9,10023.136969
TBFT,SET,1,CASE,myfit,,10,0.43
TBFT,SET,1,CASE,myfit,,11,100000
TBFT,SET,1,CASE,myfit,,12,1
TBFT,SET,1,CASE,myfit,,13,1
TBFT,SET,1,CASE,myfit,,14,1
TBFT,SET,1,CASE,myfit,,15,1
TBFT,SET,1,CASE,myfit,,16,1
TBFT,SET,1,CASE,myfit,,17,1
TBFT,SET,1,CASE,myfit,,18,1
TBFT,SET,1,CASE,myfit,,19,1
TBFT,SET,1,CASE,myfit,,20,1
TBFT,SET,1,CASE,myfit,,21,1
TBFT,SET,1,CASE,myfit,,22,1
TBFT,SET,1,CASE,myfit,,comp,pvhe
TBFT,FIX,1,CASE,myfit,,1,0
TBFT,FIX,1,CASE,myfit,,2,0
TBFT,FIX,1,CASE,myfit,,3,0
TBFT,FIX,1,CASE,myfit,,4,0
TBFT,FIX,1,CASE,myfit,,5,0
TBFT,FIX,1,CASE,myfit,,6,0
TBFT,FIX,1,CASE,myfit,,7,0
TBFT,FIX,1,CASE,myfit,,8,0
TBFT,FIX,1,CASE,myfit,,9,0
TBFT,FIX,1,CASE,myfit,,10,0
TBFT,FIX,1,CASE,myfit,,11,0
TBFT,FIX,1,CASE,myfit,,12,0
TBFT,FIX,1,CASE,myfit,,13,0
TBFT,FIX,1,CASE,myfit,,14,0
TBFT,FIX,1,CASE,myfit,,15,0
TBFT,FIX,1,CASE,myfit,,16,0
TBFT,FIX,1,CASE,myfit,,17,0
TBFT,FIX,1,CASE,myfit,,18,0
TBFT,FIX,1,CASE,myfit,,19,0
TBFT,FIX,1,CASE,myfit,,20,0
TBFT,FIX,1,CASE,myfit,,21,0
TBFT,FIX,1,CASE,myfit,,22,0
TBFT,SET,1,CASE,myfit,,tref,20
TBFT,SET,1,CASE,myfit,,tdep,0
TBFT,SOLVE,1,CASE,myfit,,1,1000,0,0
TBFT,FSET,1,CASE,myfit,


TB,SHIFT,1,1,3,1
TBTEMP,refT
TBDATA,,refT,C1,C2,,,
```

```
104
105
106 !Mesh using smart sizing just in case
107 Type,1
108 SECNUM,1
109 SMRTSIZE,5
110 VSEL,ALL
111 VMESH,ALL
112 ALLSEL,ALL       !Make sure to have selected everything again
113
114 !Min and max node in the line
115 LSEL,S,,,2         !select keypoint 3
116 NSLL,S             !select the node at keypoint 3
117 *GET,mn,NODE,,NUM,MIN,
118 *GET,mx,NODE,,NUM,MAX,
119
120
121 FINISH          !exit pre-processor
122
123 /SOLU        !enter solution menu
124
125 !Settings
126 NLGEOM,1        !Include large deflection effects
127 NEQIT,300       !Allow n substeps per iteration (good for non-linear analysis)
128 NROPT,FULL,,ON
129 NSUBST,1000,1000,1
130 AUTOTS,ON
131 ALLSEL,ALL
132
133
134 Tref,refT
135
136 !Boundary conditions and initial displacement
137 OUTRES,ALL,ALL
138
139 TIME,1
140 KBC,0          !Ramped loading
141
142 DL,50,,ALL,0
143 DL,47,,ALL,0
144 DL,48,,ALL,0
145 DL,49,,ALL,0
146
147 DLDELE,50,ROTZ
148 DLDELE,48,ROTZ
149 DLDELE,47,ROTZ
150 DLDELE,49,ROTZ
151
152 DL,2,,UY,0
153
154 BF,ALL,TEMP,Temprel
155 SOLVE
156
157
158 !Get the x-direction displacement after buckling potentially buckling
159 *GET,disp_x,node,mn,u,x
160
161 displacement = tot_disp - disp_x
162
163 time_step = 2
164 steps = 4
165
```

```
166 !Deform in prescribed amount of steps
167 *DO,i,disp_x,displacement,(displacement/steps)
168   TIME,time_step
169   DL,2,,UX,i*DispFactor
170   SOLVE
171   time_step=time_step+1
172 *ENDDO
173
174 ! Relaxation time
175 TIME,Trelax
176 SOLVE
177
178
179
180 ! Deform back to original configuration
181 time_step = Trelax+1
182 *DO,i,0,displacement,displacement/steps
183   TIME,time_step
184   DL,2,,UX,(displacement+disp_x-i)*DispFactor
185   OUTRES,ALL,ALL
186   SOLVE
187   time_step=time_step+1
188 *ENDDO
189
190
191
192 OUTRES,ALL,ALL
193
194 FINISH
195
196 /POST26
197 NUMVAR,150     !Number of variables that are available for analysis
198         ! You can lower this if you know the amount of nodes per line
199
200
201 ! I need this node to plot the moment vs the angular rotation
202 KSEL,S,,,3          !select keypoint 3
203 NSLK,S              !select the node at keypoint 3
204 *GET,K3,NODE,,NUM,MIN    !assign the ID: K3 to this node
205 ALLSEL,ALL
206
207 TIMERANGE,2,Trelax+20
208 NSOL,2,K3,U,X,UX
209
210 j = 3
211 sum = 100
212 *DO,i,mn,mx,1
213   NSEL,S,,,i          !Get the current node number in the selection
214   RFORCE,j,i,F,X,X%i%    !Get reaction force variable
215   ADD,sum,sum,j       !Sum current variable to sum variable
216   j = j + 1         !Increment variable number
217 *ENDDO
218
219
220 ALLSEL,ALL
221 ! /XRANGE, 0, 0.085, 2
222 ! /YRANGE, 0, 20, 3
223 /AXLAB, X, displacement [m]
224 /AXLAB, Y, force [N]
225 XVAR,2
226 PLVAR,sum
227
```

```
228
229 *CREATE,scratch,gui !Put my results in ResultsProto.csv file in order to see if
        I've
230 *DEL,_P26_EXPORT    !really achieved neutral stability
231 *DIM,_P26_EXPORT,TABLE,700,3
232 VGET,_P26_EXPORT(1,0),1
233 VGET,_P26_EXPORT(1,1),2
234 VGET,_P26_EXPORT(1,2),sum
235 /OUTPUT,'ResultsProto','csv','C:\Users\Thies\Documents\TU Delft\Ansys\Notepad'
        !set output file of export
236 *VWRITE,'TIME','UX','FX'                !write strings of output data in first row
237 %C, %C, %C
238 *VWRITE,_P26_EXPORT(1,0),_P26_EXPORT(1,1),_P26_EXPORT(1,2)  !write output data in
        separate columns
239 %G, %G, %G
240 *END
241 /INPUT,scratch,gui
242
243 /OUTPUT,'C:\Users\Thies\Documents\TU Delft\Ansys\Notepad\outfile','txt'
```

## II APDL code helicoidal shell

```
1  FINISH          !some commands to clear the workspace
2  /CLEAR
3  /OUTPUT
4
5  !In case of batch mode ga ik deze dus ff aanzetten zodat ik minder error gezeik
       heb
6  /NERR,0,99999999,,,0       !/NERR,0,99999999,,,0 deze werkt sws
7  /UIS,MSGPOP,4
8
9  !!!!parameters!!!!
10 E = 1.8e9    ! Young's modulus (Pa)
11 v = 0.38     ! Poisson ratio (-)
12
13 t = 0.4e-3     ! Original thickness Helicoid
14 w = 0.01     ! Original width helicoid
15 h = 0.1      ! Original length helicoid
16
17 t_scale = 1
18 w_scale = 1
19 h_scale = 1
20
21 pi=acos(-1)
22
23 refT = 20          ! Temperature (K)
24 C1 = 60          ! WLF constant  (-)
25 C2 = 280         ! WLF constant  (C)
26
27 Trelax = 2000
28 Temprel = 20
29 Tfactor = 1.0
30
31
32 !!!!preprocessing!!!!
33
34 /PREP7       !enter preprocessor menu
35
36 !Define element type
37 ET,1,SHELL181 !element type 1
38 ET,2,MPC184    !Rigid element
```

```
KEYOPT,1,5,2  !Allows for initial curvature effects

KEYOPT,2,1,1  !Allow rigid link

!Import and create geometry
~PARAIN,'Surfaceass','x_t','.\Documents\TU Delft\Ansys\Notepad\Probeersels\',
    SOLIDS,0,0
ASEL,ALL

!Play with location keypoints for parametric

!Create surface from geometry
AL,1,2,3,4

! Scale geometry: ARSCALE, NA1, NA2, NINC, RX, RY, RZ, KINC, NOELEM, IMOVE !In the
     end I did not use this

t = t*t_scale              !Thickness
ARSCALE,1,,,w_scale,,w_scale,,,1     !Width
ARSCALE,1,,,,h_scale,,,,1        !Height


!Define shell geometry
/ESHAPE
SECTYPE,1,SHELL
SECDATA,t,1,,9     !More integration points makes it more vulnerable to excessive
    distortions

SECTYPE,2,beam,RECT
SECDATA,t,t    !same for buckled beam


!Define material model
MP,EX,1,E    !set Young's modulus of mat 1
MP,PRXY,1,v    !set Poisson ratio of mat 1

/com,Curve Fitting Experimental Data Written To Twist_SDEC_1.exp !Curve fit PA12
TBFT,EADD,1,SDEC,Twist_SDEC_1.exp
TBFT,FCASE,1,NEW,PVHE,myfit
TBFT,FADD,1,VISCO,PSHEAR,5
TBFT,FADD,1,VISCO,PBULK,5
TBFT,FADD,1,VISCO,SHIFT,NONE
TBFT,FCASE,1,FINI
TBFT,SET,1,CASE,myfit,,1,0.9
TBFT,SET,1,CASE,myfit,,2,0.85
TBFT,SET,1,CASE,myfit,,3,10
TBFT,SET,1,CASE,myfit,,4,0.71
TBFT,SET,1,CASE,myfit,,5,100
TBFT,SET,1,CASE,myfit,,6,0.63
TBFT,SET,1,CASE,myfit,,7,1000
TBFT,SET,1,CASE,myfit,,8,0.55
TBFT,SET,1,CASE,myfit,,9,10000
TBFT,SET,1,CASE,myfit,,10,0.508
TBFT,SET,1,CASE,myfit,,11,24000
TBFT,SET,1,CASE,myfit,,12,1
TBFT,SET,1,CASE,myfit,,13,1
TBFT,SET,1,CASE,myfit,,14,1
TBFT,SET,1,CASE,myfit,,15,1
TBFT,SET,1,CASE,myfit,,16,1
TBFT,SET,1,CASE,myfit,,17,1
TBFT,SET,1,CASE,myfit,,18,1
TBFT,SET,1,CASE,myfit,,19,1
```

```
98  TBFT,SET,1,CASE,myfit,,20,1
99  TBFT,SET,1,CASE,myfit,,21,1
100 TBFT,SET,1,CASE,myfit,,22,1
101 TBFT,SET,1,CASE,myfit,,comp,pvhe
102 TBFT,FIX,1,CASE,myfit,,1,0
103 TBFT,FIX,1,CASE,myfit,,2,0
104 TBFT,FIX,1,CASE,myfit,,3,0
105 TBFT,FIX,1,CASE,myfit,,4,0
106 TBFT,FIX,1,CASE,myfit,,5,0
107 TBFT,FIX,1,CASE,myfit,,6,0
108 TBFT,FIX,1,CASE,myfit,,7,0
109 TBFT,FIX,1,CASE,myfit,,8,0
110 TBFT,FIX,1,CASE,myfit,,9,0
111 TBFT,FIX,1,CASE,myfit,,10,0
112 TBFT,FIX,1,CASE,myfit,,11,0
113 TBFT,FIX,1,CASE,myfit,,12,0
114 TBFT,FIX,1,CASE,myfit,,13,0
115 TBFT,FIX,1,CASE,myfit,,14,0
116 TBFT,FIX,1,CASE,myfit,,15,0
117 TBFT,FIX,1,CASE,myfit,,16,0
118 TBFT,FIX,1,CASE,myfit,,17,0
119 TBFT,FIX,1,CASE,myfit,,18,0
120 TBFT,FIX,1,CASE,myfit,,19,0
121 TBFT,FIX,1,CASE,myfit,,20,0
122 TBFT,FIX,1,CASE,myfit,,21,0
123 TBFT,FIX,1,CASE,myfit,,22,0
124 TBFT,SET,1,CASE,myfit,,tref,20
125 TBFT,SET,1,CASE,myfit,,tdep,0
126 TBFT,SOLVE,1,CASE,myfit,,1,1000,0,0
127 TBFT,FSET,1,CASE,myfit,
128
129
130 TB,SHIFT,1,1,3,1
131 TBTEMP,refT
132 TBDATA,,refT,C1,C2,,,
133
134
135 ALLSEL,ALL
136 !Mesh using smart sizing just in case
137 Type,1
138 SMRTSIZE,4,    !1 is fine, 10 is coarse
139 AMESH,ALL
140 ALLSEL,ALL       !Make sure to have selected everything again
141
142 Type,2          !select element type for mesh
143 SECNUM,2        !select section for mesh
144 LSEL,S,LINE,,3     !Select top line to remesh for rigid link
145 SMRTSIZE,4,
146 LMESH,ALL       !mesh all lines
147 ALLSEL,ALL
148
149
150 LSEL,S,,,3,,,1
151 NSLL,S
152 *GET,mn,NODE,,NUM,MIN,
153 *GET,mx,NODE,,NUM,MAX,
154 ALLSEL,ALL
155
156
157 FINISH          !exit pre-processor
158
159 /SOLU        !enter solution menu
```

```
160 ! NLDIAG,EFLG,ON
161
162 !Settings
163 NLGEOM,1       !Include large deflection effects
164 NEQIT,300      !Allow n substeps per iteration (good for non-linear analysis)
165 NROPT,FULL,,ON
166 NSUBST,1000,1000,1
167 AUTOTS,ON
168 ALLSEL,ALL
169
170 Tref,20
171
172 ALLSEL,ALL
173 OUTRES,ALL,ALL
174
175 !Constrain bottom, spine and top lines, and remove unnecessary ones
176 DL,1,,ALL,0      !Bottom line
177
178 DL,2,,ALL,0      !Symmetry axis
179 DLDELE,2,ROTY
180 DLDELE,2,UY
181
182 DL,3,,ALL,0      !Top line
183 DLDELE,3,ROTY
184 DLDELE,3,UX
185 DLDELE,3,UY
186 DLDELE,3,UZ
187
188 ! STEP 1: Twist
189 KBC,0
190 TIME,1
191 BF,ALL,TEMP,Temprel      !Add temperature at this moment
192 DL,3,,ROTY,pi/2        !Rotate mechananism
193
194 F,161,MY,-0.0005
195 ALLSEL,ALL
196 SOLVE
197
198 steps = 10
199 time_step = 2
200 *DO,i,pi/2,2*pi*Tfactor,(2*pi*Tfactor-pi/2)/steps
201   TIME,time_step
202   DL,3,,ROTY,i
203   SOLVE
204   time_step = time_step+1
205 *ENDDO
206
207 ! STEP 2: Hold
208 TIME,Trelax
209 ALLSEL,ALL
210 SOLVE
211
212 ! Step 3: Twist back
213 TIME,Trelax+1
214 steps = 16
215 time_step = Trelax+2
216 *DO,i,0,2*pi*Tfactor,2*pi*Tfactor/steps
217   TIME,time_step
218   DL,3,,ROTY,2*pi*Tfactor-i
219   SOLVE
220   time_step = time_step+1
221 *ENDDO
```

```
222
223 FINISH
224
225 /POST26
226 NUMVAR,150     !Number of variables that are available for analysis
227         !You can lower this if you know the amount of nodes per line
228
229 FILE,'Twisting','rst','.' !First entry determines location to which results are
    written
230
231 ! I need this node to plot the moment vs the angular rotation
232 KSEL,S,,,3          !select keypoint 3
233 NSLK,S              !select the node at keypoint 3
234 *GET,K3,NODE,,NUM,MIN    !assign the ID: K3 to this node
235 ALLSEL,ALL
236
237 TIMERANGE,0,Trelax+20
238 NSOL,2,K3,ROT,Y, ROTY
239
240 !Include keypoints 3 and 4, they would be skipped otherwise
241 NSEL,S,,,3
242 RFORCE,3,3,M,Y,M3
243 ALLSEL,ALL
244
245 NSEL,S,,,4
246 RFORCE,4,4,M,Y,M4
247 ALLSEL,ALL
248
249 sum = 100    !Variable number high enough that it  doesn't interfere with loop
250 j = 5        !One more than the last variable which is 4
251
252 !For i in range 1-length of selection
253 *DO,i,mn,mx,1
254   NSEL,S,,,i          !Get the current node number in the selection
255   RFORCE,j,i,M,Y,M%i%    !Get reaction force variable
256   ADD,sum,sum,j       !Sum current variable to sum variable
257   j = j + 1           !Increment variable number
258 *ENDDO
259
260 ADD,sum,sum,3,4
261
262 XVAR,2
263 PLVAR,sum
264
265 *CREATE,scratch,gui      !Put my results in Results manual.csv file in order to see
    if I've
266 *DEL,_P26_EXPORT         !really achieved neutral stability
267 *DIM,_P26_EXPORT,TABLE,800,3
268 VGET,_P26_EXPORT(1,0),1
269 VGET,_P26_EXPORT(1,1),2
270 VGET,_P26_EXPORT(1,2),sum
271 /OUTPUT,'Results manual','csv','C:\Users\Thies\Documents\TU Delft\Ansys\Notepad'
        !set output file of export
272 *VWRITE,'TIME','ROTY','MY'                !write strings of output data in first
    row
273 %C, %C, %C
274 *VWRITE,_P26_EXPORT(1,0),_P26_EXPORT(1,1),_P26_EXPORT(1,2)  !write output data in
    separate columns
275 %G, %G, %G
276 *END
277 /INPUT,scratch,gui
278
```

```
279 /OUTPUT,'C:\Users\Thies\Documents\TU Delft\Ansys\Notepad\outfile','txt'
```